DMD Fast Forward. Published on January 9, 2018 as DOI: 10.1124/dmd.117.075606
This article has not been copyedited and formatted. The final version may differ from this version.

Derivation of a system-independent Ki for Pgp-mediated digoxin transport from system-dependent IC_{50} data.

Aqsaa Chaudhry, Git Chung, Adam Lynn, Akshata Yalvigi, Colin Brown, Harma Ellens, Michael O'Connor, Caroline Lee and Joe Bentz

Drexel University, Department of Biology, Philadelphia, PA 19104 (AC, AL, AY, MO, JB)

Newcastle University, Institute for Cell and Molecular Biosciences, United Kingdom (GC, CB)

GlaxoSmithKline Pharmaceuticals, Drug Metabolism and Pharmacokinetics, King of Prussia, PA (HE)

Drexel University, Department of Biodiversity, Ecology and Earth Sciences, Philadelphia, PA, 19104 (MO)

Ardea Biosciences Inc., Translational Sciences, San Diego, CA 92121 (CL)

DMD Fast Forward. Published on January 9, 2018 as DOI: 10.1124/dmd.117.075606
This article has not been copyedited and formatted. The final version may differ from this version.

Running Title: Generation of system-independent Ki from IC_{50} curves

*Address correspondence to:

Joe Bentz

Drexel University

Biology Department

3245 Chestnut Street

Philadelphia, PA 19104

Email: bentzj@drexel.edu

Phone: 215 895 1513

Fax number: 215 895 1273

Number of text pages: 26

Number of tables: 6

Number of figures: 6

Number of reference: 35

Number of words in abstract: 249/250

Number of words in introduction: 944/750

Number of words in discussion: 2195/1500

DMD Fast Forward. Published on January 9, 2018 as DOI: 10.1124/dmd.117.075606
This article has not been copyedited and formatted. The final version may differ from this version.

Non-standard Abbreviations:

DMEM: Dulbecco's modified Eagle's medium

GF120918: N-(4-[2-(1,2,3,4-tetrahydro-6,7-dimethoxy-2-isoquinolinyl)ethyl]-phenyl)-9,10-

DMD Fast Forward. Published on January 9, 2018 as DOI: 10.1124/dmd.117.075606
This article has not been copyedited and formatted. The final version may differ from this version.

Abstract

It has been previously demonstrated that IC_{50} values for inhibition of digoxin transport across confluent polarized cell monolayers are system-dependent. Digoxin IC_{50} data from five labs participating in the P-gp IC_{50} Initiative using Caco-2, MDCKII-hMDR1 or LLC-PK1-hMDR1 cells were fitted by the structural mass action kinetic model for P-glycoprotein (P-gp) mediated transport across confluent cell monolayers. We determined the efflux active P-gp concentration (T(0)), the inhibitor elementary dissociation rate constant from P-gp (k_{rQ}), the digoxin basolateral uptake clearance (k_B) and the inhibitor binding affinity to the digoxin basolateral uptake transporter (K_{QB}). We also fitted the IC_{50} data for inhibition of digoxin transport through monolayers of primary human proximal tubule cells, HPTC. All cell systems kinetically required a basolateral uptake transporter for digoxin. The k_{rQ} of these inhibitors was cell system independent, thereby allowing calculation of a system-independent Ki. The variability in efflux active P-gp concentrations and basolateral uptake clearances in the 5 labs was about an order of magnitude. The lab-to-lab variability of these ranges can explain more than 50% of the IC_{50} variability found in the PCA plot in Bentz et al. (2013), supporting the hypothesis that the observed IC_{50} variability is primarily due to differences in expression levels of P-gp and the basolateral digoxin uptake transporter. HPTCs had 10- to 100-fold lower efflux active P-gp concentrations than the over-expressing cell lines, while their digoxin basolateral uptake clearances were similar. The HPTC basolateral uptake of digoxin was inhibited 50% by 10 μM ouabain, suggesting involvement of OATP4C1.

DMD Fast Forward. Published on January 9, 2018 as DOI: 10.1124/dmd.117.075606
This article has not been copyedited and formatted. The final version may differ from this version.

Introduction

The P-glycoprotein (P-gp) IC_{50} Initiative was established to assess inter-laboratory variability in P-gp IC_{50} determinations. The results of this study were published in Bentz et al. (2013) and Ellens et al. (2013). The data showed significant lab-to-lab variability in the reported IC_{50} values, even for labs using the same cell line (for example MDCKII-hMDR1 or Caco-2) and the same inhibitor. This result raised concern about the utility of in vitro data for predicting in vivo digoxin DDI risk (Lee et al., 2014). Despite this variability, decision criteria could be derived by receiver operating characteristic (ROC) analysis, which predicted the risk for a digoxin DDI with a low false negative rate of 12% (Ellens et al., 2013). These papers made recommendations on the most robust way to determine a P-gp IC_{50} value, recommended refined decision criteria and proposed that the decision criteria be specific for the P-gp probe substrate digoxin. These recommendations were accepted by the International Transporter Consortium (Lee et al., 2014).

Based upon previous studies (Acharya et al., 2008; Lumen et al., 2010; Agnani et al., 2011), Bentz et al. (2013) hypothesized that the IC_{50} variability was due to the intrinsic variability in the expression levels of efflux active P-gp and the digoxin basolateral uptake transporter. There are several approaches to analyzing transport across confluent cell monolayers (Zamek-Gliszczynski et al., 2013). In this work, we have used the structural mass action kinetic model (Bentz and Ellens, 2014) for P-gp to analyze a selected subset of data generated by the P-gp IC_{50} Initiative to investigate the reasons for the IC_{50} variability and whether a cell system independent Ki can be extracted from this variable IC_{50} data, as proposed in Lumen at al.

(2013). The selection criteria was focused on choosing data of a higher quality than imposed in Bentz et al. (2013) that could provide unambiguous answers to these questions and serve as the input to in vivo DDI predictions. The data from five labs was selected for this analysis. We also analyzed new data for digoxin transport across primary culture human proximal tubule cells, HPTC, using the same inhibitors (Brown et al., 2008).

The structural mass action kinetic model (Bentz & Ellens, 2014) was developed to obtain elementary kinetic parameters for P-gp mediated transport. Using this kinetic model for P-gp, we previously demonstrated that digoxin transport across MDCKII-hMDR1 and Caco-2 cells cannot be fitted by using only P-gp and digoxin passive permeability across the basolateral membrane (Acharya et al., 2008). The passive permeability alone, independently measured in the presence of GF120918 (Tran et al., 2005), does not allow enough digoxin to enter the cell to permit the experimentally measured amount of digoxin effluxed to the receiver chamber by both P-gp and passive permeability. We have proposed that this is most likely due to a basolateral uptake transporter for digoxin (Acharya et al., 2008; Agnani et al., 2011; Lumen et al., 2013), although this putative transporter remains unidentified. For the purpose of the kinetic analysis presented here and in our previous work, it is not crucial whether this contributor to basolateral uptake transport is due to a basolateral uptake transporter or to "something else". For convenience, we will refer to this contributor as the basolateral digoxin uptake transporter or, occasionally, BT, throughout this manuscript.

Previously, we have fitted the elementary kinetic rate constants of digoxin transport by P-gp

DMD Fast Forward. Published on January 9, 2018 as DOI: 10.1124/dmd.117.075606
This article has not been copyedited and formatted. The final version may differ from this version.

(Agnani et al., 2011; Lumen et al., 2013). In this work, we have used these kinetic rate constants of digoxin, as the probe-substrate, for the fitting of the IC_{50} curves using 8 P-gp inhibitors obtained from the P-gp IC_{50} Initiative to generate values for: (1) the efflux active P-gp concentration (T(0)), (2) the clearance of digoxin by the basolateral uptake transporter (k_B), (3) the inhibitor dissociation rate constant (k_{rQ}) from P-gp, and (4) the inhibitor binding affinity to the digoxin uptake transporter (K_{QB}), as described previously (Lumen et al., 2013). Note that K_{QB} depends upon both uptake transporter surface density and its binding constant to the inhibitor. Thus, for a given inhibitor, the K_{QB} values for an inhibitor across different cell lines cannot be compared in any simple way.

The function of these kinetic parameters are illustrated in Fig, 1, where BT denotes the basolateral digoxin uptake transporter. The figure illustrates that the fifteen P-gp inhibitors used in Bentz et al. (2013) are shown here to also inhibit the digoxin uptake by BT in these cells, so the IC_{50} values are the product of the convolution of the inhibition of both P-gp and BT. This is the primary cause of the P-gp IC_{50} variability reported in Bentz et al. (2013), as shown below.

The k_1 for binding of substrates to P-gp is essentially the same for all compounds used for model validation (Lumen et al., 2013; Meng et al., 2017a), consistent with a large open binding site on P-gp (Li et al., 2014). The inhibitor dissociation constant $Ki = k_{rQ}/k_1$, with respect to the inhibitor concentration in the membrane, so the system independence of k_1 allows Ki to be calculated for each inhibitor from k_{rQ} alone. Relative to the cytosolic concentration, Ki =

DMD Fast Forward. Published on January 9, 2018 as DOI: 10.1124/dmd.117.075606
This article has not been copyedited and formatted. The final version may differ from this version.

$(k_{rQ}/k_1)K_{QPC}$, where K_{QPC} is the partition coefficient of inhibitor Q into a liposome mimic of the cytosolic inner lipid monolayer of these eukaryotic cells (Tran et al., 2005; Lumen et al., 2013).

The fitting of the values for T(0), k_B and K_{QB} and the inhibitor specific values of k_{rQ} for the inhibitors from the five labs used in this work allowed us to simulate IC_{50} curves for "virtual" cell lines with kinetic parameters defined within the ranges of these parameters. This determines how much IC_{50} variability these ranges of these parameters can create. The lab-to-lab variability in transporter expression levels for just these five labs can explain more than 50% of the IC_{50} variability found in the PCA plot in Bentz et al. (2013). This supports the hypothesis that the observed IC_{50} variability in Bentz et al. (2013) was primarily due to lab-to-lab differences in expression levels of P-gp and of the basolateral digoxin uptake transporter, which the kinetic analysis used here can elucidate.

DMD Fast Forward. Published on January 9, 2018 as DOI: 10.1124/dmd.117.075606
This article has not been copyedited and formatted. The final version may differ from this version.

Materials & Methods

Experimental

For the generation of IC_{50} data for P-gp IC_{50} initiative, the methods have been reported in Bentz et al. (2013).

Materials and Methods for HPTC cells.

Cell culture reagents including High-glucose Dulbecco's modified eagles medium (HG-DMEM), Ham's F-12 Nutrient Mixture, Roswell Park Memorial Institute-1640 medium (RPMI), foetal calf serum (FCS), penicillin, streptomycin, L-glutamine, trypsin (with 0.02 % EDTA), and Dulbecco's phosphate-buffered sa (PBS) were obtained from Sigma-Aldrich, UK. SingleQuot kit renal epithelial growth medium supplements and growth factors were purchased from Lonza, Switzerland. Percoll was bought from GE Healthcare, UK, type 2 collagenase from Worthington Biochemicals, USA, and 10X HBSS from Invitrogen, USA. Radiolabelled substrates were sourced from Hartmann Analytics, Germany, and Perkin Elmer, UK. All other chemicals were from Sigma-Aldrich, UK, and were of the highest quality available.

HPTC cell culture

Primary human proximal tubule cells (HPTC) used in this study were isolated from human kidney donors that were not suitable for transplant. Informed consent and ethical approval for the use of human renal tissue for primary culture and drug safety studies approved by the Ethical Review Board of the Tissue Bank supplying the tissue. These kidneys were kept on ice after removal from the body and processed within 18 hours. All cell culture work was

DMD Fast Forward. Published on January 9, 2018 as DOI: 10.1124/dmd.117.075606
This article has not been copyedited and formatted. The final version may differ from this version.

performed in a class II vertical laminar flow hood to ensure sterility. The protocol for human HPTC isolation was adapted from Brown et al. (2008). The procedure was as follows: Under sterile conditions, macroscopically normal tissue was decapsulated and cortex and outer stripe of outer medulla (if present) were dissected, cut into pieces of about 1 mm^3 and digested in collagenase solution (Worthington), final concentration 300 units/mg tissue in RMPI 1640 media. The suspension was shaken vigorously for 2 h at 37°C then passed through a 120μm sieve. The resulting cell suspension was loaded on top of a discontinuous Percoll (Pharmacia) gradient made up in RMPI 1640 media with densities of 1.04 and 1.07 g/ml. After centrifugation at 3000rpm for 25 min in a 4x200ml swing-out rotor, cells from the intersection were carefully aspirated, washed and brought into culture as a mixed population of proximal tubular (PTC) and distal tubular and cortical collecting duct cells (DTC) seeded directly onto 6.5mm 0.4μm pore size polycarbonate Transwell filter supports (Costar) at a density of 50 000 cells/filter.

HPTC transport measurements

Transepithelial flux measurements of digoxin across monolayers of human tubular epithelial cells were measured essentially as previously described (Brown et al., 2008). Cell monolayers grown on permeable filter supports were extensively washed 4x in a modified Krebs' buffer (mmol/l) : NaCl 140; KCl 5.4; $MgSO_4$ 1.2; KH_2PO_4 0.3; NaH_2PO_4 0.3; $CaCl_2$ 2; glucose 5; Hepes 10 buffered to pH 7.4 at 37^0C with Tris base. Filters were then placed in 12-well plastic plates, each well containing 1ml of prewarmed Krebs or Krebs plus inhibitor with a further 0.5ml of identical solution added to the apical chamber. Monolayers were preincubated for 1

DMD Fast Forward. Published on January 9, 2018 as DOI: 10.1124/dmd.117.075606
This article has not been copyedited and formatted. The final version may differ from this version.

hour at 37^0C. Basolateral to apical fluxes of digoxin and mannitol were measured in paired resistance matched monolayers. Monolayers were paired according to their transepithelial resistance, additionally monolayers were excluded if the transepithelial resistance of the monolayer corrected for the resistance of the filter was less than 60 $\Omega.cm^2$. Flux was initiated by adding [^{3}H]-digoxin (1μCi/ml) and [^{14}C] mannitol (0.1μCi/ml) to the basolateral chamber. A 250μl sample was removed from the apical chamber after a 60 min flux period. [^{3}H] or [^{14}C] activity in the samples was determined by liquid scintillation spectrophotometry using a Beckman liquid scintillation counter. At the end of the flux period, the remaining solutions were aspirated off and the filters washed 4x in a 500ml volume of ice-cold Krebs' buffer at pH 7.4 to remove extracellular isotope. The cell monolayers were then excised from the filter insert and the cell associated isotope determined by liquid scintillation counting.

Kinetic fitting for all cells

Unless specifically noted, all calculations, including statistics, were performed using a 64 bit installation of MATLAB Version 7.11 (Release 2010b). Logistic regressions (logistic fits), parameter and standard error estimates were fitted using non-linear least squares regression from MATLAB's statistics toolbox. Standard errors of log(IC_{50}) estimates were calculated as recommended by Lyles et al. (2008). Linear least squares regressions were performed using MATLAB (Press et al. 2007; Quinn and Keough 2002). Analysis of variance (ANOVA) and analysis of covariance (ANCOVA) were calculated via general linear models (Rao 1998; Quinn and Keough 2002). The transport kinetics fittings used a MATLAB program published in Agnani et al. (2011) and the program is freely available.

DMD Fast Forward. Published on January 9, 2018 as DOI: 10.1124/dmd.117.075606
This article has not been copyedited and formatted. The final version may differ from this version.

Calculation of Ki

The binding constant of the inhibitor Q in the plasma membrane to P-gp is defined as $Ki=k_{1Q}/k_{rQ}$, where k_{1Q} is the association rate constant of the inhibitor Q from the membrane to P-gp and k_{rQ} is the dissociation rate constant of the inhibitor from P-gp back into the membrane. Based upon the system independence of k_1, we set $k_{1Q}=k_1$ (Lumen et al., 2013). $Ki=K_{QPC}k_1/k_{rQ}$ is the system independent dissociation constant of the inhibitor relative to the aqueous concentration of the inhibitor in the cytosol. We used a partition coefficient $K_{QPC}=350$ for all inhibitors used in this work, which is the value we measured for quinidine binding to 0.1 μm liposomes composed of a phosphatidylethanolamine/ phosphatidylserine/cholesterol (1:1:1) mol ratio (Lumen et al., 2013). This lipid composition roughly mimics the cytosolic face of the plasma membrane (van Meer et al., 2008). Verapamil had a measured partition coefficient of 650, which would give a Ki roughly half as large (Lumen et al., 2013). None of the other inhibitors have known partition coefficients measured using this system. k_{1Q} has been measured for MDCKII-hMDR1-NKI cells for several P-gp substrates, including quinidine and verapamil, and was found to be well fitted as 1e8 $M^{-1}s^{-1}$ (Agnani et al., 2011; Lumen et al., 2013). The same value has been assumed for the LLC-PK1-hMDR1-NKI cells. However, Meng et al. (2017a) found for Caco-2 cells that k_{1Q} was about 1.7-fold larger. This means that the Ki for an inhibitor with the Caco-2 cells would be 1.7-fold smaller than with MDCKII-hMDR1-NKI cells. Since mammalian plasma membranes appear to be similar with respect to lipid acyl chain composition (van Meer et al., 2008), P-gp's elementary rate constants should not depend strongly on which plasma membrane it inhabits, which appears to be the case.

DMD Fast Forward. Published on January 9, 2018 as DOI: 10.1124/dmd.117.075606
This article has not been copyedited and formatted. The final version may differ from this version.

Unstirred water layer.

There has been renewed interest in the unstirred water layer (UWL) enveloping the plasma membrane as a kinetic factor in total substrate permeation (Ghosh et al.,2014; Shibayama et al., 2015). The UWL is important when total transport is measured. Our kinetic model avoids this complication because the UWL contribution to transport is isolated to the passive permeability component, measured in the presence of GF120918 (Tran et al., 2005). This assumes that 2μM GF120918 does not significantly affect the UWL, which is reasonable. This allows us to measure specifically the kinetics of P-gp and BT transport and inhibition.

DMD Fast Forward. Published on January 9, 2018 as DOI: 10.1124/dmd.117.075606
This article has not been copyedited and formatted. The final version may differ from this version.

Results

Acharya et al. (2008) and Lumen et al. (2013) previously showed that a basolateral digoxin uptake transporter was required in two of the three overexpressing cell lines used here. So the kinetic model used here has this uptake transporter incorporated (Fig 1). If a data set did not kinetically require a basolateral digoxin uptake transporter, the value of its kinetic parameter would be zero.

The parameters required to fit the IC_{50} curves for inhibition of probe-substrate transport in this model are:

1) T(0) (M, mols of P-gp per L of acyl chains in the bilayer, Tran et al. (2005)) is the initial efflux active concentration of P-gp prior to drug binding, which depends strongly on the microvilli morphology (Meng et al., 2017b). We fit the concentration of P-gp in the apical membrane needed to efflux the digoxin/probe substrate concentration into the apical chamber over time, which is the efflux active concentration of P-gp prior to drug binding. Efflux from the rest of the P-gp in the apical membrane is reabsorbed back into the same or adjacent microvilli prior to reaching the apical chamber, in a futile cycle.
2) k_B (s^{-1}) measures the digoxin clearance rate constant across the basolateral membrane due to the basolateral digoxin uptake transporter (BT). The identity of BT is not known nor is its surface density.
3) k_{rQ} (s^{-1}) is the elementary dissociation rate constant of the inhibitor (Q) from P-gp back into the apical membrane. A smaller value of k_{rQ} corresponds to a stronger binding of the inhibitor to P-gp.

DMD Fast Forward. Published on January 9, 2018 as DOI: 10.1124/dmd.117.075606
This article has not been copyedited and formatted. The final version may differ from this version.

4) K_{QB} (M^{-1}) is the binding affinity of the inhibitor to the BT from the basolateral compartment. K_{QB} is a convolution of the surface density of BT and the binding constant for the inhibitor to BT. The term affinity, rather than binding constant, is used since the identity and the value of the surface density of BT is unknown.

These four kinetic parameters are necessary and sufficient to fit all of the IC_{50} curves analyzed in this work, as shown below. We can calculate the inhibitor dissociation constant, Ki, from P-gp into the membrane from the inhibitor k_{rQ} and k_1 (see Materials and Methods). We have found previously that k_1 is essentially the same for all of the drugs we have studied in both MDCKII-hMDR1-NKI and Caco-2 cells (Agnani et al., 2011, Lumen et al., 2013; Meng et al., 2017a). %CV is the coefficient of variation as a percentage between the data and the fitted data points. It gives a quantitative rank order for the quality of the fit to the data.

Criteria for choosing data sets to fit. In Bentz et al. (2013) and Ellens et al. (2013), the sole qualifying criteria for a data set was that the t-statistic $t_{\alpha\beta}>3$, which yields a 95% confidence that measured IC_{50} is within 4-fold of the true IC_{50} (O'Connor et al., 2014). The choice of data sets from Bentz et al., (2013) used for fitting the above described 4 parameters from IC_{50} curves in this work was based on more rigorous criteria derived from preliminary fittings focused on obtaining unambiguous data fits. Here, we have replaced $t_{\alpha\beta}$ with t_β defined in O'Conner et al. (2014), which is simpler to calculate and a nearly perfect approximation for $t_{\alpha\beta}$.

DMD Fast Forward. Published on January 9, 2018 as DOI: 10.1124/dmd.117.075606
This article has not been copyedited and formatted. The final version may differ from this version.

At least 4 inhibitors out of the 8 tested by the lab must satisfy the following two criteria:

1) t_β>5, which implies a 95% confidence that fitted IC_{50} is within 3-fold of the true IC_{50} (O'Connor et al., 2014).
2) Lab average negative control (NC, no inhibitor) and positive control (PC, maximum inhibition) must both have CV<20%. This is crucial because two of the four essential kinetic parameters, i.e. T(0) and k_B, are specific to the cells and cannot depend on the inhibitor. Thus, two crucial parts of the IC_{50} curve depend on the lab average value NC and PC for the cells grown in that lab. Variations of NC and/or PC across inhibitors, which was more common for the NC data in Bentz et al. (2013), suggests that the cells in that lab varied in transporter expression levels from experiment to experiment, so the IC_{50} fits would vary. Note that the value of NC will depend on the initial concentration of digoxin used, which varied widely across labs, ~100 fold, see Supplemental Data Table S1 for examples or Bentz et al. (2013).

Table 1 shows those labs that matched the quality criteria in terms of the lab average NC and PC controls for 4 or more inhibitors and only these inhibitor data were fitted in this work. The average of NC and of PC, their standard deviations and coefficients of variation are shown. It was important to have at least one LLC-PK1-hMDR1 lab in this analysis, which determined the maximum NC %CV allowed. The inhibitors left out for a lab did not show any consistent estimates for kinetic parameters.

DMD Fast Forward. Published on January 9, 2018 as DOI: 10.1124/dmd.117.075606
This article has not been copyedited and formatted. The final version may differ from this version.

Table 2 shows the fitted values for the parameters that characterized this IC_{50} data. The IC_{50}, t_β, lab average t_β and β are shown for each chosen lab and the chosen inhibitors for that lab.

Fitting protocol. The values for T(0) and k_B for a particular cell system were fixed first by simultaneously fitting all qualified IC_{50} data sets from the lab in question, as described previously, using an exhaustive fitting approach (Agnani et al., 2011; Lumen et al., 2013). Thus, for each lab there is one consensus value for T(0) and for k_B, both of which are only cell dependent, not inhibitor dependent. The second round of fits for each lab used these fixed values for T(0) and k_B for each lab, but refitted the values for k_{rQ} and K_{QB} for each inhibitor. Since there were 4-8 qualified inhibitors for each chosen lab and five chosen labs, several independent k_{rQ} values were fitted, at least twice (mibefradil) and up to five times (ranolazine). The other inhibitors had 3-4 independent fits for k_{rQ}.

Across all the labs, the independent k_{rQ} values for each inhibitor were relatively clustered, indicating that this parameter appeared essentially cell independent. These individual k_{rQ} values are shown in Supplemental Data Table S70. Table 3 shows the average, the low and high estimates for krQ at the 95% confidence level and the statistically significant 1 digit consensus value for each k_{rQ}, for all the overexpressing cell lines, i.e. Caco-2, MDCKII-hMDR1-NKI and LLC-PK1-hMDR1-NKI.

DMD Fast Forward. Published on January 9, 2018 as DOI: 10.1124/dmd.117.075606
This article has not been copyedited and formatted. The final version may differ from this version.

A complete refit of the data was done using the fixed values of the consensus k_{rQ} values for each inhibitor. Using this consensus k_{rQ}, rather than the independently fit values, made little difference in the goodness of fit, as measured by the coefficient of variation for the fit relative to the data. This was because the re-fits allowed T(0), k_B and K_{QB} for each lab to adjust slightly to having the fixed k_{rQ} value. As shown in more detail in Agnani et al. (2011), the global minima for these multi-parameter kinetic fits lie within shallow "multi-dimensional valleys", which makes mass action kinetic and evolutionary sense. As shown below, these same consensus k_{rQ} values were used to fit the IC_{50} data curve for the primary culture HPTC. This suggests strongly that the elementary rate constant k_{rQ} is essentially system independent.

Table 4 shows the final fits of the qualified data, together with the CV of the fit and the Ki. Of course, when the true partition coefficients K_{QPC} of the inhibitors are measured the Ki values for each inhibitor may change somewhat from the values shown in Table 4.

Bentz et al. (2013) also had data from 7 other P-gp inhibitors used in the P-gp IC50 Initiative that was lower quality than the 8 inhibitors in Tables 3 and 4 with respect to t_β values, as explained there. Data from selected labs, $t_\beta > 3$ for these inhibitors, for six of these P-gp inhibitors (felodipine, nifedipine, nitrendipine, sertraline, telmisartan and troglitazone) were fitted using their consensus k_{rQ} values. Initial fittings of these data showed that using their consensus values for each of these inhibitors, as opposed to individual fits, made no significant difference to the quality of the fits. All fits and the fitted kinetic parameters are shown in

DMD Fast Forward. Published on January 9, 2018 as DOI: 10.1124/dmd.117.075606
This article has not been copyedited and formatted. The final version may differ from this version.

Supplemental Data Tables S1-S3 and Supplemental Data Figures S1-S24. All amiodarone data from Bentz et al. (2013) was too poor to fit for unknown reasons.

All 4 kinetic parameters are required to fit the IC_{50} curves. We performed fitting studies to test whether all of these fitted parameters are necessary and sufficient to fit the data,. The fit (line) for carvedilol inhibition of digoxin transport across a confluent cell monolayer of MDCKII-hMDR1-NKI cells is shown in Figures 2A-C and Figures 3A-B. Figure 2A shows the fit to the carvedilol IC_{50} curve for digoxin transport with a model that only contained P-gp and not the basolateral digoxin uptake transporter, so k_B=0 (Figures 2A-C). k_{rQ} was fixed at the value shown in Table 4. This model clearly does not fit the data, especially at the NC. Changing the P-gp efflux active concentration 10-fold from $1e^{-3}$M (Figure 2A) to $1e^{-2}$M (Figure 2B) or 1/10-fold to $1e^{-4}$M (Figure 2C) did not improve the fit of digoxin transport kinetics. So, P-gp efflux active concentration does not significantly affect the fit to NC.

When the basolateral digoxin uptake transporter was added to the model, or some other mechanism of enhanced digoxin influx through the basolateral membrane, the predicted curve for carvedilol inhibition of digoxin transport kinetics fits much better. Figure 3A shows that the negative control (NC), where carvedilol concentration goes to zero, can now be fitted. That is k_B's primary contribution to these fits, i.e. allowing enough digoxin uptake into the cells for the measured amount of P-gp mediated efflux to occur in the absence of inhibitor. At higher inhibitor concentrations, the fit "floats" above the data. Accounting for the inhibitor binding

DMD Fast Forward. Published on January 9, 2018 as DOI: 10.1124/dmd.117.075606
This article has not been copyedited and formatted. The final version may differ from this version.

affinity to the basolateral digoxin uptake transporter (BT), K_{QB}, so that the inhibitor inhibits both P-gp and BT, allows a good fit at the PC, as shown in Figure 3B

Carvedilol required all four kinetic parameters in order to fit the digoxin inhibition IC_{50} curve. The same was true for the other inhibitors. All final fits are shown in Supplemental Data Table S4 and Supplemental Data Figures S25-S53.

PCA analysis of IC_{50} variability. We examined the variability of T(0), k_B and K_{QB} measured here as potential causes for the variability in IC_{50} values across the chosen 5 labs from the P-gp IC_{50} initiative and the HPTC. k_{rQ} was fixed at the consensus value for each inhibitor, Table 4, and does not contribute significant variability in this calculation. Fig. 4 shows the PCA plot for IC_{50} data simulated for virtual cell lines based on the ranges of kinetic parameters (T(0), k_B, k_{rQ} and K_{QB}), shown in Tables 4 and 5B. PCA axis 1 is essentially the average of $\log_{10}\{IC_{50}$ (M)$\}$ over all qualified inhibitors within each lab, as was the case in Bentz et al. (2013). The amplitude of the second axis of this PCA is very small since in the simulation the only remaining variabilities are the fixed k_{rQ} values for each inhibitor, since no simulated experimental error was added.

Fitting transport kinetics for primary cell culture monolayers of human proximal tubule cells, HPTC. The inhibition of digoxin transport through confluent cell monolayers composed of primary human proximal tubule cells (HPTC) using the same inhibitors were fitted by the

DMD Fast Forward. Published on January 9, 2018 as DOI: 10.1124/dmd.117.075606
This article has not been copyedited and formatted. The final version may differ from this version.

kinetic analysis as well, using the fixed consensus k_{rQ} values in Table 3. Figure 5 shows the data average (empty squares, n=3), its standard deviation (bars, n=3) and the best fit (line) for ketoconazole inhibition of digoxin transport across a confluent monolayer of HPTC cells. When a basolateral digoxin uptake transporter, BT, is not incorporated, the fit was poor (Figure 5A, k_B=0), as digoxin transport is not fitted at low inhibitor concentrations. When BT is added to the model without binding/inhibition by the inhibitor, K_{QB}=0, digoxin is fitted at the smaller inhibitor concentrations, i.e. the NC can be fitted. There is enough BT mediated uptake of digoxin into the cells for the appropriate level of P-gp mediated efflux to occur (Figure 5B). However, digoxin transport inhibition at the higher inhibitor concentrations near PC is not fitted well. When inhibition of BT is accounted for by K_{QB}, then the observed data is fit well by the model (Figure 5C). K_{QB} for ketoconazole causes about a 50% inhibition of digoxin transport. The HPTC cells, with smaller efflux active P-gp concentrations, show a much greater role of inhibitor binding to BT than in the P-gp over-expressing cell lines, shown in Fig. 4A&B.

The kinetic parameters of inhibition of digoxin transport conducted in HPTC are shown in Table 5. Table 5A shows the IC_{50}, t_β and the Hill coefficient or slope factor β for these data, which came from 10 out of a total of 13 kidneys evaluated for inhibition. This data was not filtered through the same quality criteria as used for the overexpressing cells, but instead just used t_β>3, except for ranolazine, where t_β=2.4 (Table 5A). This ranolazine data was included because it was the only data for this inhibitor for the HPTC cells. The IC_{50} values were typically lower than the values observed with the overexpressing cells, mostly due to the lower efflux active P-gp concentration in these primary cells, as explained in Lumen et al., (2010).

DMD Fast Forward. Published on January 9, 2018 as DOI: 10.1124/dmd.117.075606
This article has not been copyedited and formatted. The final version may differ from this version.

The slope factor β was also smaller than those for the overexpressing cells. Although estimated β values for the HPTC include a few values near or greater than 1, the mean of the estimates is approximately 0.71 (Std error = 0.062), and the 95% confidence interval for the values (0.58-0.85) does not include 1.0. Thus the HPTC cells have a lower average $\beta<1$ estimate than the cultured cells. A hypothesis for this behavior is given in the discussion.

Table 5B shows this final fitting of the qualified data along with the CV of the fit. These cells have roughly 10 to 100-fold less efflux active P-gp than the over-expressing cell lines used in the P-gp IC_{50} Initiative and the fraction of total transport due to the basolateral digoxin uptake transporter is greater (Fig 5B), thus the impact of inhibition of BT by the inhibitors on the IC_{50} is greater. In addition, the consensus values for k_{rQ}, Table 4, worked well with these HPTC cells, expanding the system independence of this elementary kinetic parameter. K_{QB} values were similar to those shown in Table 4 for the over-expressing cells. We note that the kinetic parameters can vary significantly between different kidney samples for the same inhibitor. For example, the IC_{50}/Ki ratio with carvedilol varied 25-fold between two kidney preps, which was entirely due to the variability in the IC_{50} values, Table 5A. Interestingly, the IC_{50} variability is largely due to the variability of k_B and K_{QB}, not the efflux active P-gp. The same is true for the ketoconazole, quinidine and verapamil data. This highlights the importance of the basolateral digoxin uptake transporter and its inhibition in any in vivo DDI predictions. All fits are shown in Supplemental Data Table S5 and Supplemental Data Figures S54-S67.

DMD Fast Forward. Published on January 9, 2018 as DOI: 10.1124/dmd.117.075606
This article has not been copyedited and formatted. The final version may differ from this version.

Potential Involvement of OATP4C1 in basolateral uptake of digoxin in HPTC monolayers.

Fig. 6A shows that digoxin uptake into the HPTC cells was 50% inhibited with about 10 μM of the OATP4C1 inhibitor ouabain, with a roughly linear inhibition curve, i.e. not a sigmoidal curve as observed for the other inhibitors. Digoxin uptake into the cells is significantly greater in the presence of GF120918, where P-gp is fully inhibited, than in the control cells, where P-gp is fully active. Fig. 6B shows that digoxin transport across the HPTC cells was only about 20-25% inhibited with 30 μM of the OATP4C1 inhibitor ouabain, also with a roughly linear, not sigmoidal, inhibition curve.

The inhibition of digoxin uptake into and transport through the HPTC cells by T3, 0-30 μM, was only somewhat reduced at and above 10 μM T3. This was similar to the uptake results in Mikkaichi et al., (2004). The data for T3 inhibition of digoxin uptake and digoxin transport across the HPTC confluent cell monolayer is shown in the Supplemental Table S6 and Supplemental Data Figures S68-S69.

DMD Fast Forward. Published on January 9, 2018 as DOI: 10.1124/dmd.117.075606
This article has not been copyedited and formatted. The final version may differ from this version.

Discussion

We have used the structural mass action kinetic model for digoxin transport through a confluent monolayer of P-gp overexpressing polarized cells to (1) derive system independent P-gp inhibitor dissociation rate constants for calculation of system-independent Ki's and (2) further explore potential mechanistic factors that contribute to the variability in IC_{50} values observed in the P-gp IC_{50} Initiative. A subset of the IC_{50} data generated by the P-gp IC_{50} Initiative participants was selected for this work, based on data quality criteria described in the results section. We used the data from two Caco-2 labs, two MDCKII-hMDR1-NKI labs and one LLC-PK1-hMDR1-NKI lab. Newly generated data for digoxin transport inhibition across primary human proximal tubule cell monolayers, HPTC, was also included in this analysis using the same inhibitors.

The structural mass action kinetics model for P-gp-mediated transport has been extensively validated as a diagnostic tool to determine the efflux active P-gp concentration on several cell lines and to identify kinetically required uptake transporters in the transport of P-gp substrates across confluent cell monolayers (Acharya et al., 2008; Agnani et al., 2011; Lumen et al., 2013; Bentz and Ellens, 2014; Meng et al., 2017a,b). The IC_{50} curve of digoxin transport across confluent cell monolayers was analyzed using this model. The kinetic parameters needed to fit the data shown in Figures 2, 3 and 5 were the efflux active P-gp concentration (T(0)), uptake clearance of digoxin by the basolateral digoxin uptake transporter (k_B), the dissociation constant of the inhibitor from P-gp (k_{rQ}) and the affinity of the inhibitor to the basolateral uptake transporter (K_{QB}). In addition, to execute these IC_{50} fits, the kinetic parameters k_1, k_r and k_2 for

the probe-substrate, digoxin in this case, were required and were obtained from Lumen et al. (2013). As shown in the results section, these kinetic parameters were necessary and sufficient to fit IC_{50} data in P-gp overexpressing cell lines and the primary culture HPTC to within experimental error. Importantly, the k_{rQ} (and therefore the calculated Ki) for a given inhibitor was found to be system-independent over the cell lines used here.

Our kinetic analysis found that all 8 P-gp inhibitors in all cell lines were kinetically required to bind to and inhibit the digoxin basolateral uptake transporter, Tables 4 and 5B. This means that any IC_{50} value reported in Bentz et al. (2013) could be due to inhibitor binding to P-gp, or inhibitor binding to the digoxin basolateral uptake transporter, or inhibitor binding to both, so that the measured IC_{50} was a complex convolution of both binding events. The calculated IC_{50} values for the basolateral digoxin uptake transporter and for P-gp are sufficiently similar that current commercial IC_{50} fitting software would be hard pressed to unambiguously deconvolve these two intertwined contributions to the IC_{50} data.

In Bentz et al. (2013), a Principal Component Analysis, PCA, showed that the largest variability was due essentially to the differences in the average $\log_{10}\{IC_{50}(M)\}$ over the inhibitors between the different labs, which was PCA axis 1 in Figure 7 of that paper. This result raised concerns about the utility of in vitro data for predicting in vivo digoxin DDI risk (Lee et al., 2014). Here, IC_{50} curves were simulated using all combinations of efflux active P-gp and the kinetic parameters from within the ranges shown in Tables 4 and 5B. Figure 4 shows the PCA analysis

DMD Fast Forward. Published on January 9, 2018 as DOI: 10.1124/dmd.117.075606
This article has not been copyedited and formatted. The final version may differ from this version.

on these simulated curves, with no added random error in the data. PCA axis 1 here was essentially the average of the $\log_{10}\{IC_{50}\}$, same as in Bentz et al. (2013), covers more than 50% of the range of axis 1 found in Bentz et al. (2013). Thus, most of the IC_{50} variability found in Bentz et al. (2013) can be explained by the cells in each lab, regardless of origin, expressing different efflux active P-gp concentrations and of basolateral digoxin uptake transporter expression levels. The remaining variability in Bentz et al. (2013) is most likely to be due to experimental error, inclusion of data from labs with $t_\beta \leq 5$ containing NC and PC variations and, finally, the convolution of P-gp and BT inhibition within the fitting of the inhibition data to a single logistic IC_{50} curve.

The kinetic need for a basolateral uptake transporter to explain transport of P-gp substrates across a P-gp expressing polarized cell monolayer is not unique to digoxin. We have found that both loperamide and vinblastine kinetically require a basolateral uptake transporter in MDCKII-hMDR1-NKI, MDCKII-hMDR1-NIH and Caco-2 cells (Acharya et al., 2008; Lumen et al., 2013). If a P-gp substrate uses a BT, then how can that be shown? Lumen et al. (2013) showed by simulations that a basolateral uptake transporter could be observed when the passive permeability without transporters was less than about 320 nm/s. When this is so, the deficit of probe-substrate reaching the apical chamber is because not enough probe-substrate is entering the cell from the basolateral membrane to reach P-gp. When the passive permeability is larger than this threshold, then that deficit become insignificant compared with the total probe-substrate transport. This passive permeability threshold matched our findings that digoxin, loperamide and vinblastine kinetically required the basolateral uptake transporter, while amprenavir, ketoconazole, quinidine and verapamil did not (Lumen et al., 2013). Lumen et al.

(2013) also showed for Caco-2 and MDCKII-hMDR1-NIH cells that ketoconazole and verapamil inhibited digoxin transport through the basolateral digoxin uptake transporter. Thus, not kinetically requiring the basolateral uptake transporter does not mean that there is no interaction with that transporter.

The identity of the basolateral digoxin uptake transporter in all these cells remains unknown. The possibility of a digoxin transporter in Caco-2 cells has been reported (Lowes et al., 2003). Taub et al. (2011) showed that digoxin is not a substrate of OATPs 1A2, 1B1, 1B3 and 2B1, but was a substrate of a sodium dependent transporter endogenously expressed in HEK293 cells. The kinetic modeling of the basolateral digoxin uptake transporter in MDCKII-hMDR1-NKI cells by Agnani et al. (2011) found that it was better fitted as a bidirectional passive transporter as compared to an active digoxin importer.

In Mikkaichi et al. (2004), MDCK cells, whose "endogenous expression of OATP4C1 in MDCK cell was not detected", were transfected with human OATP4C1. Confluent monolayers of these cells were used to examine digoxin uptake into and the digoxin flux across these monolayers as a function of the OATP4C1 inhibitors ouabain and T3. Their figure 5A showed that digoxin uptake into the cells was logistically inhibited to about 50% at about 0.4 μM ouabain. T3 showed no significant reduction of digoxin uptake at 0 to 30 μM (Mikkaichi et al., 2004). In our study of ouabain, digoxin uptake into HPTC cells was inhibited essentially linearly, not logistically, at ouabain concentrations between 0.1 and 30 μM, with an inhibition of about 50% at 10 μM ouabain. OATP4C1 might be involved in the basolateral

DMD Fast Forward. Published on January 9, 2018 as DOI: 10.1124/dmd.117.075606
This article has not been copyedited and formatted. The final version may differ from this version.

uptake of digoxin in this system. The fact that ouabain's inhibition curve of basolateral uptake in the HPTC cells is basically linear, rather than logistical, suggests that there could be a second basolateral digoxin uptake transporter involved in this complex system of primary isolated cells. As to whether or not ouabain affects P-gp transport has not been reported. It has been reported that ouabain had no effect on P-gp ATPase activity (Shapiro & Ling, 1994). Brouillard et al. (2001) reported that ouabain induced P-gp expression, but that is unlikely to effect the immediate inhibition of digoxin transport by P-gp in this work.

β in the IC_{50} logistic or Hill equation is called the slope factor, because it is fitted to the slope of the IC_{50} curve at the IC_{50} (O'Connor et al., 2014). $\beta > 1$ is also historically considered an indicator of cooperativity in substrate binding (Hill, 1913). The slope factor is used in all commercial IC_{50} fitting packages, so it is part of every published IC_{50} fit, yet it is rarely reported or discussed. While there have been many studies on the cooperativity of substrates binding to P-gp based upon the ATPase activity, there is no clear consensus, as reviewed in Lumen et al. (2011). The structural mass action kinetic model used here has only a single substrate binding site per P-gp, so there cannot be cooperativity in the model. Tran et al. (2005) showed the fit to data was sensitive only to the nmol transported to the apical chamber, not on how many sites were effluxing per P-gp. With twice as many sites per P-gp, the fitted P-gp efflux rate constant, k_2, was just half of the fitted value with a single binding site.

In Bentz et al (2013), the β values averaged near 1, but there was a wide range between minimum and maximum values, Table 6 here. For the higher quality data sets used in this

work, with roughly 4-fold fewer fitted data points, the ranges were significantly smaller and better centered on β=1 (Table 6). These data suggest that the range of fitted β values has little, if anything, to do with the number of cooperative binding sites in P-gp. The average slope factor β in HPTC is significantly less than 1 (Table 5A). The simplest hypothesis that explains this difference from the overexpressing cells is that the HPTC express two different basolateral digoxin uptake transporters with similar IC_{50} values. The interaction of their respective IC_{50} values would reduce the slope of the inhibition curve at the IC_{50}, i.e. $\beta<1$. This speculation is consistent with the linear, rather than logistical, inhibition curve of digoxin uptake by ouabain in HPTC (Figure 6A).

P-gp vesicles have been suggested as a simpler and possibly superior system for determination of P-gp IC_{50} values. However, the vesicle IC_{50} data generated by the P-gp IC_{50} initiative using N-methyl-quinidine as probe substrate was also very variable from lab-to lab (Bentz et al., 2013). Currently these vesicles are typically derived from mammalian or insect cell membranes, which contain a variety of endogenous transporters, just like the polarized cell systems, and could vary from lab-to-lab in expression levels of P-gp and other transporters.

Conclusions.

We have previously demonstrated that the elementary rate constants for P-gp-mediated transport (k_1, k_2 and k_r) obtained using our mass action kinetics model are essentially the same in both MDCKII-hMDR1-NKI and Caco-2 cells for amprenavir, quinidine, loperamide and

digoxin, i.e. they are essentially system independent. Here we have shown that k_{rQ} is also system independent for the cells used, including with the primary cell culture HPTC. We can therefore calculate a system independent P-gp specific Ki using highly variable IC_{50} data, even when another transporter or two are involved in transport of the probe substrate.

The criteria for selecting qualified data sets here were based upon having IC_{50} data curves from multiple labs for multiple inhibitors. These criteria can be adapted to single lead compound. It requires at least 3 completely independent IC_{50} data curves for the inhibitor of interest. For these curves, the average of the negative and of the positive controls must each have a %CV<20%. Each of the IC_{50} curves must have $t_{\beta}>5$. It is best to simultaneously fit all data curves to obtain the consensus elementary rate constants, but they could be fitted separately and then averaged as was done for k_{rQ} in Table 3. The k_1, k_r and k_2 for the probe-substrate used must be known and are already available for amprenavir, digoxin, ketoconazole, loperamide, quinidine, verapamil and vinblastine (Lumen et al., 2013).

For the purpose of the kinetic analysis presented here, and in our previous work, it is not crucial whether the basolateral uptake clearance of the probe-substrate is due to a basolateral uptake transporter or to “something else”. However, a proposed “non-transporter” mechanism for this enhanced basolateral membrane permeability of the probe-substrate must have a plausible mechanism for the inhibition of this enhanced permeability as a function of increased inhibitor concentration to account for the effect of K_{QB} on the fit.

DMD Fast Forward. Published on January 9, 2018 as DOI: 10.1124/dmd.117.075606
This article has not been copyedited and formatted. The final version may differ from this version.

The final point is how to use the structural mass action kinetic model to obtain in vivo DDI predictions. Basically, our Matlab program can replace the linearized Michaelis-Menten programs within existing in vivo PBPK computer programs. At present, this appears most easily accomplished within the Matlab SimBiology framework, which has access to other required Matlab programs. Our analysis provides the necessary elementary rate constants from in vitro experiments, all of which appear system independent. While there are good biophysical reasons for expecting the elementary rate constants for P-gp transport to be essentially system independent, that is not the case for the microvilli morphology dependent efflux active P-gp and the, as yet, unidentified basolateral and apical uptake transporter(s). The need for in vivo data fitting is seen clearly here in the HPTC data, with large kidney-to-kidney variability in IC_{50} values for the same inhibitor that was due mostly to variability in the basolateral digoxin uptake transporter clearance and inhibition, not in P-gp activity. So using the in vitro derived elementary rate constants, the in vivo PBPK model can fit in vivo data for the efflux active P-gp, the basolateral and apical uptake transporter clearances and the inhibitor affinities for these uptake transporters. These fits would allow the formulation of in vivo DDI predictions.

DMD Fast Forward. Published on January 9, 2018 as DOI: 10.1124/dmd.117.075606
This article has not been copyedited and formatted. The final version may differ from this version.

Footnotes

A. Chaudhry, G. Chung and A. Lynn contributed equally

DMD Fast Forward. Published on January 9, 2018 as DOI: 10.1124/dmd.117.075606
This article has not been copyedited and formatted. The final version may differ from this version.

Authorship Contributions

Participated in research design: Brown, O'Connor, Lee, Ellens and Bentz

Conducted experiments: Chung

Contributed new reagents or analytic tools: O'Connor and Bentz

Performed data analysis: Chaudhry, Chung, Lynn, Yalvigi, Brown, O'Connor, Lee, Ellens and Bentz

Wrote or contributed to the writing of the manuscript: Chung, Brown, O'Connor, Lee, Ellens and Bentz

References

Acharya P, O'Connor MP, Polli JW, Ayrton A, Ellens H and Bentz J (2008). Kinetic identification of membrane transporters that assist P-glycoprotein-mediated transport of digoxin and loperamide through a confluent monolayer of MDCKII-hMDR1 cells. *Drug Metab Dispos* **36**: 452-460.

Agarwal S, Arya V, and Zhang L (2012). Review of P-gp inhibition data in recently approved New Drug Applications: utility of the proposed $[I_1]/IC_{50}$ and $[I_2]/IC_{50}$ criteria in the P-gp decision tree. *J Clin Pharmacol* doi:10.1177/0091270011436344.

Agnani D, Acharya P, Martinez E, Tran TT, Abraham F, Tobin F and Bentz J (2011). Fitting the elementary rate constants of the P-gp transporter network in the hMDR1-MDCK confluent cell monolayer using a particle swarm algorithm. *PLoS ONE* **6:** 10, e25086

Bentz J and Ellens H (2014). A Structural Model for the Mass Action Kinetic Analysis of P-gp Mediated Transport Through Confluent Cell Monolayers. In: Enzyme Kinetics in Drug Metabolism – Fundamentals and Applications, Chapter 14, pp.289-316. Eds. S. Nagar, U.A. Argikar, and D. J. Tweedie. Humana Press, 2014.

Bentz, J, O'Connor MP, Bednarczyk D, Coleman J, Lee C, Palm J, Pak YA, Perloff ES, Reyner E, Balimane P, Brännström M, Chu X, Funk C, Guo A, Hanna I, Herédi-Szabó K, Hillgren K, Li L, E. Hollnack-Pusch E, Jamei M, Lin X, Mason AK, Neuhoff S, Patel A, Podila L, Plise E, Rajaraman GG, Salphati L, Sands E, Taub ME, Taur J, Weitz D, Wortelboer HM, Xia CQ, Xiao G, Yabut J, Yamagata T, Zhang L and Ellens H (2013). Variability in P-glycoprotein inhibitory potency (IC_{50}) using various in vitro experimental systems: implications for universal digoxin DDI risk assessment decision criteria. *Drug Metab Dispos* **41**: 1347-1366.

Brouillard F, Tondelier D, Edelman A & Baudouin-Legros M. (2001). Drug resistance induced by ouabain via the stimulation of MDR1 gene expression in human carcinomatous pulmonary cells. Cancer Res. 2001 Feb 15;61(4):1693-8.

Brown CD, Sayer R, Windass AS, Haslam IS, De Broe ME, D'Haese PC, Verhulst A. (2008). Characterisation of human tubular cell monolayers as a model of proximal tubular xenobiotic handling. *Toxicol Appl Pharmacol*., 233(3):428-38. doi: 10.1016/j.taap.2008.09.018. Epub 2008 Oct 1.

Cook JA, Feng B, Fenner KS, Kempshall S, Liu R, Rotter C, Smith DA, Troutman MD, Ullah M and Lee CA (2010). Refining the in vitro and in vivo critical parameters for p-glycoprotein,

I/IC50 and I2/IC50, that allow for the exclusion of drug candidates from clinical digoxin interaction studies. *Molecular Pharmaceutics* **7**:398-411

Ellens H, Deng S, Coleman J, Bentz J, Taub ME, Ragueneau-Majlessi I, Chung SP, Herédi-Szabó K, Neuhoff S, Palm J, Balimane P, Zhang L, Jamei M, Hanna I, O'Connor M, Bednarczyk D, Forsgard M, Chu X, Funk C, Guo A, Hillgren KM, Li L, Pak AY, Perloff ES, Rajaraman G, Salphati L, Taur JS, Weitz D, Wortelboer HM, Xia CQ, Xiao G, Yamagata T and Lee CA (2013). Application of receiver operating characteristic analysis to refine the prediction of potential digoxin drug interactions. *Drug Metab Dispos*. (41):1367-74. doi: 10.1124/dmd.112.050542.

Fenner KS, Troutman MD, Kempshall S, Cook JA, Ware JA, Smith DA and Lee CA (2009). Drug-drug interactions mediated through P-glycoprotein: clinical relevance and in vitro-in vivo correlation using digoxin as a probe drug. *Clin Pharm Ther* **85**:173-181

Ghosh A, Scott DO and Maurer TS (2014). Towards a unified model of passive drug permeation I: origins of the unstirred water layer with applications to ionic permeation. *Eur J Pharm Sci* 52:109-24. doi: 10.1016/j.ejps.2013.10.004. Epub 2013 Nov 7.

Hill AV (1913). The Combinations of Haemoglobin with Oxygen and with Carbon Monoxide. I. Biochem J. 7(5):471-80.

Jones HM, Chen Y, Gibson C, Heimbach T, Parrott N, Peters SA, Snoeys J, Upreti VV, Zheng M, and Hall SD (2015). Physiologically based pharmacokinetic modeling in drug discovery and development: a pharmaceutical industry perspective. *Clin Pharmacol Ther* **97:**247-262.

Lee CA, Kalvass JC, Galetin A and Zamek-Gliszczynski MJ (2014). ITC commentary on the prediction of digoxin clinical drug-drug interactions from in vitro transporter assays. Clin Pharmacol Ther. 96(3):298-301. doi: 10.1038/clpt.2014.94.

Li J, Jaimes KF, Aller SG (2014). Refined structures of mouse P-glycoprotein. Protein Sci. Jan;23(1):34-46. doi: 10.1002/pro.2387. Epub 2013 Nov 15.

Loo TW and Clarke DM (2000). Drug-stimulated ATPase activity of human P-glycoprotein is blocked by disulfide cross-linking between the nucleotide-binding sites. *J Biol Chem* **275:**19435-19438.

Lowes S, Cavet ME and Simmons N (2003). Evidence for a non-MDR1 component in digoxin secretion by human intestinal Caco-2 epithelial layers. *Eur J Pharmacol* **458** 49–56.

Lumen AA, Acharya P, Polli JW, Ayrton A, Ellens H and Bentz J (2010). If the K_I is defined by the free energy of binding to P-glycoprotein, which kinetic parameters define the IC_{50} for the Madin-Darby Canine Kidney II cell line overexpressing human Multidrug Resistance 1 confluent cell monolayer? *Drug Metab Dispos* **38**: 260-269.

Lumen AA (2011). Mechanistic Understanding of P-gp Mediated Transport and Inhibition Kinetics across a Confluent Monolayer of MDCKII-hMDR1 cells using a Mass Action Kinetic model. *Ph.D Dissertation, Drexel University.*

Lumen AA, Li L, Li J, Ahmed Z, Meng Z, Owen A, Ellens H, Hidalgo IJ, and Bentz J (2013). Transport inhibition of digoxin using several common P-gp expressing cell lines is not necessarily reporting only on inhibitor binding to P-gp. *PLoS One* **8:**e69394.

Lyles RH, Poindexter C, Evans A, Brown M, Cooper CR (2008). Nonlinear model-based estimates of IC for studies involving continuous therapeutic dose-response data. Contemporary Clinical Trials 29:878-886.

Meng Z, Ellens H and Bentz J (2017a). Extrapolation of elementary rate constants of P-glycoprotein mediated transport from MDCKII-hMDR1-NKI to Caco-2 cells. *Drug Metab Dispos* 45:190-197. doi: 10.1124/dmd.116.072140.

Meng Z, Le Marchand SJ, Agnani D, Szapacs ME, Ellens H and Bentz J (2017b). Microvilli morphology can affect efflux active P-glycoprotein in confluent MDCKII-hMDR1-NKI and Caco-2 cell monolayers. *Drug Metab Dispos* 45:145-151. doi: 10.1124/dmd.116.072157.

Mikkaichi T, Suzuki T, Onogawa T, Tanemoto M, Mizutamari H, Okada M, Chaki T, Masuda S, Tokui T, Eto N, Abe M, Satoh F, Unno M, Hishinuma T, Inui K, Ito S, Goto J and Abe T (2004). Isolation and characterization of a digoxin transporter and its rat homologue expressed in the kid- ney. Proc. Natl. Acad. Sci. U.S.A., 101: 3569–3574.

Michaelis L, Menten ML, Johnson KA, Goody RS. (2011). The original Michaelis constant: translation of the 1913 Michaelis-Menten paper. Biochemistry. 2011 Oct 4;50(39):8264-9. doi: 10.1021/bi201284u. Epub 2011 Sep 9.

O'Connor MP, Lee C, Ellens H and Bentz J (2014). A novel application of t-statistics to objectively assess the quality of IC_{50} fits for P-glycoprotein and other transporters. Pharma Res Per, 2(5), 2014, e00078, doi: 10.1002/prp2.78

Press WH, Teukolsky SA, Vetterling WT and Flannery BP (2007) Numerical Recipes: The Art of Scientific Computing (3rd Ed). Cambridge Univ. Press, Cambridge.

Quinn GP, Keough MJ (2002). Experimental Design and Data Analysis for Biologists. Cambridge Univ. Press, Cambridge, U.K.

Rao PV (1998). Statistical Research Methods in the Life Sciences. Duxbury Press, Pacific Grove, CA.

Shapiro AB and Ling V (1994). ATPase activity of purified and reconstituted P-glycoprotein from Chinese hamster ovary cells. J Biol Chem. 269(5):3745-54.

Shibayama T, Morales M, Zhang X, Martinez-Guerrero LJ, Berteloot A, Secomb TW, and Wright SH (2015). Unstirred Water Layers and the Kinetics of Organic Cation Transport. *Pharm Res* **32:**2937-2949.

Taub ME, Mease K, Sane RS, Watson CA, Chen L, Ellens H, Hirakawa B, Reyner EL, Jani M, Lee CA. (2011). Digoxin is not a substrate for organic anion-transporting polypeptide transporters OATP1A2, OATP1B1, OATP1B3, and OATP2B1 but is a substrate for a sodium-

dependent transporter expressed in HEK293 cells. Drug Metab Dispos. 2011 Nov;39(11):2093-102. doi: 10.1124/dmd.111.040816. Epub 2011 Aug 17.

Tran TT, Mittal A, Aldinger T, Polli JW, Ayrton A, Ellens H, and Bentz J (2005). The elementary mass action rate constants of P-gp transport for a confluent monolayer of MDCKII-hMDR1 cells. *Biophys J* **88:**715-738.

van Meer G, Voelker DR, and Feigenson GW (2008). Membrane lipids: where they are and how they behave. *Nat Rev Mol Cell Biol* **9:**112-124.

Zamek-Gliszczynski MJ, Lee CA, Poirier A, Bentz J, Chu X, Ellens H, Ishikawa T, Jamei M, Kalvass JC, Nagar S, Pang KS, Korzekwa K, Swaan PW, Taub ME, Zhao P, Galetin A, and International Transporter C (2013). ITC recommendations for transporter kinetic parameter estimation and translational modeling of transport-mediated PK and DDIs in humans. *Clin Pharmacol Ther* **94:**64-79.

DMD Fast Forward. Published on January 9, 2018 as DOI: 10.1124/dmd.117.075606
This article has not been copyedited and formatted. The final version may differ from this version.

Figure Legends

Figure.1

Biological mechanism of digoxin transport inhibition. The top portion (above the dashed line) shows digoxin transport in the absence of inhibitor, where the basolateral uptake transporter clearance is k_B (s^{-1}), making its fitted value a convolution of transporter surface density and the binding constant K_Q of the inhibitor to the transporter. Digoxin then diffuses within the plasma membrane (Tran et al., 2005) with an association rate constant to P-gp of k_1 ($M^{-1}s^{-1}$) and binds to P-gp with a binding constant of K_C (M^{-1}). Digoxin is then either dissociated back into the bilayer, which is most frequent, or effluxed into the apical chamber with a rate constant k_2 (s^{-1}), which is rare. For digoxin, roughly $1x10^4$ molecules bound to P-gp return to the apical bilayer for every 1 that is effluxed by P-gp into the apical chamber (Lumen et al., 2013). The bottom portion of the figure (below the dashed line) shows the case when there is also a P-gp inhibitor. If the inhibitor only binds to P-gp and not to the uptake transporter, then the IC_{50} is due solely to P-gp. However, we show in Tables 4, 5B and Supporting Data Table S2 that carvedilol, diltiazem, isradipine, mibefradil, nicardipine, nifedipine, nitrendipine, quinidine, ranolazine, sertraline, telmisartin, troglitizone and verapamil all bind to the basolateral uptake transporter, thereby inhibiting digoxin's uptake into the cells. It remains to be shown whether probe substrates like loperamide and vinblastine, which also kinetically require a basolateral uptake transporter, would likewise be inhibited by these P-gp inhibitors (Lumen et al., 2013). Thus, for the P-gp IC50 Initiative data, the IC_{50} is a convolution of the inhibition of P-gp and inhibition of the basolateral uptake transporter.

DMD Fast Forward. Published on January 9, 2018 as DOI: 10.1124/dmd.117.075606
This article has not been copyedited and formatted. The final version may differ from this version.

Figure 2

Inhibition of digoxin transport through a confluent cell monolayer of MDCKII-hMDR1-NKI cells by carvedilol. The squares are the data points with standard deviations. The lines are the fits to the data. The inhibitor dissociation constant from P-gp, $k_{rQ}(s^{-1})$, is fixed at the consensus value found for all the cells used, as explained in Table 4. Fig. 2A (with T(0)=1e-3 M, k_B=0 s^{-1}, k_{rQ}=1e4 (s^{-1}) and K_{QB}=0 M^{-1}) shows the best fit without the basolateral uptake transporter, which is a very poor fit. The NC, which occurs with little or no inhibitor, cannot be reached. Fig. 2B shows the fit with a higher P-gp efflux active concentration of T(0)=1e-2 M, which is the value for closely packed P-gp, i.e. the maximum possible (Tran et al., 2005; Agnani et al., 2011), the other kinetic parameters are as in Fig. 2A. The best fit is very still poor because NC cannot be reached. Fig. 2C shows that a lower P-gp efflux surface active density of T(0)=1e-4 M. Clearly, altering the P-gp level cannot alter fits enough to reach the NC. All eight digoxin/inhibitor pairs had the best kinetic fit when the inhibitors bound to both the basolateral transporter and P-gp.

Figure 3

Transport of digoxin through a confluent cell monolayer of MDCKII-hMDR1-NKI cells with a basolateral uptake transporter, without and with inhibitor binding to the uptake transporter. The squares are the data points with standard deviations. The lines are the fits to the data. The same data as in Fig. 2 is fitted here with the basolateral uptake clearance, $k_B(s^{-1})$. Fig. 3A (with

DMD Fast Forward. Published on January 9, 2018 as DOI: 10.1124/dmd.117.075606
This article has not been copyedited and formatted. The final version may differ from this version.

T(0)=1e-3 M, k_B=30 s^{-1}, k_{rQ}=1e4 ($s^{-}1$) and K_{QB}=0 M^{-1}) shows a good fit to NC, but not allowing the inhibitor to bind to the uptake transporter makes a poor fit to the positive control plateau, PC. The PC fit without binding of the inhibitor is about 15% too high at the PC. Additional inhibition is required for a good fit. Fig. 3B (with K_{QB}=1e5 M^{-1}) and with all other parameters the same as Fig. 3A shows a good fit to PC. K_{QB} is called an affinity constant since it is a convolution of the uptake transporter surface density and the inhibitor's binding constant to the uptake transporter. While the PC correction may not look large, that smallness appears to be largely due to these cells overexpressing P-gp, as shown below in Fig. 5 for the HPTC cells.

Figure 4

PCA plot for the variability of the IC_{50} values with simulated data for "virtual" cells using the kinetic parameters from the five labs from the P-gp IC_{50} Initiative, Table 4, and the HPTC data, Table 5B. T(0), the efflux active P-gp concentration, ranged from 1e-5 to 5e-3 M; k_B, the basolateral uptake transporter clearance, ranged from 5-30 s^{-1}; and K_{QB}, the affinity constant of the inhibitor to the basolateral uptake transporter ranged from 2e4 to 1e6 M^{-1}. For each inhibitor, the consensus values of k_{rQ}, the inhibitor dissociation constant from P-gp, Table 4, were used. These ranges, in all combinations of the parameters, were used to simulate IC_{50} data curves, fit for the IC_{50} values and then used to make the PCA plot. The color of the symbols denotes the value of k_B and their shape denotes the value of K_{QB}, as indicated on the right hand legend. The value for T(0) was not indicated, as a third element embedded into the symbols makes the plot unintelligible. However, the values can be inferred. On the right hand side of the graph, for example, there are nine black stars which represent: k_B=50 s^{-1} (black), K_{QB}=1e6

DMD Fast Forward. Published on January 9, 2018 as DOI: 10.1124/dmd.117.075606
This article has not been copyedited and formatted. The final version may differ from this version.

M^{-1} (a star shape), and the nine values [1e-5, 2e-5, 5e-5, 1e-4, 2e-4, 5e-4, 1e-3, 2e-3, 5e-3] M for T(0) in order from left to right. That is the trend throughout the plot.

Figure 5

Digoxin transport through a confluent cell monolayer of primary human proximal tubule kidney cells (HPTC) with inhibition by ketoconazole. The squares are the data points with standard deviations. The lines are the fits to the data. Fig. 5A (with T(0)=1.5e-5 M, k_B=0 s^{-1}, k_rQ=3e4 (s^-1) and K_{QB}=0 M^{-1}) is fitted with just P-gp, i.e. no basolateral uptake clearance. The fit is very poor and looks like Fig 2. Fig. 5B (with k_B=45s^{-1} and all the other parameters the same as Fig. 5A) gives a good fit to NC, but a poor fit to PC, notably worse than Fig 3A. The PC fit without binding of the inhibitor is about 50% off. Fig. 5C (with K_{QB}=2e6 $M^{-1}$and all the other parameters the same as Fig. 5B) gives a good fit to PC. K_{QB} is called an affinity constant since it is a convolution of the uptake transporter surface density and the inhibitor's binding constant to the uptake transporter.

Figure 6

Digoxin uptake in and transport through a confluent cell monolayer of primary human proximal tubule kidney cells (HPTC) inhibited by ouabain. Fig. 6A shows the inhibition of digoxin uptake into the HPTC cells by ouabain. 10 μM ouabain inhibits digoxin uptake by about 50%.

DMD Fast Forward. Published on January 9, 2018 as DOI: 10.1124/dmd.117.075606
This article has not been copyedited and formatted. The final version may differ from this version.

The decreased transport is mostly linear rather than logistic, as discussed. Fig. 6B shows the inhibition of digoxin transport, $J_{B>A}$, through the HPTC cells by ouabain. 30 μM ouabain only inhibits digoxin B>A transport by 20-25%. The decreased transport is mostly linear rather than logistic, as discussed.

DMD Fast Forward. Published on January 9, 2018 as DOI: 10.1124/dmd.117.075606
This article has not been copyedited and formatted. The final version may differ from this version.

Tables with footnotes

Table 1. Average values for negative (NC) and positive (PC) control values in the different overexpressing cell systems for the qualified inhibitors with %CV<20% for both NC and PC, and t_{β}>5.

Cells[a]	Lab[a]	NC or PC [b] (number of inhibitors chosen)	Lab average (nm/s)[b]	Lab average SD (nm/s)[b]	%CV[c]
MDCK	2	NC (8)	198	16	8
		PC (8)	36	3	8
	7	NC (4)	179	12	7
		PC (4)	32	1	3
Caco-2	6	NC (7)	312	22	7
		PC (7)	119	7	6
	11	NC (6)	112	12	11
		PC(6)	27	4	15
LLC-PK	2	NC (4)	84	17	20
		PC (4)	33	4	12

[a] MDCK, Caco-2 and LLC-PK stand for MDCKII-hMDR1-NKI, Caco-2 cells and LLC-PK1-hMDR1-NKI cells, respectively. More specific descriptions of the cells and lab numbers were described in Bentz et al. (2013). This shorthand is used in all tables herein.

[b] NC is the negative control, the permeability coefficient of digoxin in the absence of inhibitor.

PC is the positive control, the permeability coefficient of digoxin with maximum inhibition of P-gp and BT with 2μM GF120918 (Tran et al., 2005; Acharya et al., 2008). SD is the standard deviation for the NC or PC of the chosen inhibitors.

[c] %CV is the ratio of lab average NC or PC divided by the SD, expressed as a percentage.

DMD Fast Forward. Published on January 9, 2018 as DOI: 10.1124/dmd.117.075606
This article has not been copyedited and formatted. The final version may differ from this version.

Table 2. IC_{50} values, t_β-statistic values for inhibitors and IC_{50} slope factor β

Cell[a]	Lab[a]	Inhibitor	IC_{50}[b]	t_β[c]	Lab average $\langle t_\beta \rangle$[d]	β[e]
MDCK	2	Carvedilol	6.8	11.5		1.0
	2	Diltiazem	53.9	7.4		0.7
	2	Isradipine	35.4	7.0		1.0
	2	Mibefradil	7.3	11.0		1.0
	2	Nicardipine	2.6	7.7		1.0
	2	Quinidine	8.4	9.0		1.6
	2	Ranolazine	68.2	10.7		1.3
	2	Verapamil	11.8	14.9	9.8	1.2
	7	Carvedilol	8.1	11.2		1.5
	7	Nicardipine	5.5	14.5		1.1
	7	Ranolazine	114.0	5.3		1.8
	7	Verapamil	32.2	19.7	12.7	1.1
Caco-2	6	Carvedilol	0.7	10.7		0.9
	6	Diltiazem	8.3	17.3		1.2
	6	Isradipine	7.2	14.8		0.9
	6	Nicardipine	1.0	6.8		1.1
	6	Quinidine	2.3	14.8		1.0
	6	Ranolazine	9.8	10.7		1.0
	6	Verapamil	1.8	13.0	12.6	1.0
	11	Carvedilol	1.4	7.0		1.1
	11	Diltiazem	5.7	10.5		0.9

	11	Isradipine	2.6	8.6		0.6
	11	Nicardipine	1.8	8.5		1.4
	11	Quinidine	2.3	7.5		0.9
	11	Ranolazine	15.3	15.3	9.6	1.6
LLC-PK	2	Mibefradil	4.5	8.5		1.2
	2	Quinidine	15.7	6.9		1.2
	2	Ranolazine	55.4	5.7		1.2
	2	Verapamil	8.6	6.1	6.8	1.0

[a] Cell and Lab number as indicated in Bentz et al. (2013)

[b] IC_{50} values are taken from Bentz et al. (2013).

[c] t_β was calculated as described in O'Connor et al. (2014). This data quality statistic measures the goodness-of fit of the experimental IC_{50} data to a logistic curve, the expected shape of an IC_{50} curve. The present work required that $t_\beta > 5$ for all data analyzed, a lower limit defined from preliminary analysis.

[d] $\langle t_\beta \rangle$, the lab average for t_β was calculated for the qualified inhibitors.

[e] β is the slope factor for the IC_{50} curve in the Hill equation (Hill, 1913), calculated from the fit to the logistic equation (O'Connor et al., 2014). It is used in all commercial software fitting programs for IC_{50} plots as the slope factor estimate of the IC_{50} curve as it passes through the estimated IC_{50}. Any other interpretations of its meaning, e.g. binding cooperativity, are inapplicable to P-gp as analyzed in these data fits, see Discussion.

DMD Fast Forward. Published on January 9, 2018 as DOI: 10.1124/dmd.117.075606
This article has not been copyedited and formatted. The final version may differ from this version.

Table 3. Average fitted values for k_rQ for dissociation from P-gp.

Drug	$<k_{rQ}>$ [a]	Lo (95% CI) [b]	Hi (95% CI) [b]	Consensus k_{rQ} [c]
Carvedilol	9.6E+03	1.8E+03	2.7E+04	1E+04
Diltiazem	6.5E+04	3.1E+02	6.8E+05	7E+04
Isradipine	5.9E+04	6.9E+02	4.9E+05	6E+04
Mibefradil	8.2E+03	1.0E+03	1.5E+04	8E+03
Nicardipine	6.7E+03	1.4E+02	2.3E+04	7E+03
Quinidine	1.3E+04	2.8E+03	3.2E+04	1E+04
Ranolazine	5.1E+04	4.2E+03	9.7E+04	5E+04
Verapamil	2.2E+04	7.4E+03	5.0E+04	2E+04

[a] Fits were performed over $\log_{10}\{k_{rQ}\}$ fits and for each inhibitor these $\log_{10}$ values were averaged and transformed (10^x) to $<k_{rQ}>$.

[b] k_{rQ} was treated as log-normally distributed. Hence statistics including confidence intervals were calculated on $\log_{10}\{k_{rQ}\}$. 95% confidence interval bounds on k_{rQ} were determined by inverse transformation (10^x) of the intervals on $\log_{10}\{k_{rQ}\}$. The lower (Lo) and upper (Hi) 95% confidence interval bounds are shown.

[c] Consensus k_{rQ} is the one digit estimate to $<k_{rQ}>$.

DMD Fast Forward. Published on January 9, 2018 as DOI: 10.1124/dmd.117.075606
This article has not been copyedited and formatted. The final version may differ from this version.

Table 4. P-gp Efflux Active Concentration and Elementary Kinetic Parameters for the qualified overexpressing cells.

Cell	Lab	Inhibitor	T(0) (M)[a]	k_B (s^{-1})[a]	k_{rQ} (s^{-1})[b]	K_{QB} (M^{-1})[c]	%CV[c]	Ki[d] (μM)	IC_{50}/Ki[e]
MDCK	2	Carvedilol	1E-03	30	1E+04	1E+05	0.17	0.3	24
	2	Diltiazem	"	"	7E+04	1E+04	0.32	2.0	27
	2	Isradipine	"	"	6E+04	7E+04	0.42	2.0	21
	2	Mibefradil	"	"	8E+03	7E+03	0.15	0.2	32
	2	Nicardipine	"	"	7E+03	2E+04	0.28	0.2	13
	2	Quinidine	"	"	1E+04	2E+04	0.23	0.3	29
	2	Ranolazine	"	"	5E+04	5E+03	0.30	1.0	48
	2	Verapamil	"	"	2E+04	3E+03	0.22	0.6	21
	7	Carvedilol	2E-03	27	1E+04	1E+05	0.50	0.3	28
	7	Nicardipine	"	"	7E+03	5E+04	0.25	0.2	28
	7	Ranolazine	"	"	5E+04	3E+03	0.44	1.0	80
	7	Verapamil	"	"	2E+04	3E+03	0.48	0.6	56
Caco-2	6	Carvedilol	3E-04	30	1E+04	2E+05	0.29	0.2	4
	6	Diltiazem	"	"	7E+04	2E+04	0.22	1.0	7
	6	Isradipine	"	"	6E+04	1E+04	0.12	1.0	7
	6	Nicardipine	"	"	7E+03	5E+04	0.26	0.1	9
	6	Quinidine	"	"	1E+04	1E+04	0.58	0.2	14
	6	Ranolazine	"	"	5E+04	1E+04	0.29	0.8	12

DMD Fast Forward. Published on January 9, 2018 as DOI: 10.1124/dmd.117.075606
This article has not been copyedited and formatted. The final version may differ from this version.

	6	Verapamil	"	"	2E+04	2E+04	0.22	0.3	5
	11	Carvedilol	4E-04	15	1E+04	2E+05	0.57	0.2	8
	11	Diltiazem	"	"	7E+04	1E+05	0.31	1.0	5
	11	Isradipine	"	"	6E+04	1E+05	0.40	1.0	3
	11	Nicardipine	"	"	7E+03	5E+04	0.23	0.1	15
	11	Quinidine	"	"	1E+04	1E+04	0.31	0.2	14
	11	Ranolazine	"	"	5E+04	1E+05	0.29	0.8	18
LLC-PK	2	Mibefradil	1E-03	5	8E+03	5E+05	0.17	0.2	20
	2	Quinidine	"	"	1E+04	5E+04	0.40	0.3	55
	2	Ranolazine	"	"	5E+04	2E+04	0.16	1.0	39
	2	Verapamil	"	"	2E+04	1E+04	0.22	0.6	15

[a] T(0), the P-gp efflux active concentration (mols P-gp per liter of membrane) and k_B, the basolateral plasma membrane uptake transporter clearance for digoxin (s^{-1}), are inhibitor independent, i.e. they are fitted simultaneously for all qualified inhibitors for each lab.

[b] k_{rQ} is the consensus dissociation constant of inhibitor from P-gp from Table 3 and K_{QB} is the affinity constant of the inhibitor binding to the basolateral digoxin uptake transporter, BT.

[c] %CV is the coefficient of variation for the fit versus the data expresses as a percentage.

[d] $Ki=10^6/(K_{QPC}k_{1Q}/k_{rQ})$ (μM) is the system independent dissociation constant of the inhibitor measured relative to the aqueous concentration of the inhibitor in the cytosol. Most of the inhibitors we used do not have a partition coefficient, K_{QPC}, measured by the technique we used (Tran et al., 2005; Lumen et al., 2013). So we used a value of 350 for all inhibitors, which is

DMD Fast Forward. Published on January 9, 2018 as DOI: 10.1124/dmd.117.075606
This article has not been copyedited and formatted. The final version may differ from this version.

the value we measured for quinidine binding to 0.1 μm liposomes composed of a phosphatidylethanolamine/ phosphatidylserine/cholesterol (1:1:1) mol ratio (Lumen et al., 2013). This roughly mimics the cytosolic face of the plasma membrane (Lumen et al., 2013). Verapamil had a measured partition coefficient of 650, which would give a Ki roughly half as large as that shown in this Table (Lumen et al., 2013). None of the other inhibitors in this work have known partition coefficients measured using this uniform system. k_{1Q} has been measured for MDCKII-hMDR1-NKI cells for several P-gp substrates, including quinidine and verapamil, and was found to be well fitted as 1e8 $M^{-1}s^{-1}$ (Agnani et al., 2011; Lumen et al., 2013). The same value has been assumed for the LLC-PK1-hMDR1-NKI cells. However, Meng et al. (2017a) found for Caco-2 cells that k_{1Q} was about 1.7-fold larger. This means that the Ki for an inhibitor with the Caco-2 cells would be 1.7-fold smaller than with MDCKII-hMDR1-NKI cells.

[e] IC_{50}/Ki is the IC_{50} divided by the dissociation constant of the inhibitor to P-gp, both in the units of μM, so it is dimensionless.

DMD Fast Forward. Published on January 9, 2018 as DOI: 10.1124/dmd.117.075606
This article has not been copyedited and formatted. The final version may differ from this version.

Table 5A. IC_{50} values, t_β-statistic values for inhibitors and IC_{50} slope factor β

Cell	Kidney #[a]	Inhibitor	IC_{50}[b]	t_β[c]	β[d]
HPTC	6	Carvedilol	1.4	4.8	0.6
	10[e]	"	0.05	7.7	0.9
	13	Diltiazem	1.1	5.0	0.8
	8	Isradipine	8.7	6.7	0.4
	2	Ketoconazole	9.8	4.4	0.5
	3	"	0.7	3.1	0.9
	11	"	2.8	5.9	0.4
	7	Mibefradil	4.2	9.1	0.8
	4	Nicardipine	0.8	5.0	1.2
	13	"	0.3	5.2	0.8
	1	Quinidine	0.7	7.5	0.6
	2	"	3.1	3.7	1.1
	12	Ranolazine	1.8	2.4	2.8
	1	Verapamil	1.1	4.5	0.5
	10[e]	"	0.16	4.9	0.6

[a] Numbers give the chronological order of receipt of the human kidneys, as a simple means to identify the source of the data.

[b] IC_{50} values were calculated as described in O'Connor et al. (2014).

DMD Fast Forward. Published on January 9, 2018 as DOI: 10.1124/dmd.117.075606
This article has not been copyedited and formatted. The final version may differ from this version.

[c] t_β was calculated as described in O'Connor et al. (2014). This data quality statistic measures the sigmoidicity of the experimental IC_{50} curve, the expected shape of an IC_{50} curve. Because these were primary cells the criteria for qualification was set at $t_\beta>3$, as in Bentz et al. (2013).

[d] β is the slope factor for the IC_{50} curve in the Hill equation used in all commercial software fitting programs which is the slope of the IC_{50} curve as it passes through the IC_{50}..

[e] The IC_{50} value for kidney 10 is significantly smaller than the other IC50 values. The reason is unknown.

Table 5B. P-gp Efflux Active Concentration and Elementary Kinetic Parameters

for the data in Table 5A.

Cells	Kidney #[a]	Inhibitor	T(0) (M)[a]	k_B (s^{-1})[a]	k_{rQ} (s^{-1})[b]	K_{QB} (M^{-1})[c]	%CV[d]	Ki[e] (μM)	IC_{50}/Ki
HPTC	6	Carvedilol	3E-05	17	1E+04	1E+05	0.13	0.3	4.9
	10	"	1E-05	2	1E+04	7E+06	0.04	0.3	0.2
	13	Diltiazem	3E-05	15	7E+04	2E+06	0.09	2.0	0.6
	8	Isradipine	2E-04	8	6E+04	1E+04	0.18	1.7	5.1
	2	Ketoconazole	3E-05	20	3E+04	1E+04	0.19	0.9	11.4
	3	"	2E-05	45	3E+04	2E+06	0.09	0.9	0.8
	11	"	1E-05	40	3E+04	1E+05	0.08	0.9	3.3
	7	Mibefradil	2E-04	15	8E+03	5E+03	0.08	0.2	18.4
	4	Nicardipine	1E-05	20	7E+03	5E+05	0.05	0.2	4.0
	13	"	3E-05	15	7E+03	5E+05	0.08	0.2	1.5
	1	Quinidine	2E-05	9	1E+04	1E+04	0.04	0.3	2.5
	2	"	3E-05	20	1E+04	2E+05	0.16	0.3	10.9
	12	Ranolazine	3E-05	9	5E+04	4E+05	0.08	1.4	1.3
	1	Verapamil	2E-05	9	2E+04	3E+05	0.08	0.6	1.9
	10	"	1E-05	2	2E+04	3E+03	0.04	0.6	0.3

DMD Fast Forward. Published on January 9, 2018 as DOI: 10.1124/dmd.117.075606
This article has not been copyedited and formatted. The final version may differ from this version.

[a] T(0), the P-gp efflux active concentration (mols P-gp per liter of membrane) and k_B, the basolateral plasma membrane uptake transporter clearance (s^{-1}), are fitted independently for each kidney.

[b] k_{rQ} is the consensus dissociation constant of inhibitor from P-gp, Table 3.

[c] K_{QB} is the affinity constant of the inhibitor binding to the uptake transporter.

[d] %CV is the coefficient of variation for the fit to the IC50 curve expressed as a percentage.

[e] Ki=1e6/(K_{QPC}*k_{1Q}/k_{rQ}) (μM)). Defined in Footnote [d] in Table 4. K_Q= k_{1Q}/k_{rQ}.

DMD Fast Forward. Published on January 9, 2018 as DOI: 10.1124/dmd.117.075606
This article has not been copyedited and formatted. The final version may differ from this version.

Table 6. Effect of data quality on the slope factor

	IC50 fits from all labs for all data sets with $t_\beta > 3$ (Bentz et al., 2013) [a]				
	Number of fits	β (average) [a]	%CV [b]	min [c]	max [c]
MDCK	48	1.3	50	0.3	3.6
Caco-2	70	1.1	31	0.6	2.4
LLC-PK1	13	1.4	64	0.6	3.3
	IC50 fits from those labs which qualified in this work, e.g. $t_\beta > 5$ [d]				
	Number of fits	β (average)	%CV	min	max
MDCK	12	1.2	26	0.7	1.8
Caco-2	13	1.0	24	0.6	1.6
LLC-PK1	4	1.2	9	1.0	1.2

[a] Total number of fitted data sets (t_β>3) for the slope factor β from Bentz et al. (2013), Supplemental Data S2 of that paper.

[b] Coefficient of variation for fitted β expressed as a percentage.

[c] Minimum and maximum values for β.

[d] These data are from Table 2.

Fig 1

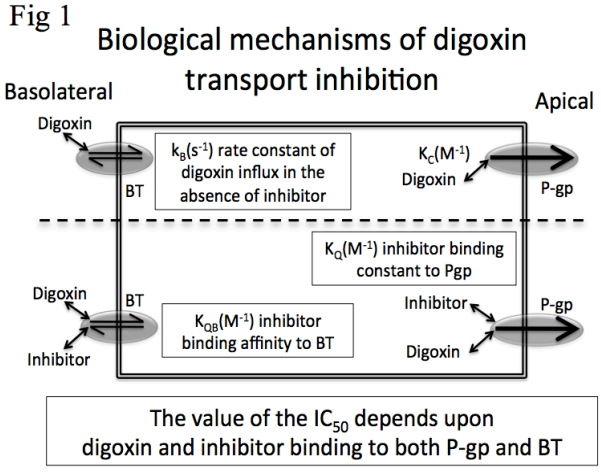
Biological mechanisms of digoxin transport inhibition
Basolateral
Apical
Digoxin
$k_B(s^{-1})$ rate constant of digoxin influx in the absence of inhibitor
BT
$K_C(M^{-1})$
Digoxin
P-gp
$K_O(M^{-1})$ inhibitor binding constant to Pgp
Digoxin
BT
$K_{OB}(M^{-1})$ inhibitor binding affinity to BT
Inhibitor
P-gp
Inhibitor
Digoxin
The value of the IC_{50} depends upon digoxin and inhibitor binding to both P-gp and BT

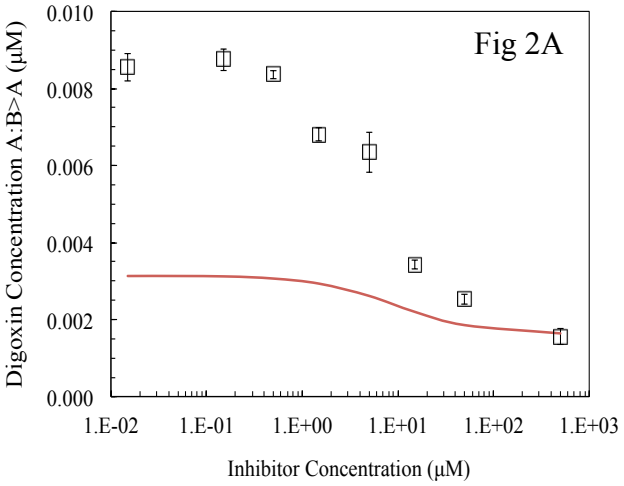
Fig 2A
Digoxin Concentration A:B>A (μM)
0.010
0.008
0.006
0.004
0.002
0.000
1.E-02
1.E-01
1.E+00
1.E+01
1.E+02
1.E+03
Inhibitor Concentration (μM)

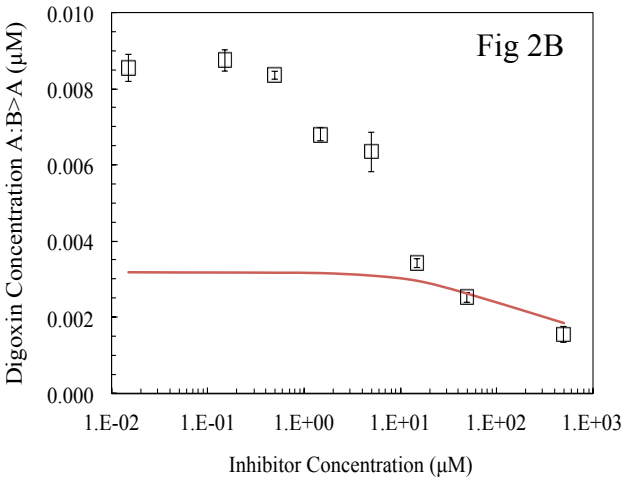
Fig 2B
Digoxin Concentration A:B>A (μM)
0.010
0.008
0.006
0.004
0.002
0.000
1.E-02
1.E-01
1.E+00
1.E+01
1.E+02
1.E+03
Inhibitor Concentration (μM)

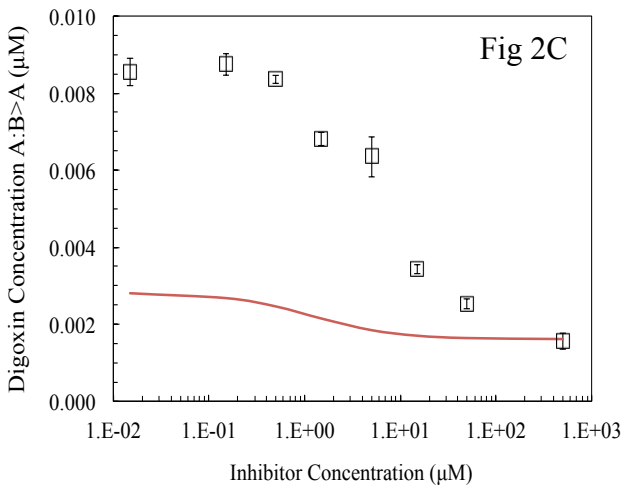
Fig 2C
Digoxin Concentration A:B>A (μM)
0.010
0.008
0.006
0.004
0.002
0.000
1.E-02
1.E-01
1.E+00
1.E+01
1.E+02
1.E+03
Inhibitor Concentration (μM)

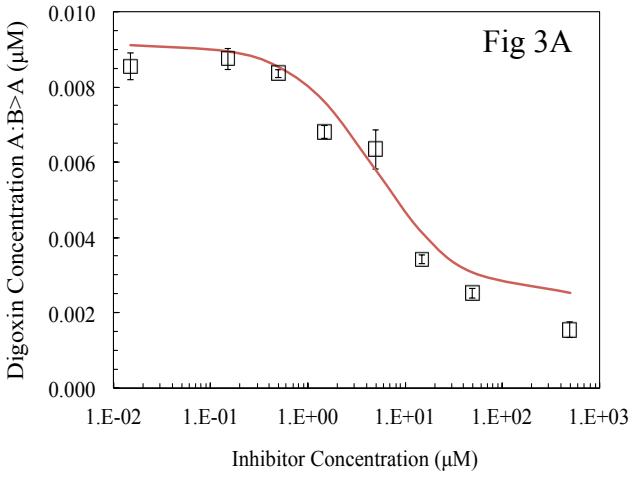
Fig 3A
Digoxin Concentration A:B>A (µM)
0.010
0.008
0.006
0.004
0.002
0.000
1.E-02
1.E-01
1.E+00
1.E+01
1.E+02
1.E+03
Inhibitor Concentration (µM)

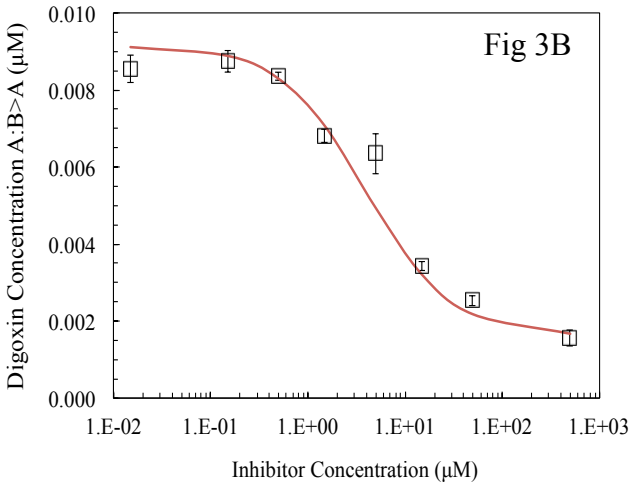
Fig 3B
Digoxin Concentration A:B>A (µM)
0.010
0.008
0.006
0.004
0.002
0.000
1.E-02
1.E-01
1.E+00
1.E+01
1.E+02
1.E+03
Inhibitor Concentration (µM)

Fig 4

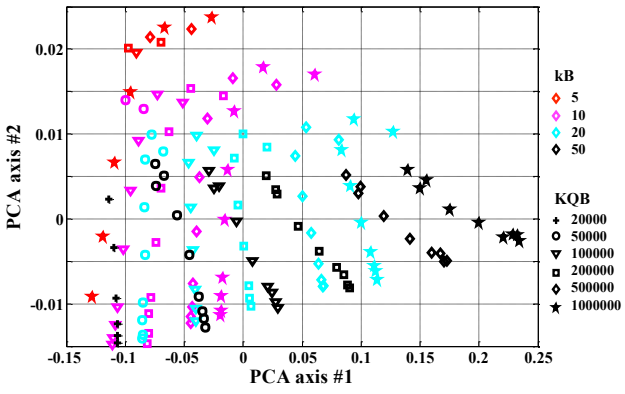
PCA axis #2
PCA axis #1
0.02
0.01
0
-0.01
-0.15
-0.1
-0.05
0
0.05
0.1
0.15
0.2
0.25
kB
5
10
20
50
KQB
20000
50000
100000
200000
500000
1000000

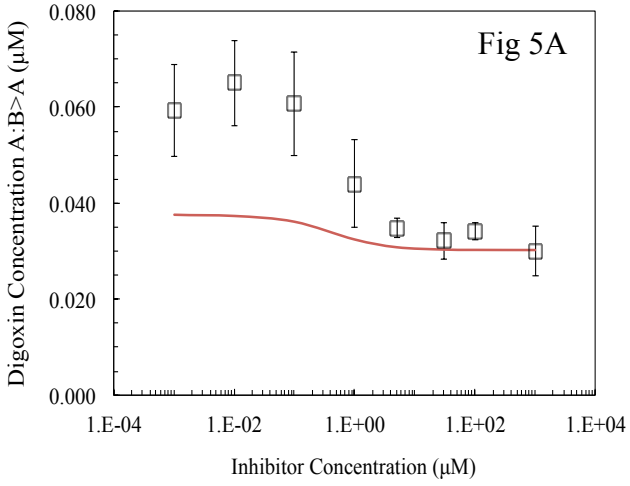
Fig 5A
Digoxin Concentration A:B>A (μM)
0.080
0.060
0.040
0.020
0.000
1.E-04
1.E-02
1.E+00
1.E+02
1.E+04
Inhibitor Concentration (μM)

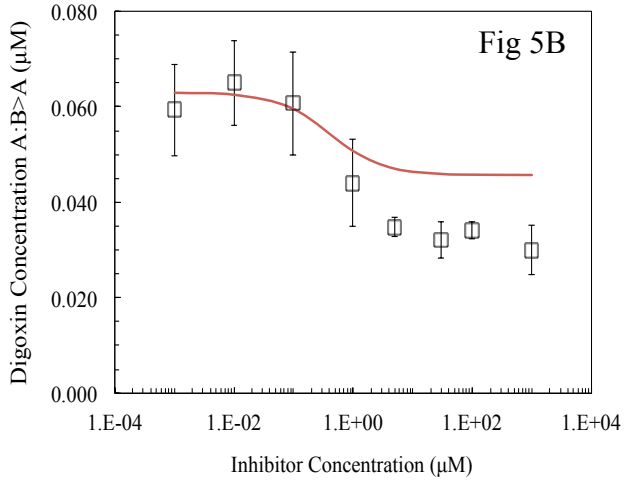
Fig 5B
Digoxin Concentration A:B>A (μM)
0.080
0.060
0.040
0.020
0.000
1.E-04
1.E-02
1.E+00
1.E+02
1.E+04
Inhibitor Concentration (μM)

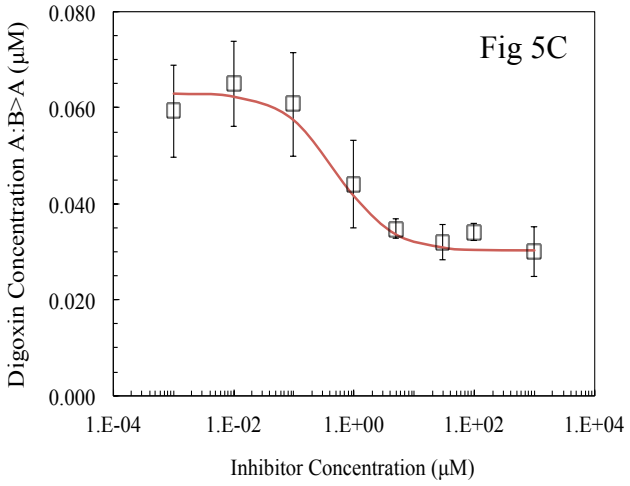
Fig 5C
Digoxin Concentration A:B>A (μM)
0.080
0.060
0.040
0.020
0.000
1.E-04
1.E-02
1.E+00
1.E+02
1.E+04
Inhibitor Concentration (μM)

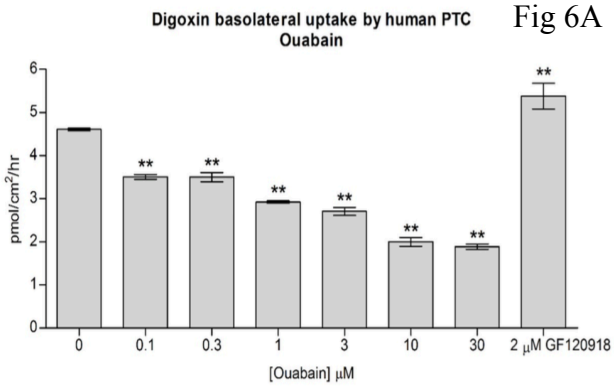
Digoxin basolateral uptake by human PTC
Ouabain
pmol/cm2/hr
0
1
2
3
4
5
6
**
**
**
**
**
**
**
0
0.1
0.3
1
3
10
30
2 μM GF120918
[Ouabain] μM

Fig 6A

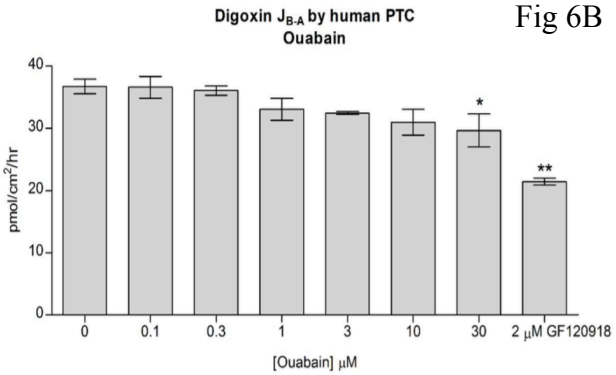
Digoxin J8-A by human PTC
Ouabain
pmol/cm2/hr
0
10
20
30
40
*
**
0
0.1
0.3
1
3
10
30
2 μM GF120918
[Ouabain] μM

Fig 6B

Supplemental Data for Drug Metabolism and Disposition (2018):

Derivation of a system-independent Ki for Pgp-mediated digoxin transport from system-dependent IC50 data.

Aqsaa Chaudhry, Git Chung, Adam Lynn, Akshata Yalvigi, Colin Brown, Harma Ellens,

Michael O'Connor, Caroline Lee and Joe Bentz

Drexel University, Department of Biology, Philadelphia, PA 19104 (AC, AL, AY, MO, JB)

Newcastle University, Institute for Cell and Molecular Biosciences, United Kingdom (GC, CB)

GlaxoSmithKline Pharmaceuticals, Drug Metabolism and Pharmacokinetics, King of Prussia, PA (HE)

Drexel University, Department of Biodiversity, Ecology and Earth Sciences, Philadelphia, PA, 19104 (MO)

Ardea Biosciences Inc., Translational Sciences, San Diego, CA 92121 (CL)

Supplemental Data Contents:

1. Parameters and figures for the Group 2 P-gp inhibitors
    a. Table S1: IC_{50} values, t_{β}-statistic values for inhibitors and IC_{50} slope factor β
    b. Table S2: P-gp Efflux Active Concentration and Elementary Kinetic Parameters
    c. Table S3: Legends for Figs. S1-S24
    d. Supplemental Data Figures S1-S24
2. Figures for the data of Tables 2 and 4 in the main paper
    a. Table S4: Legends for Figs. S25-S53
    b. Supplemental Data Figures S25-S53
3. Figures for the data of Tables 6A and 6B in the main paper
    a. Table S5: Legends for Figs. S54-S67
    b. Supplemental Data Figures S54-S67
4. Figures for the HPTC data of T3 inhibition of digoxin uptake and $J_{B\rightarrow A}$ transport in the main paper
    a. Table S6: Legends for Figs. S68-S69
    b. Supplemental Data Figures S68-S69
5. Supplemental Data Table S7 for Individual Lab fits for $\log_{10}\{k_{rQ}\}$ for Main Table 3.

Supplemental Data Table S1. IC_{50} parameters for the 7LI (Bentz et al., 2013)

Inhibitor	Cell Line	Lab	Initial [DGX] (μM)[d]	IC_{50} (μM)[a]	t_β[a]	β
Felodipine	MDCK[e]	L02	0.12	33.9	7.7	1.7
		L03	0.05	12.7	6.7	0.8
	Caco-2	L07	5	4.4	5.4	1.0
		L11	0.1	56.4	3.6	2.6
	LLCPK[e]	L01	5	30.9	8.2	1.1
Nifedipine	Caco-2	L06	0.0125	69.0	10.5	1.2
		L07	5	59.1	4.5	0.6
		L11	0.1	38.2	4.6	0.6
Nitrendipine	MDCKII	L02	0.12	75.8	11.4	1.3
		L03	0.05	9.6	4.0	0.2
	Caco-2	L06	0.0125	15.8	11.7	0.6
		L07	5	2.5	9.2	0.6
		L08	10	38.8	1.7	4.7
		L11	0.1	28.1	5.6	0.7
Sertraline	MDCKII	L01	0.12	19.6	10.8	1.3
Telmisartan	Caco-2	L02	1	18.1	5.5	1.6
		L10	0.05	10.1	8.3	1.2
	LLCPK	L02	5	26.7	6.6	1.0
Troglitazone	Caco-2	L02	1	17.2	7.6	1.2
		L06	0.0125	13.8	7.2	1.0
		L07	5	8.3	4.3	1.5
		L10	0.05	172.7	0.4	2.5
		L11	0.1	7.0	6.0	1.6
	LLC-PK	L02	5	36.3	3.2	1.1

Footnotes to Table

[a] T(0) is the P-gp efflux active surface density and k_B is the basolateral uptake clearance as fitted for the 8 better inhibitors in Table 5 of the main paper, since these parameters should not depend on inhibitor.

[b] k_{rQ} is the consensus inhibitor P-gp dissociation constant for all labs shown. K_{QB} is the affinity for the basolateral uptake transporter for the inhibitor for each lab.
[c] %CV is the coefficient of variation between the data and the fit.
[d] [DGX] is the initial concentration of digoxin in the basolateral chamber. This explains why the NC values for digoxin vary widely for the different labs.
[e] MDCK refers to the MDCKII-hMDR1-NKI cells and LLCPK refers to LLC-PK1-hMDR1-NKI cells for the labs shown.

Supplemental Data Table S2. Best fits for the 7LI (Bentz et al., 2013)

Inhibitor	Cell Line	Lab	T(0) (M)[a]	k_B (s^{-1})[a]	k_{rQ} (s^{-1})[b]	K_{QB} (M^{-1})[b]	%CV fit[c]	
Felodipine	MDCK[d]	L02	1e-3	30	7e4	3e4	0.21	
		L03	2e-3	10	"	1e5	0.65	
	Caco-2	L07	2e-4	7	"	1e4	0.19	
		L11	4e-4	15	"	1e4	0.49	
	LLCPK[d]	L01	5e-4	7	"	3e3	1.0	
Nifedipine	Caco-2	L06	3e-4	30	5e5	5e4	0.67	
		L07	2e-4	7	"	5e4	0.10	
		L11	4e-4	15	"	3e4	0.47	
Nitrendipine	MDCK	L02	1e-3	30	8e4	1e4	0.23	
		L03	2e-3	10	"	1e5	0.54	
	Caco-2	L06	3e-4	30	"	1e3	0.60	
		L07	2e-4	7	"	3e4	0.18	
		L08	2e-4	0.7	"	1e5	0.04	
		L11	4e-4	15	"	5e3	0.79	
Sertraline	MDCK	L01	2e-3	30	1e5	1e5	0.17	
Telmisartan	Caco-2	L02	1e-3	8	1e4	5e3	0.53	
		L10	3.5e-4	8	"	5e3	0.12	
	LLCPK	L02	2e-3	7	"	3e4	0.14	
Troglitazone	Caco-2	L02	1e-3	8	3e4	1e5	0.18	
		L06	3e-4	30	"	1e3	0.72	
		L07	2e-4	7	"	1e5	0.23	
		L10	3.5e-4	8	"	1e4	0.20	
		L11	4e-4	15	"	4e5	0.47	
	LLCPK	L02	2e-3	7	"	2e4	0.25	

Footnotes to Table

[a] T(0) is the P-gp efflux active surface density and k_B is the basolateral uptake clearance as fitted for the 8 better inhibitors in Table 5 main paper, since these parameters should not depend on inhibitor.

[b] k_{rQ} is the consensus inhibitor P-gp dissociation constant for all labs shown. K_{QB} is the affinity for the basolateral uptake transporter inhibitor for each lab.

[c] %CV is the coefficient of variation between the data and the fit.

[d] MDCK refers to the MDCKII-hMDR1-NKI cells for the labs shown and LLCPK refers to LLC-PK1-hMDR1-NKI cells for the labs shown.

Supplementary Data Table S3. Figure Legends for Tables S1 and S2. (symbols show the B>A digoxin transport data, error bars show the data standard deviation and the line shows the fit to the data

Fig. S1. Inhibition by felodipine with Caco-2 cells from L07.
Fig. S2. Inhibition by felodipine with Caco-2 cells from L11.
Fig. S3. Inhibition by felodipine with MDCK-hMDR1-NKI cells from L02.
Fig. S4. Inhibition by felodipine with MDCK-hMDR1-NKI cells from L03.
Fig. S5. Inhibition by felodipine with LLC-PK1-hMDR1-NKI cells from L01.
Fig. S6. Inhibition by nifedipine with Caco-2 cells from L06.
Fig. S7. Inhibition by nifedipine with Caco-2 cells from L07.
Fig. S8. Inhibition by nifedipine with Caco-2 cells from L11.
Fig. S9. Inhibition by nitrendipine with Caco-2 cells from L06.
Fig. S10. Inhibition by nitrendipine with Caco-2 cells from L07.
Fig. S11. Inhibition by nitrendipine with Caco-2 cells from L08.
Fig. S12. Inhibition by nitrendipine with Caco-2 cells from L11.
Fig. S13. Inhibition by nitrendipine with MDCK-hMDR1-NKI cells from L02.
Fig. S14. Inhibition by nitrendipine with MDCK-hMDR1-NKI cells from L03.
Fig. S15. Inhibition by sertraline with MDCK-hMDR1-NKI cells from L01.
Fig. S16. Inhibition by telmisartan with Caco-2 cells from L02.
Fig. S17. Inhibition by telmisartan with Caco-2 cells from L10.
Fig. S18. Inhibition by telmisartan with LLC-PK1-hMDR1-NKI cells from L02.
Fig. S19. Inhibition by troglitazone with Caco-2 cells from L02.
Fig. S20. Inhibition by troglitazone with Caco-2 cells from L06.
Fig. S21. Inhibition by troglitazone with Caco-2 cells from L07.
Fig. S22. Inhibition by troglitazone with Caco-2 cells from L10.
Fig. S23. Inhibition by troglitazone with Caco-2 cells from L11.
Fig. S24. Inhibition by troglitazone with LLC-PK1-hMDR1-NKI cells from L02.

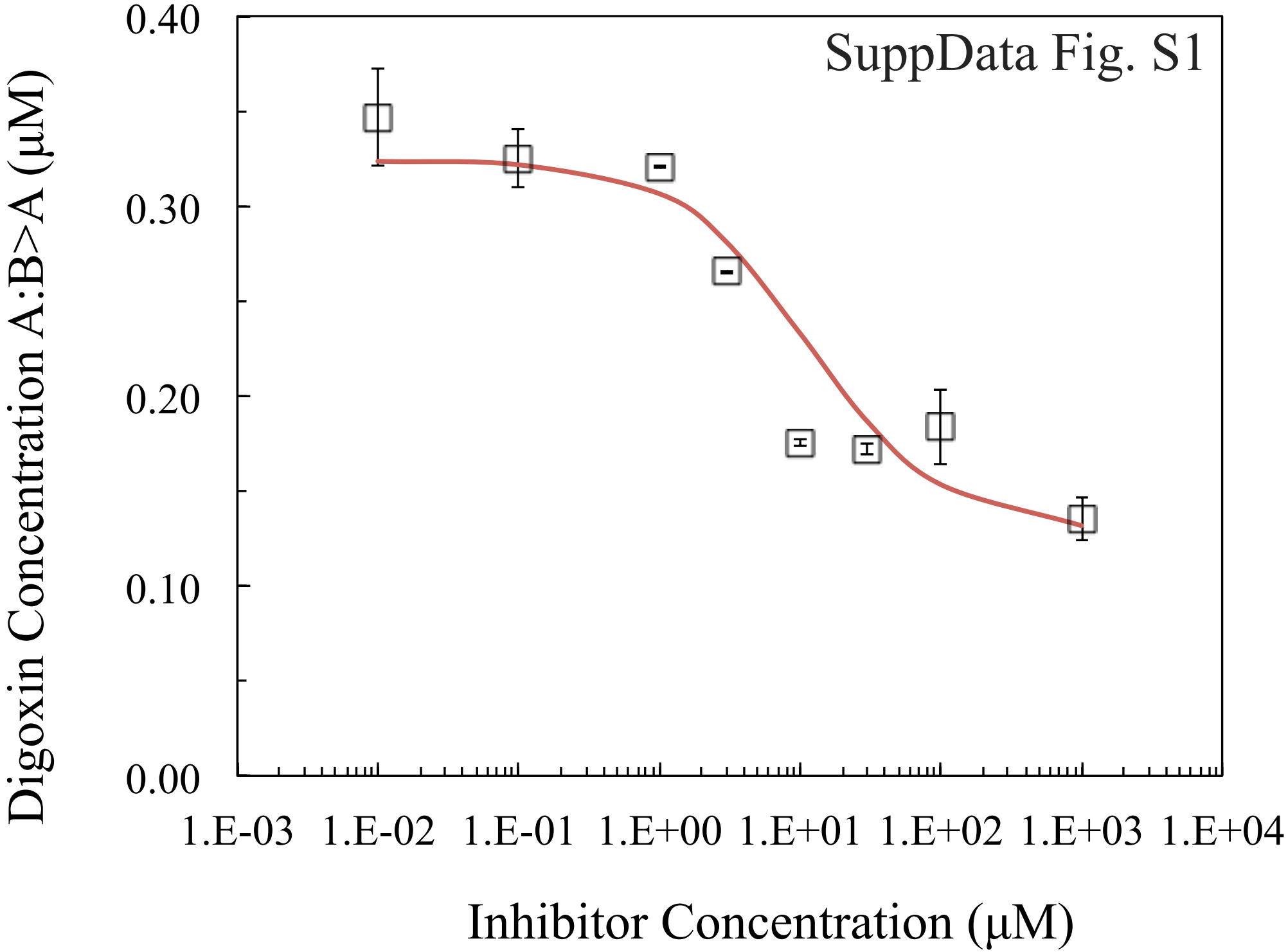
SuppData Fig. S1
0.40
0.30
0.20
0.10
0.00
Digoxin Concentration A:B>A (μM)
1.E-03
1.E-02
1.E-01
1.E+00
1.E+01
1.E+02
1.E+03
1.E+04
Inhibitor Concentration (μM)

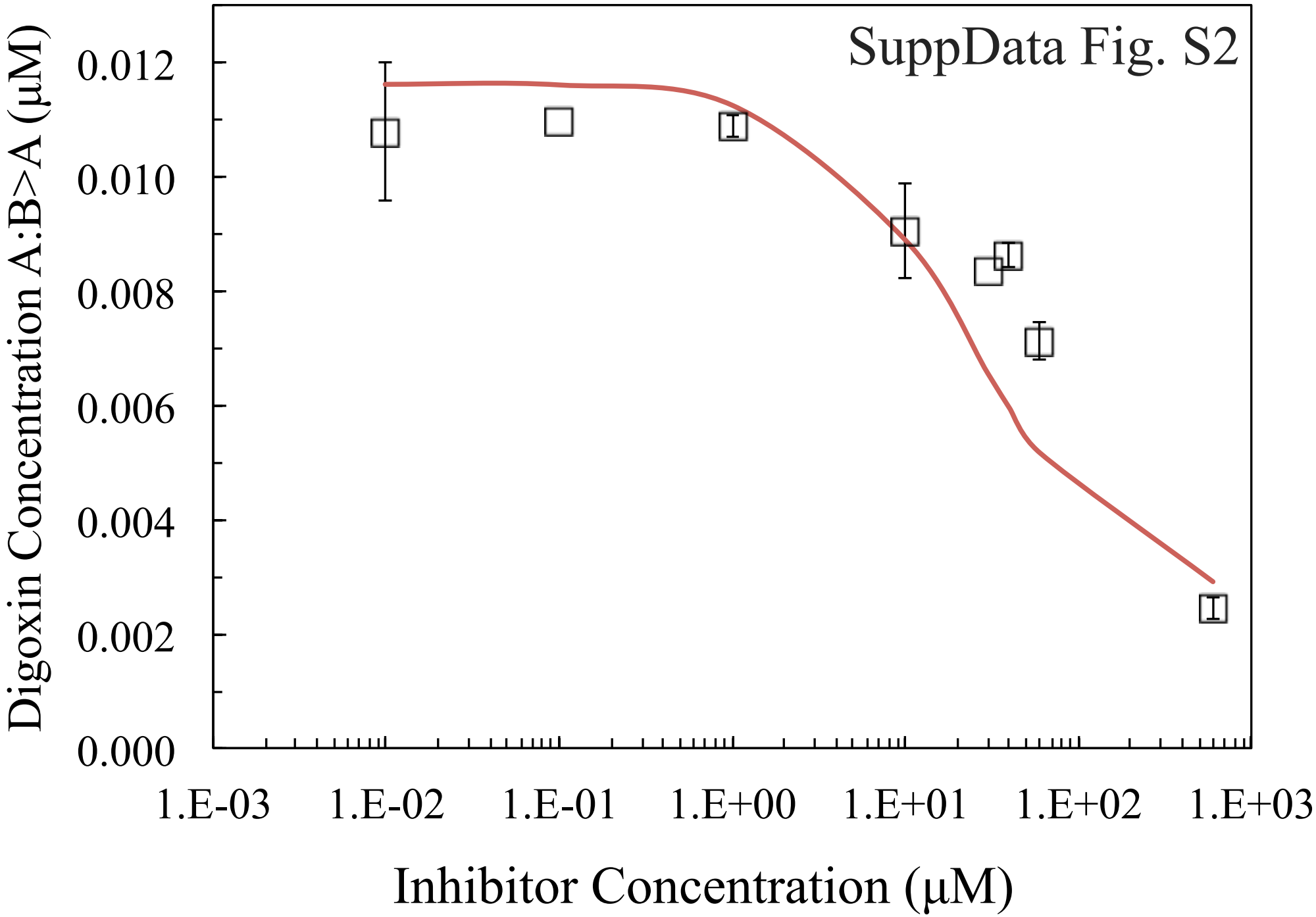
SuppData Fig. S2
Digoxin Concentration A:B>A (μM)
0.012
0.010
0.008
0.006
0.004
0.002
0.000
1.E-03
1.E-02
1.E-01
1.E+00
1.E+01
1.E+02
1.E+03
Inhibitor Concentration (μM)

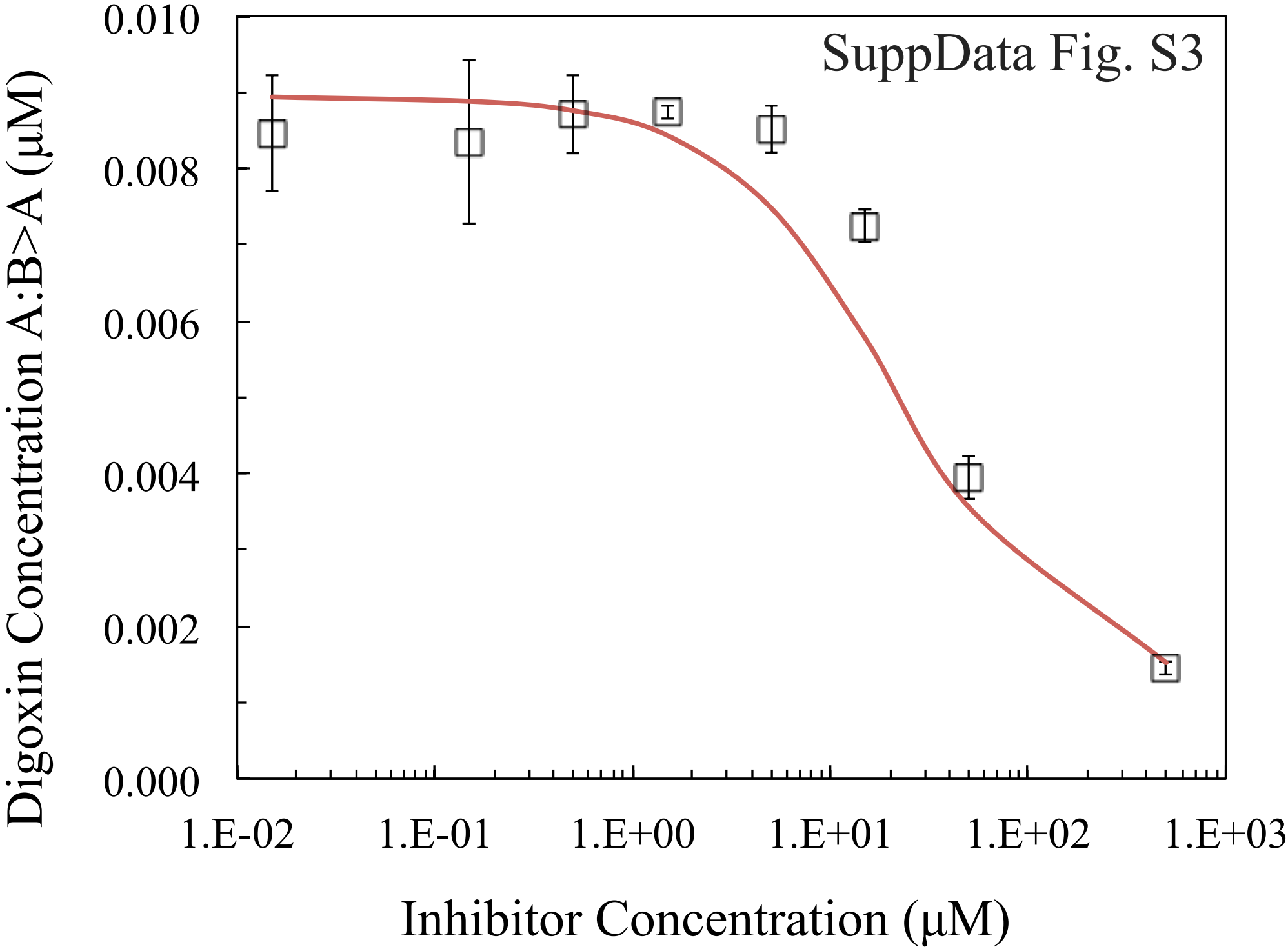
SuppData Fig. S3
Digoxin Concentration A:B>A (µM)
0.010
0.008
0.006
0.004
0.002
0.000
1.E-02
1.E-01
1.E+00
1.E+01
1.E+02
1.E+03
Inhibitor Concentration (µM)

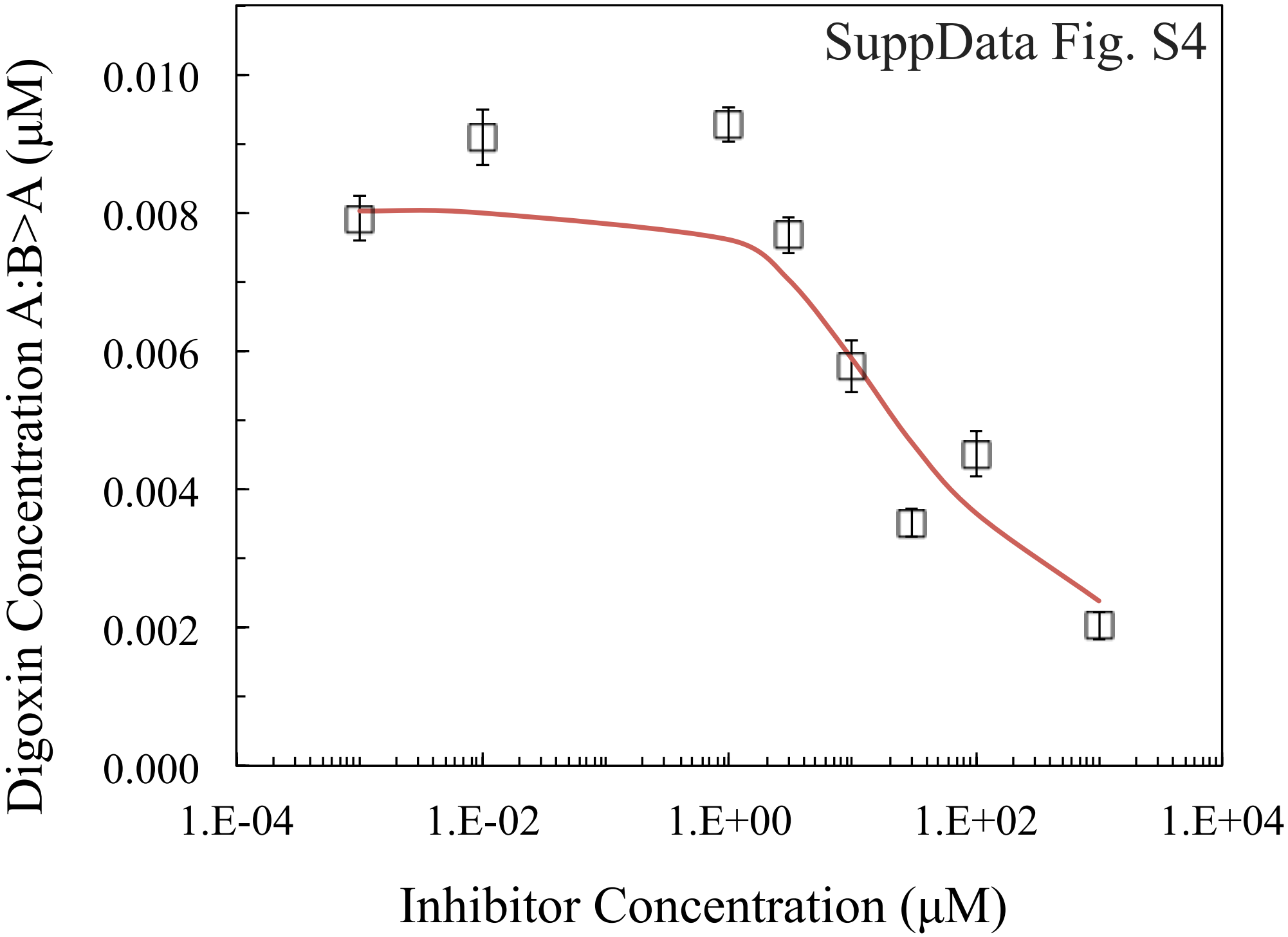
SuppData Fig. S4
Digoxin Concentration A:B>A (μM)
0.010
0.008
0.006
0.004
0.002
0.000
1.E-04
1.E-02
1.E+00
1.E+02
1.E+04
Inhibitor Concentration (μM)

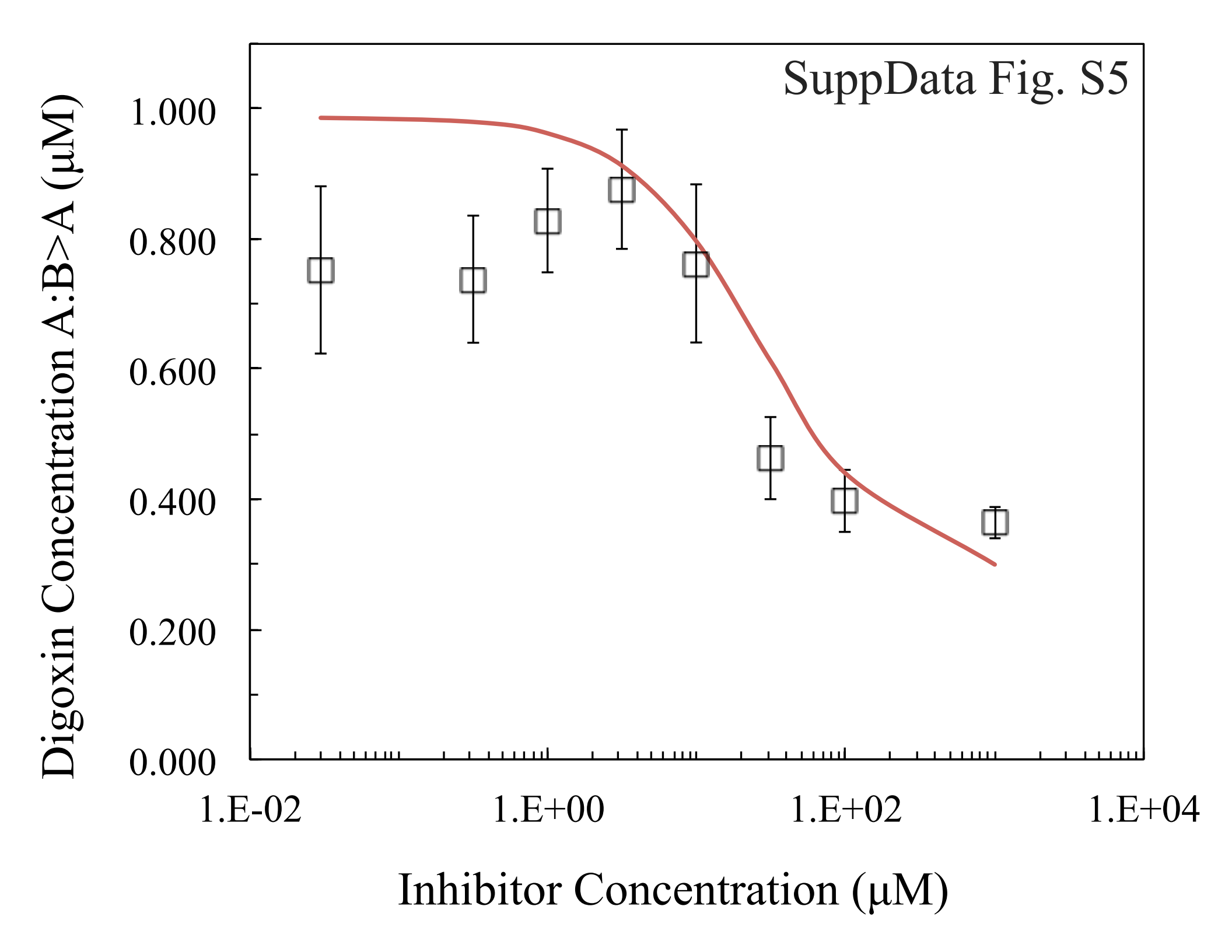
SuppData Fig. S5
Digoxin Concentration A:B>A (µM)
1.000
0.800
0.600
0.400
0.200
0.000
1.E-02
1.E+00
1.E+02
1.E+04
Inhibitor Concentration (µM)

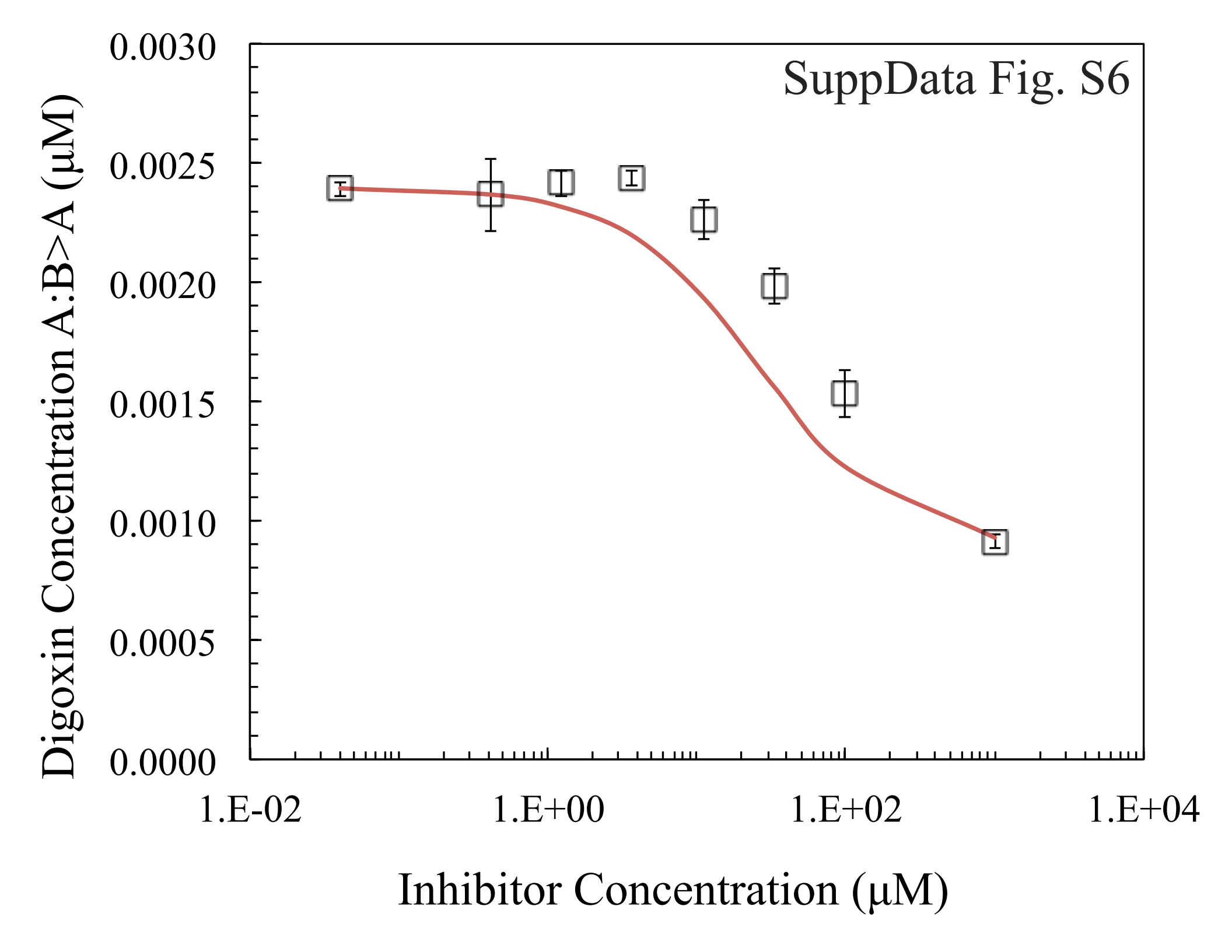
SuppData Fig. S6
Digoxin Concentration A:B>A (µM)
0.0030
0.0025
0.0020
0.0015
0.0010
0.0005
0.0000
1.E-02
1.E+00
1.E+02
1.E+04
Inhibitor Concentration (µM)

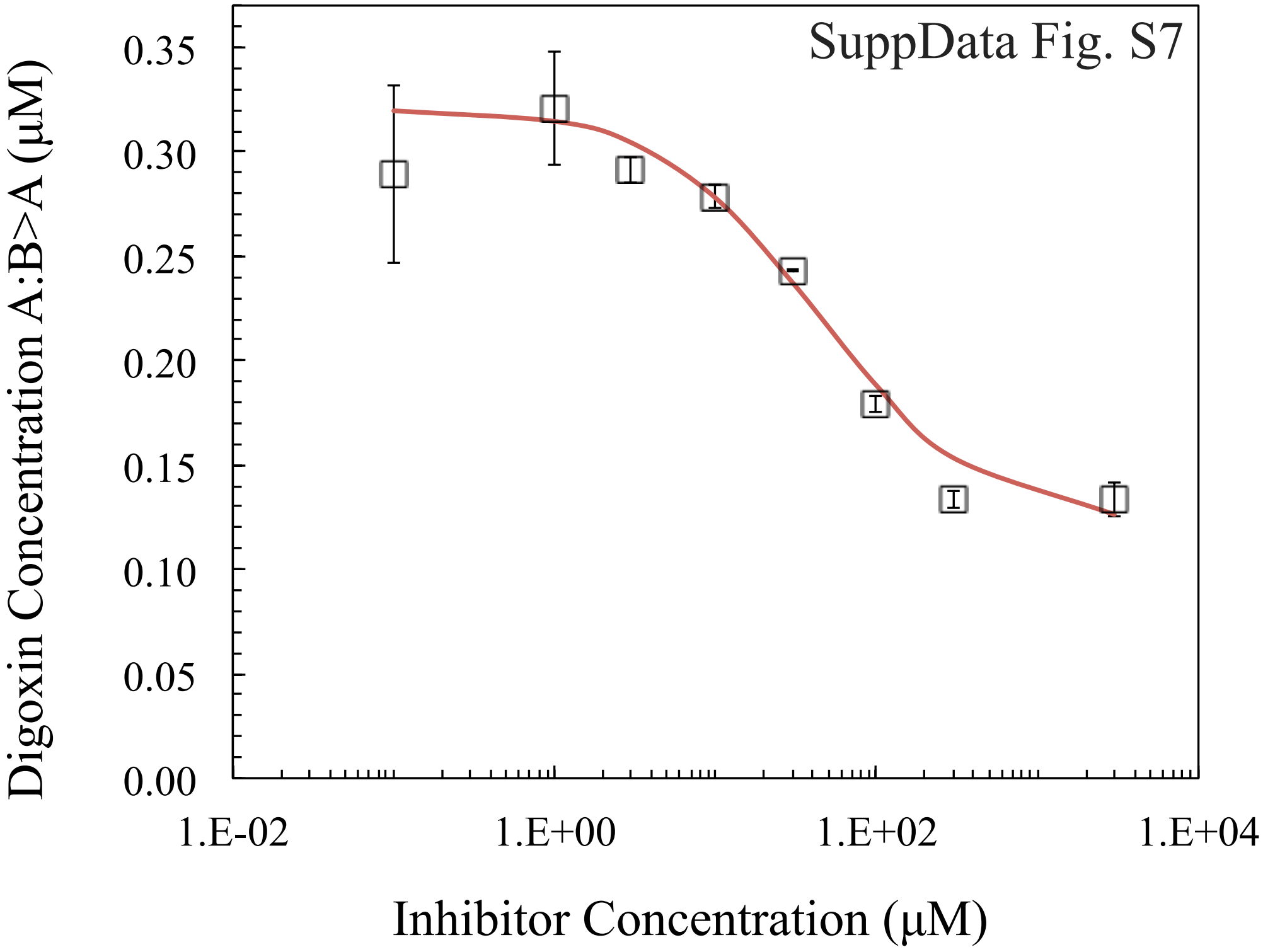
SuppData Fig. S7
Digoxin Concentration A:B>A (μM)
0.35
0.30
0.25
0.20
0.15
0.10
0.05
0.00
1.E-02
1.E+00
1.E+02
1.E+04
Inhibitor Concentration (μM)

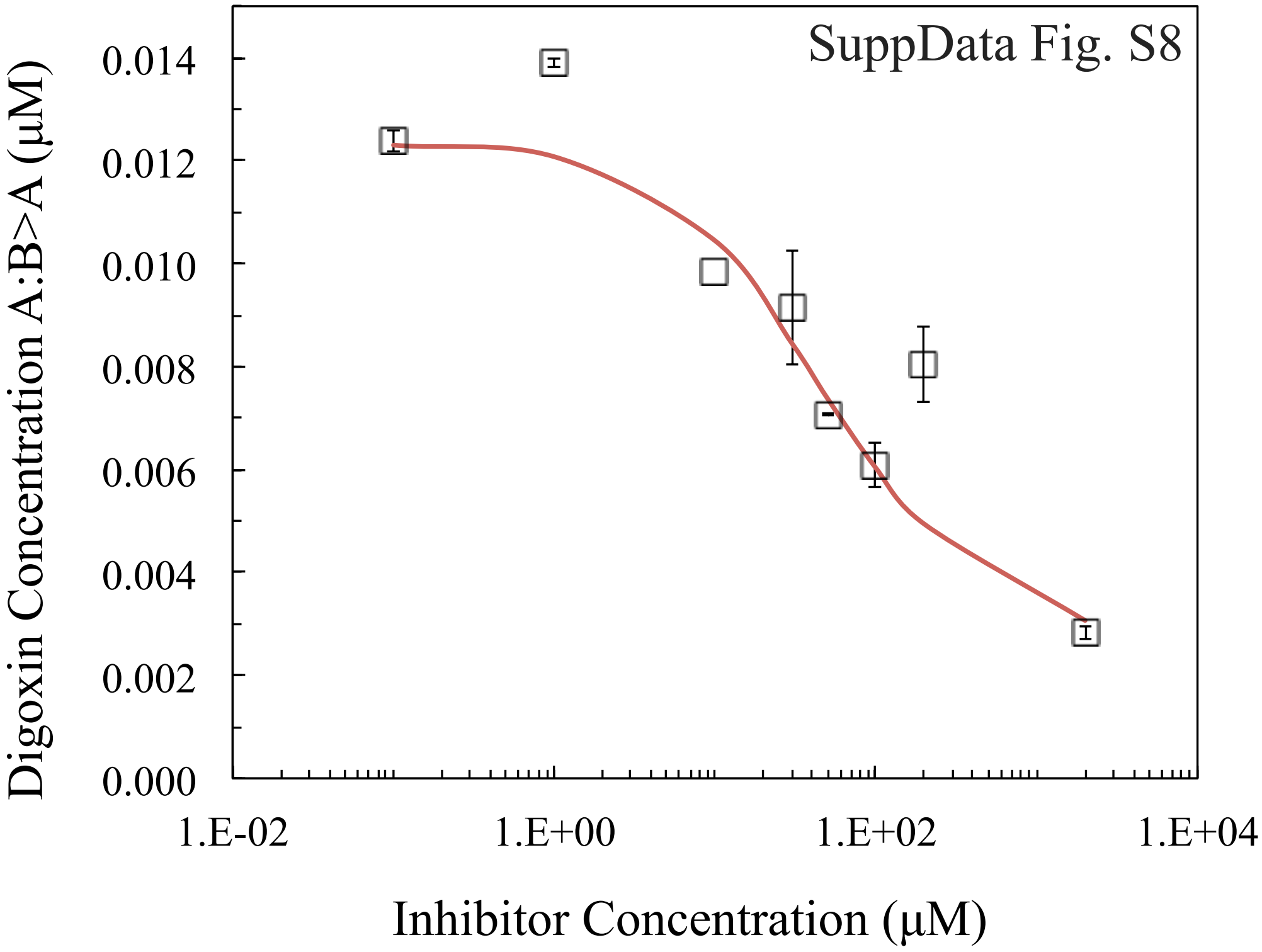
SuppData Fig. S8
Digoxin Concentration A:B>A (µM)
0.014
0.012
0.010
0.008
0.006
0.004
0.002
0.000
1.E-02
1.E+00
1.E+02
1.E+04
Inhibitor Concentration (µM)

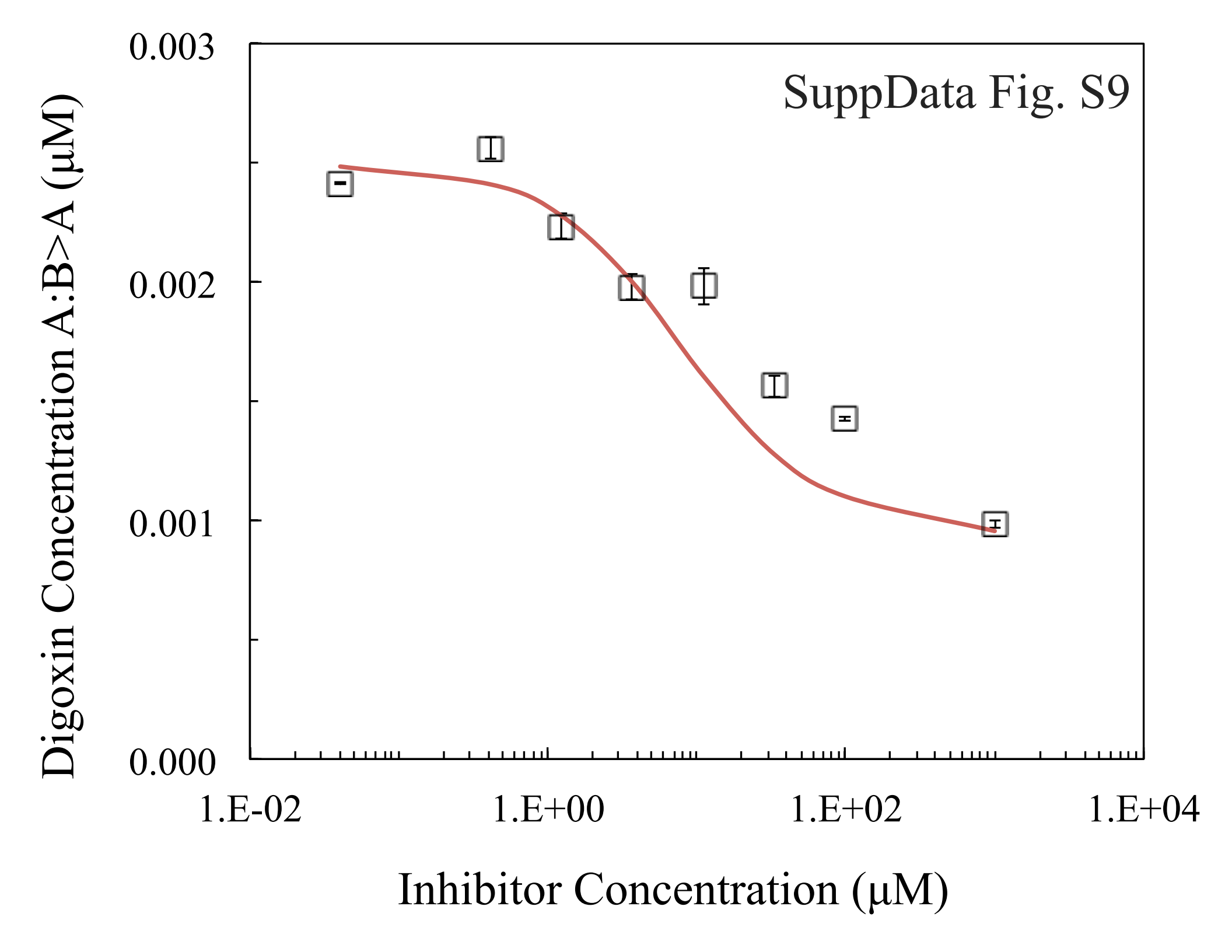
SuppData Fig. S9
Digoxin Concentration A:B>A (μM)
0.003
0.002
0.001
0.000
1.E-02
1.E+00
1.E+02
1.E+04
Inhibitor Concentration (μM)

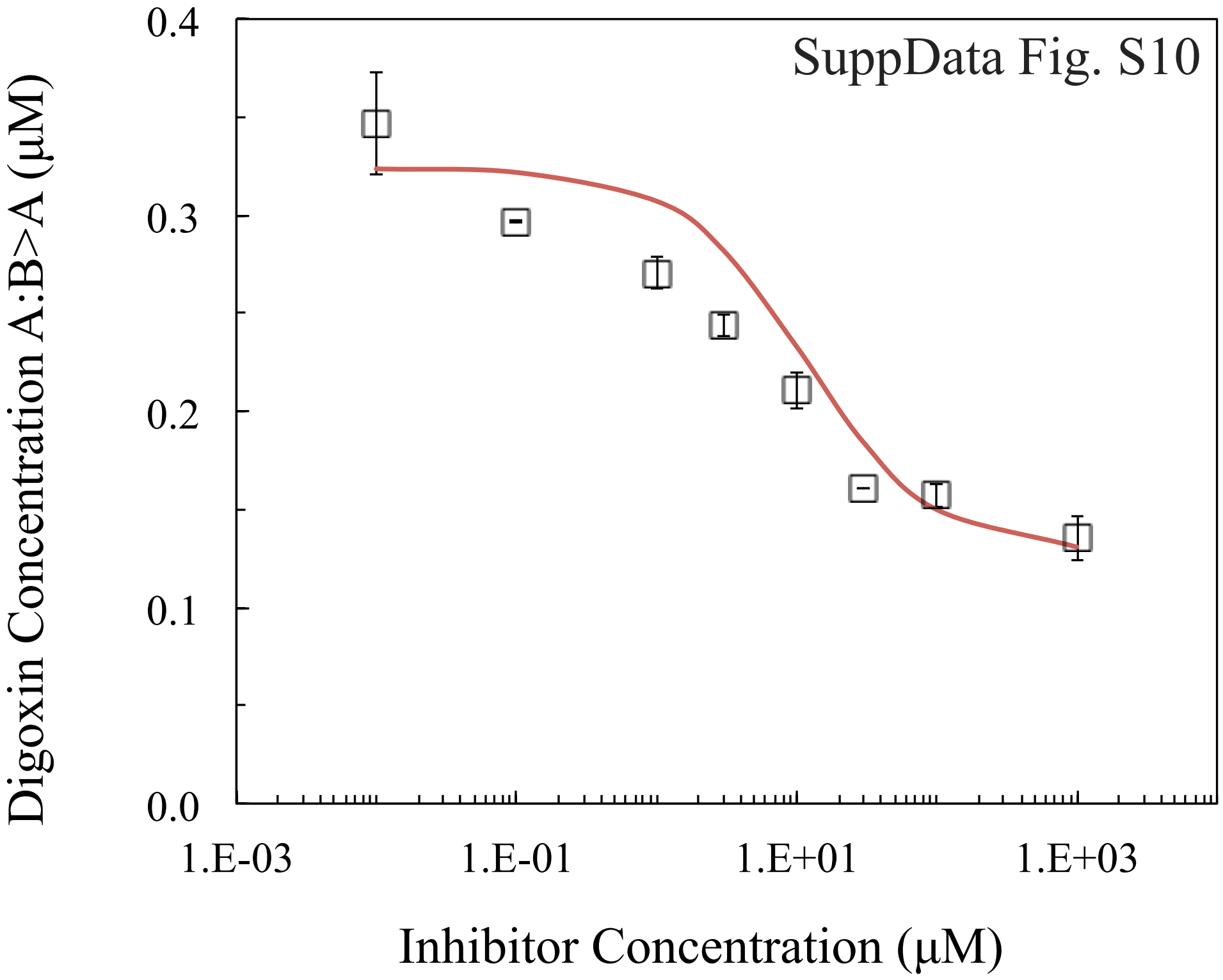
SuppData Fig. S10
Digoxin Concentration A:B>A (μM)
0.4
0.3
0.2
0.1
0.0
1.E-03
1.E-01
1.E+01
1.E+03
Inhibitor Concentration (μM)

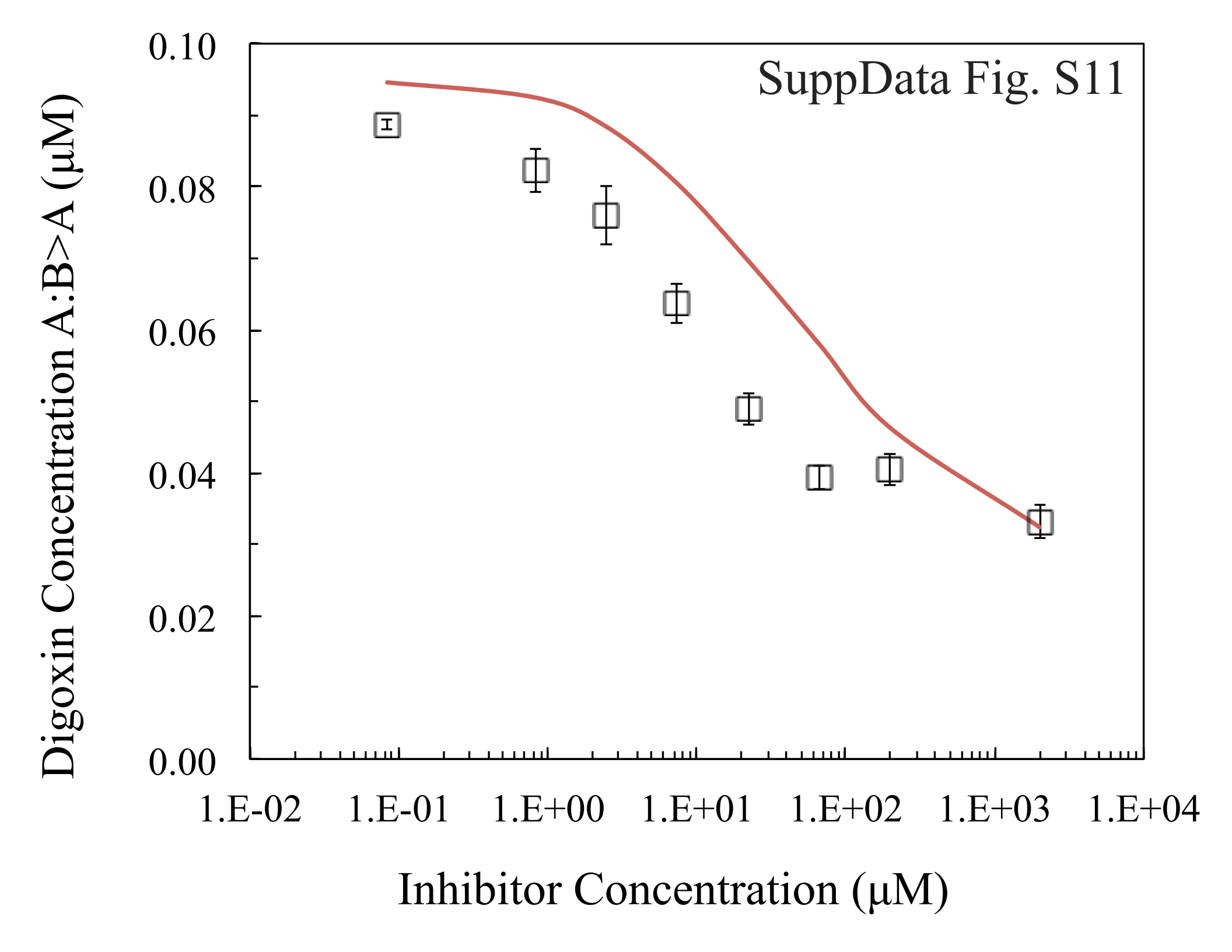
SuppData Fig. S11
Digoxin Concentration A:B>A (µM)
0.10
0.08
0.06
0.04
0.02
0.00
1.E-02
1.E-01
1.E+00
1.E+01
1.E+02
1.E+03
1.E+04
Inhibitor Concentration (µM)

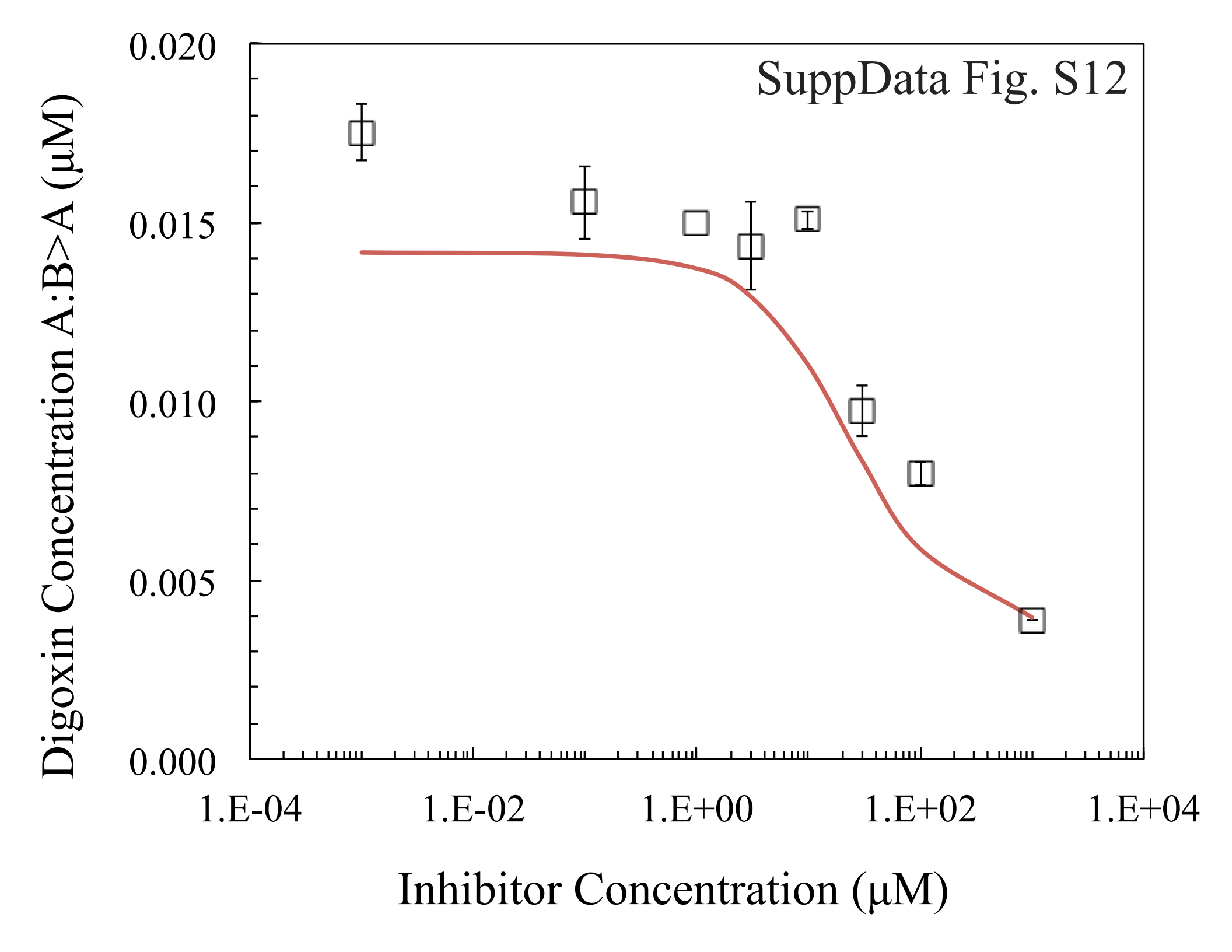
SuppData Fig. S12
Digoxin Concentration A:B>A (μM)
0.020
0.015
0.010
0.005
0.000
1.E-04
1.E-02
1.E+00
1.E+02
1.E+04
Inhibitor Concentration (μM)

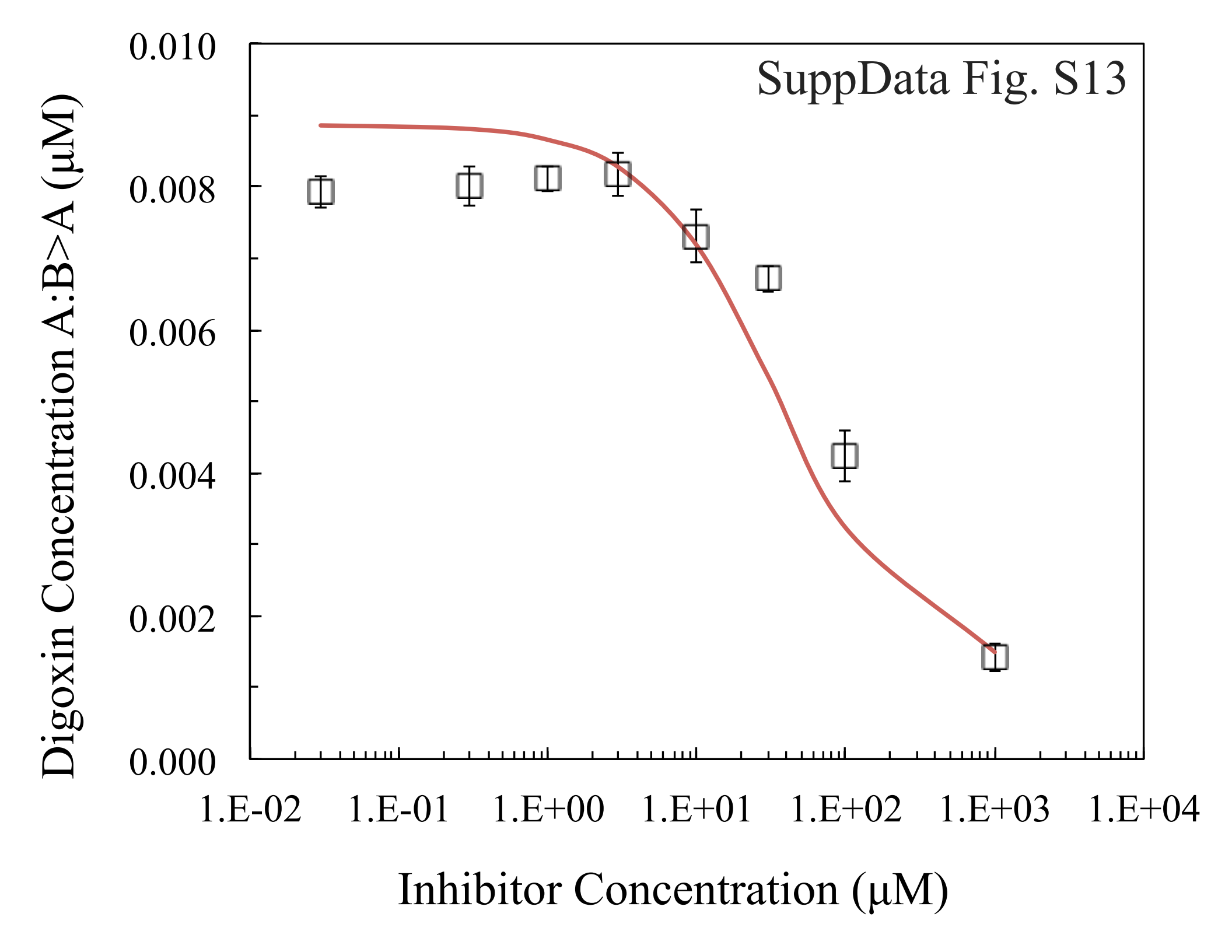
SuppData Fig. S13
0.010
0.008
0.006
0.004
0.002
0.000
Digoxin Concentration A:B>A (μM)
1.E-02
1.E-01
1.E+00
1.E+01
1.E+02
1.E+03
1.E+04
Inhibitor Concentration (μM)

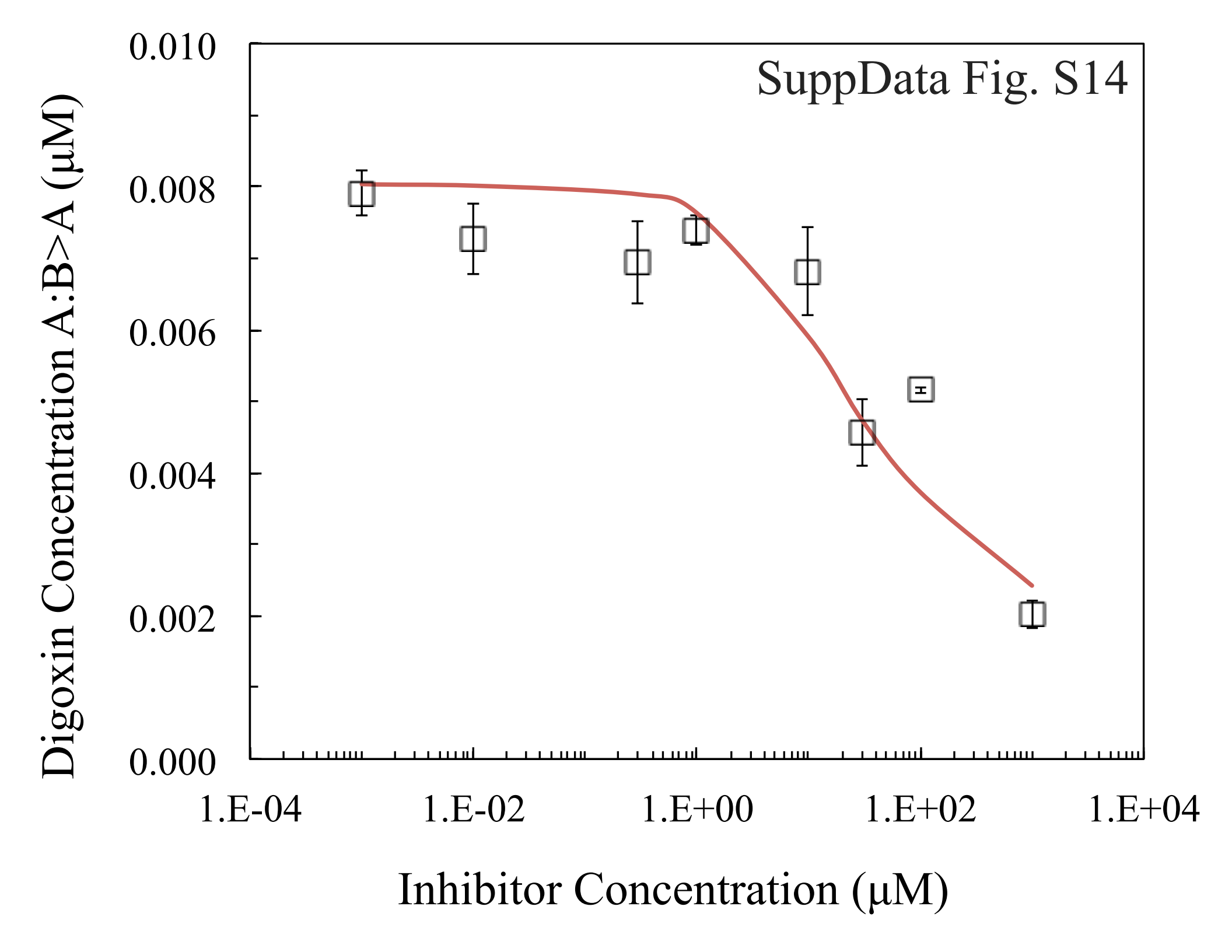
SuppData Fig. S14
Digoxin Concentration A:B>A (μM)
0.010
0.008
0.006
0.004
0.002
0.000
1.E-04
1.E-02
1.E+00
1.E+02
1.E+04
Inhibitor Concentration (μM)

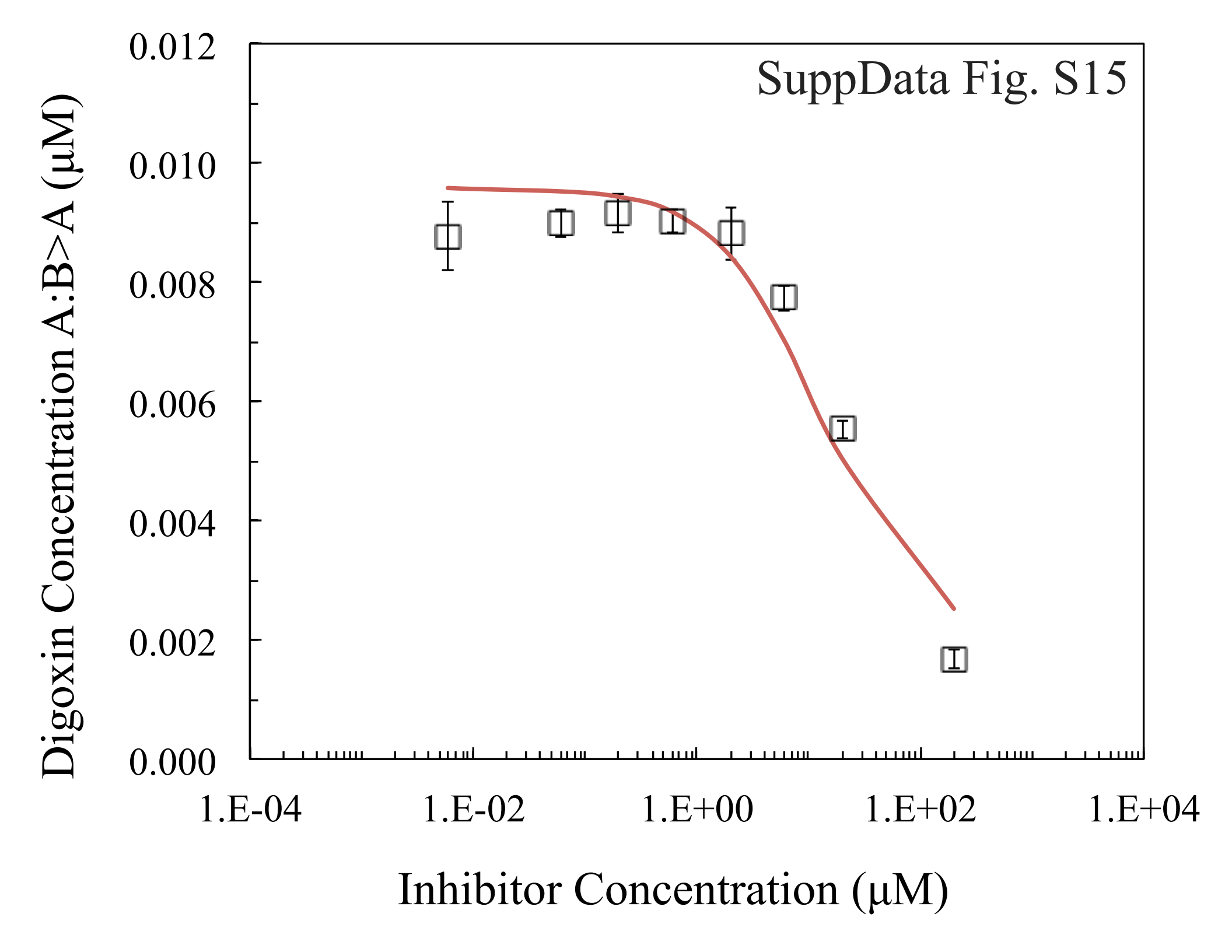
SuppData Fig. S15
0.012
0.010
0.008
0.006
0.004
0.002
0.000
Digoxin Concentration A:B>A (µM)
1.E-04
1.E-02
1.E+00
1.E+02
1.E+04
Inhibitor Concentration (µM)

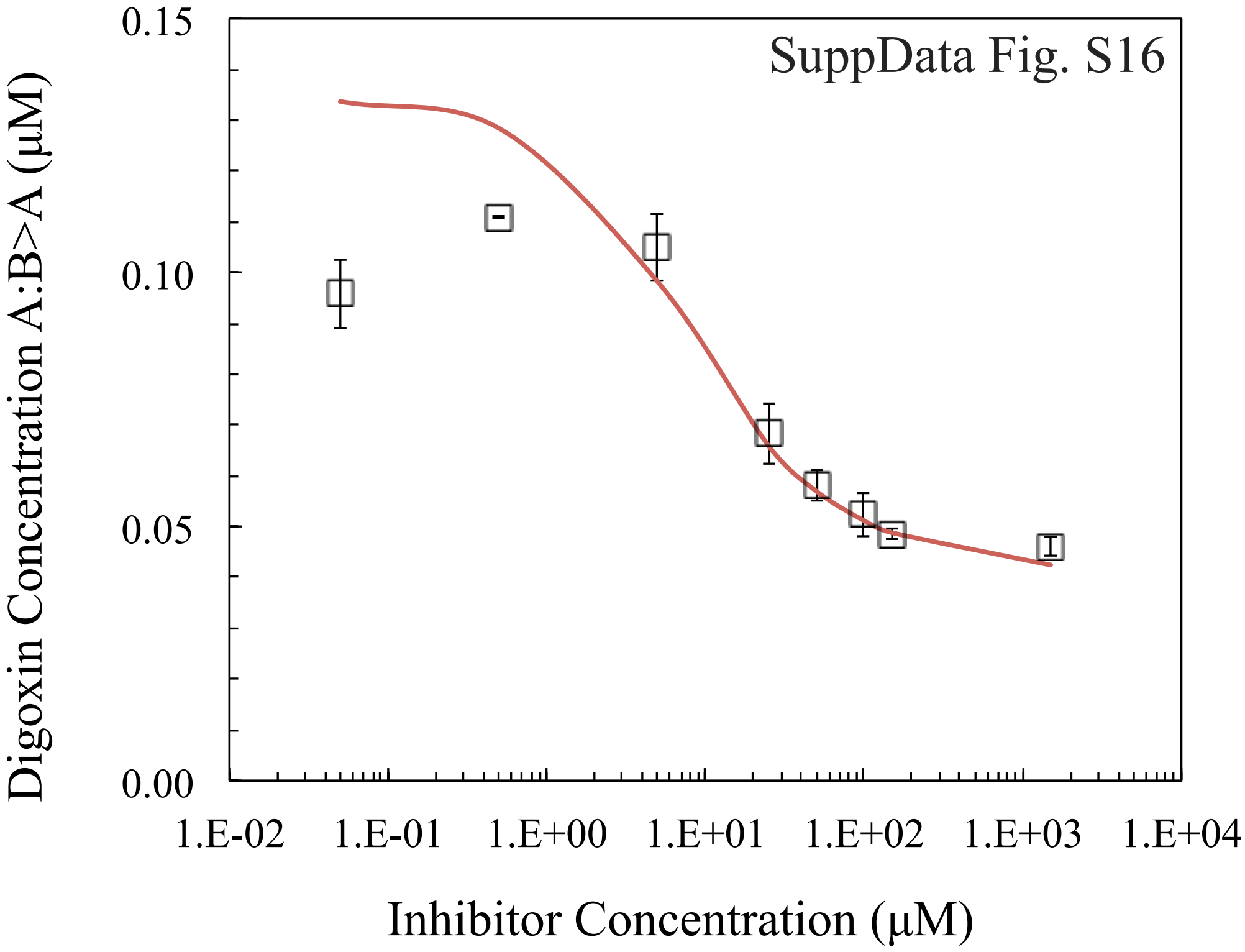
SuppData Fig. S16
Digoxin Concentration A:B>A (μM)
0.15
0.10
0.05
0.00
1.E-02
1.E-01
1.E+00
1.E+01
1.E+02
1.E+03
1.E+04
Inhibitor Concentration (μM)

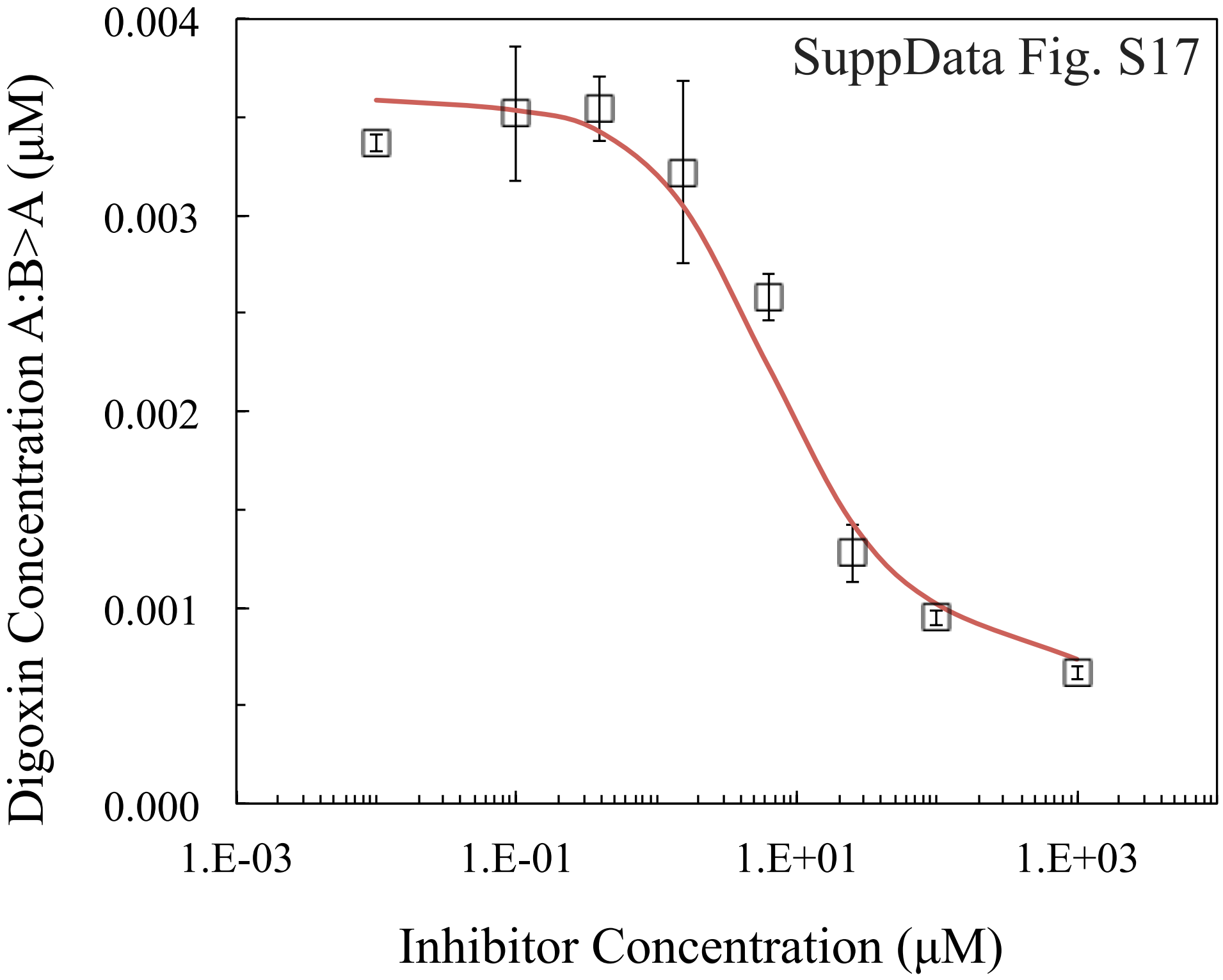
SuppData Fig. S17
Digoxin Concentration A:B>A (μM)
0.004
0.003
0.002
0.001
0.000
1.E-03
1.E-01
1.E+01
1.E+03
Inhibitor Concentration (μM)

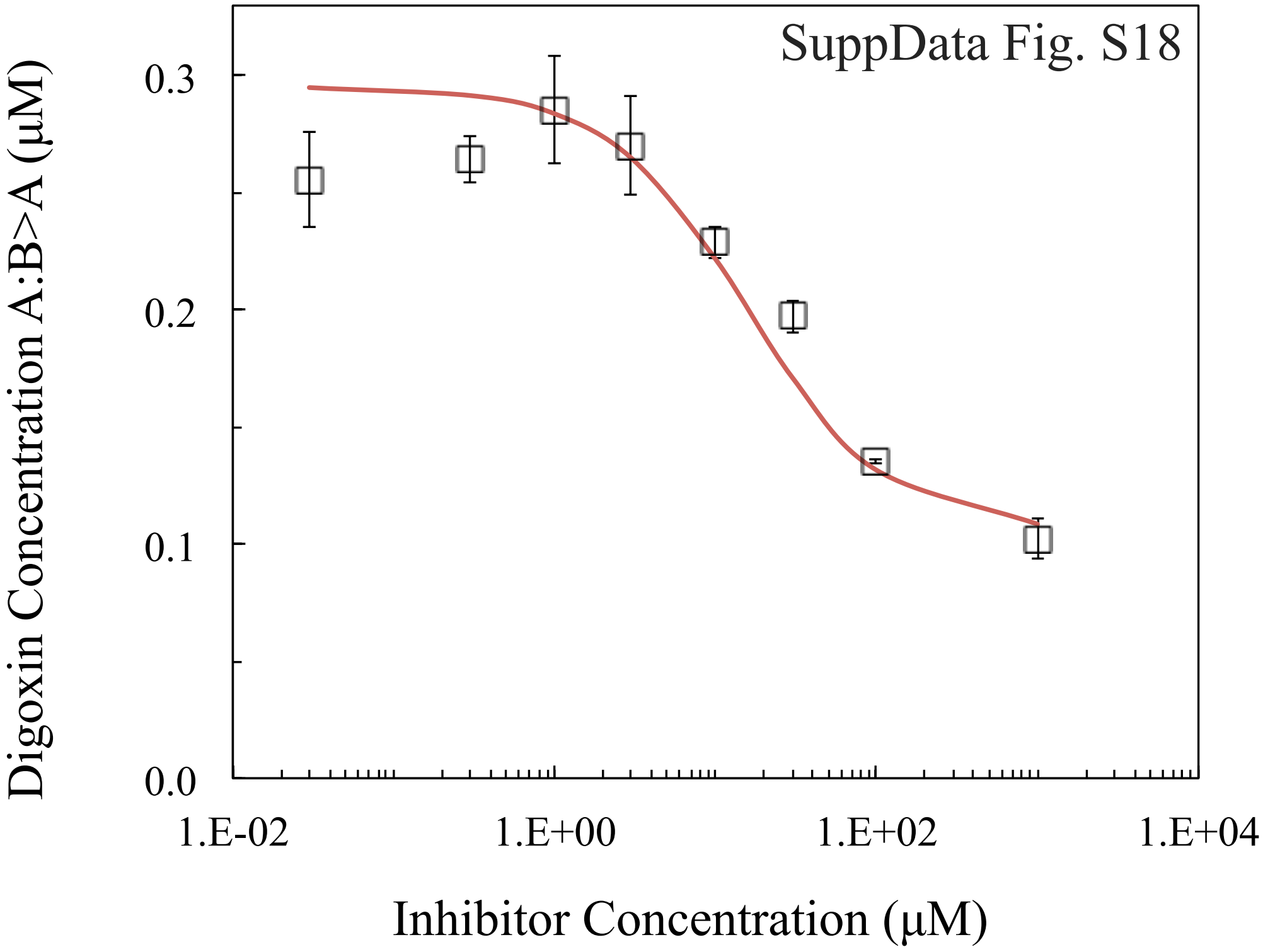
SuppData Fig. S18
Digoxin Concentration A:B>A (μM)
0.3
0.2
0.1
0.0
1.E-02
1.E+00
1.E+02
1.E+04
Inhibitor Concentration (μM)

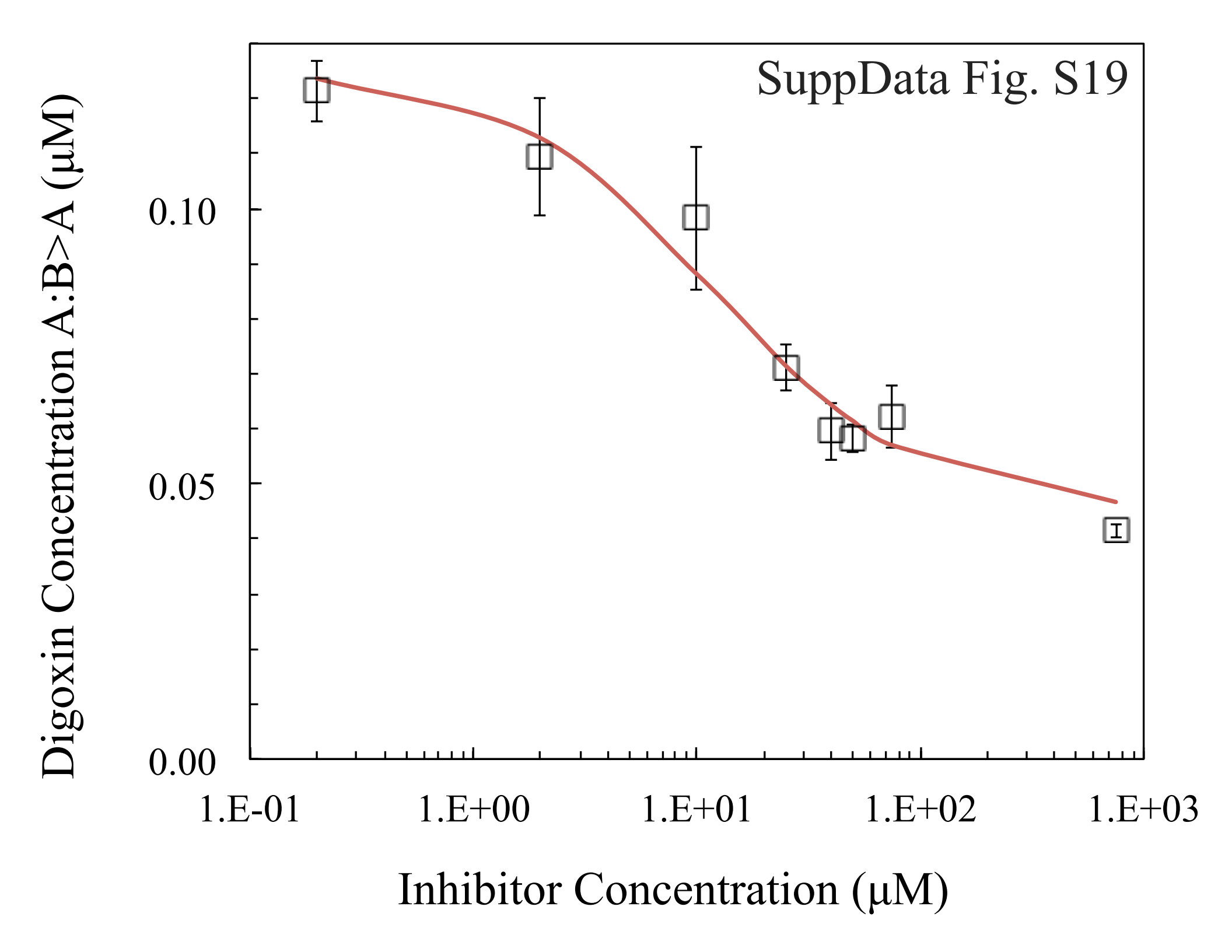
SuppData Fig. S19
Digoxin Concentration A:B>A (μM)
0.10
0.05
0.00
1.E-01
1.E+00
1.E+01
1.E+02
1.E+03
Inhibitor Concentration (μM)

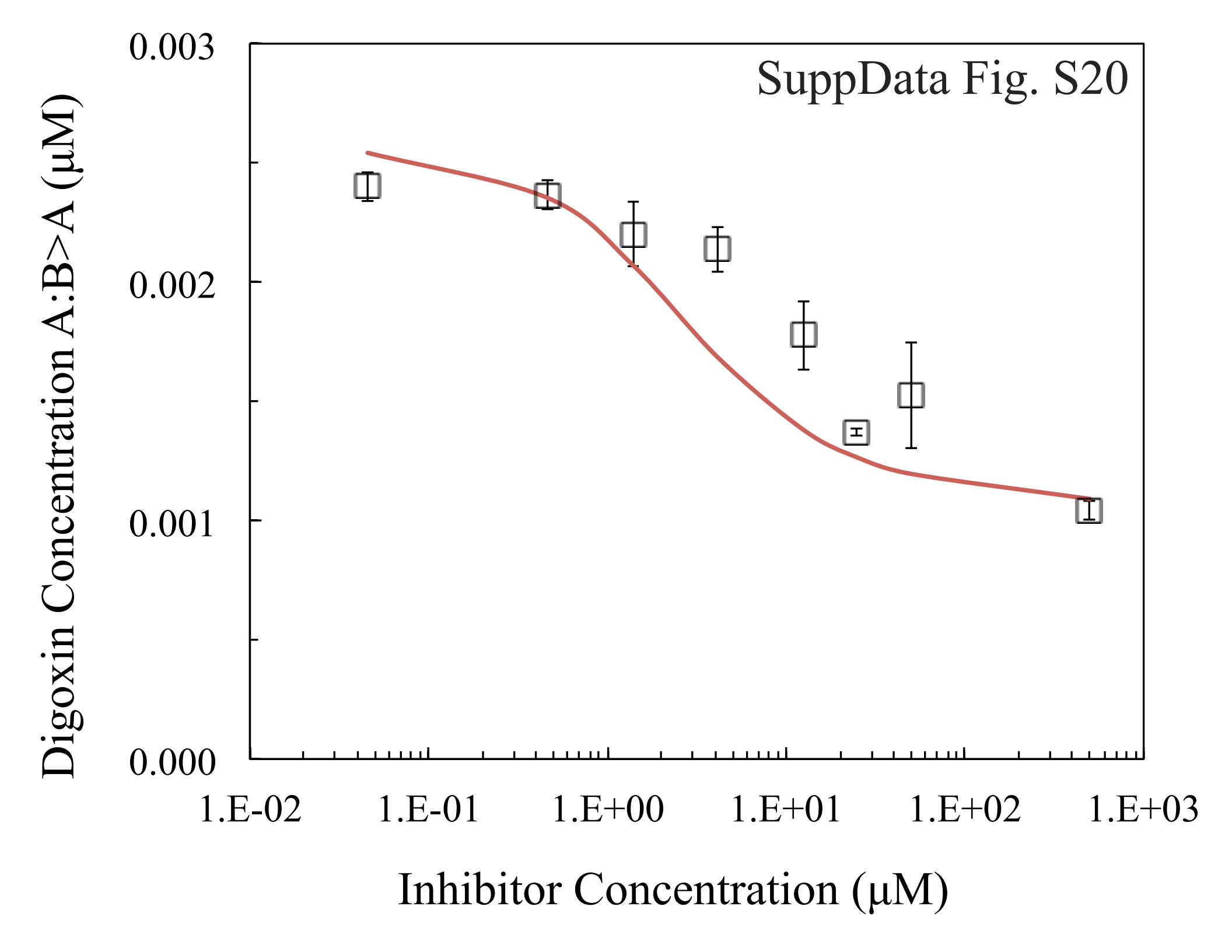
SuppData Fig. S20
Digoxin Concentration A:B>A (μM)
0.003
0.002
0.001
0.000
1.E-02
1.E-01
1.E+00
1.E+01
1.E+02
1.E+03
Inhibitor Concentration (μM)

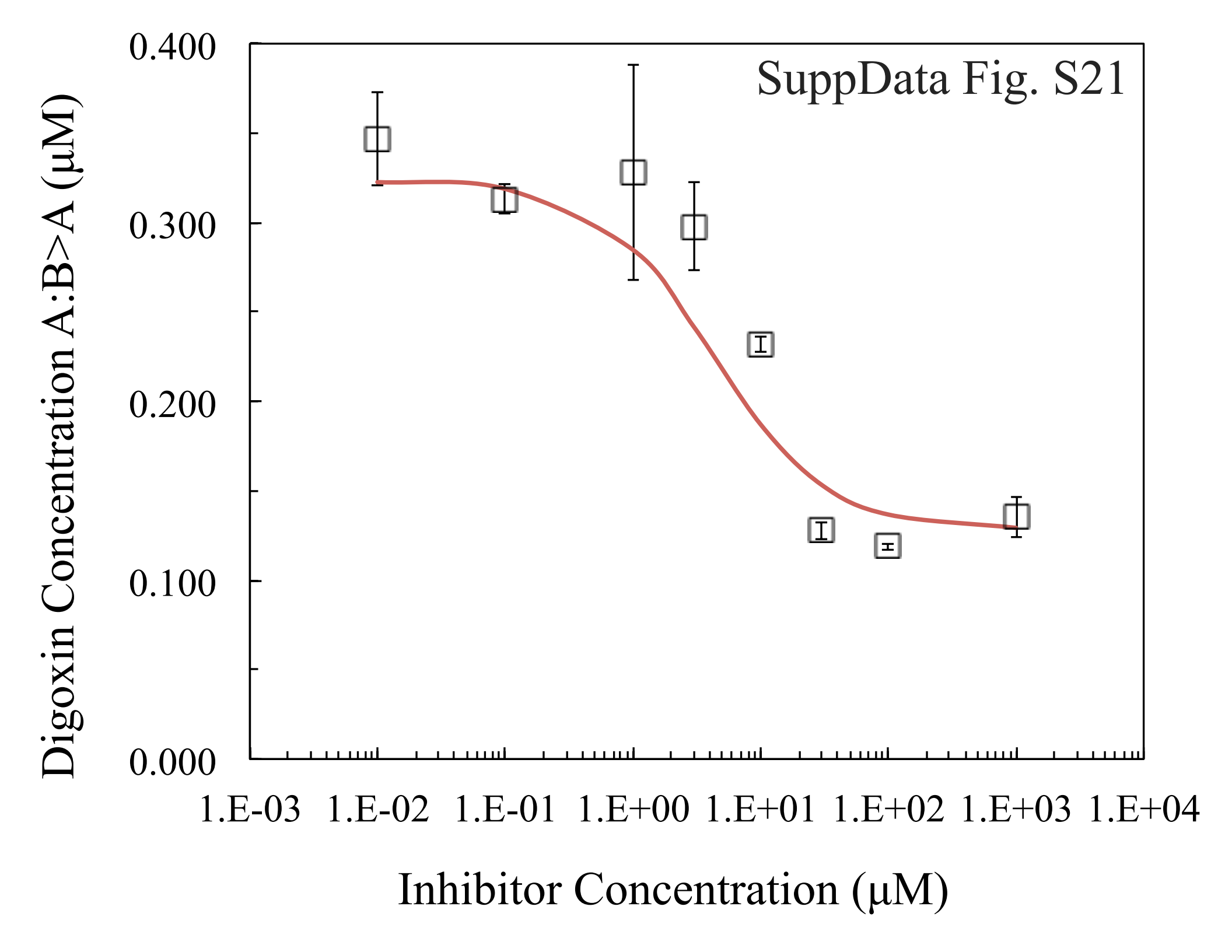
SuppData Fig. S21
Digoxin Concentration A:B>A (µM)
0.400
0.300
0.200
0.100
0.000
1.E-03
1.E-02
1.E-01
1.E+00
1.E+01
1.E+02
1.E+03
1.E+04
Inhibitor Concentration (µM)

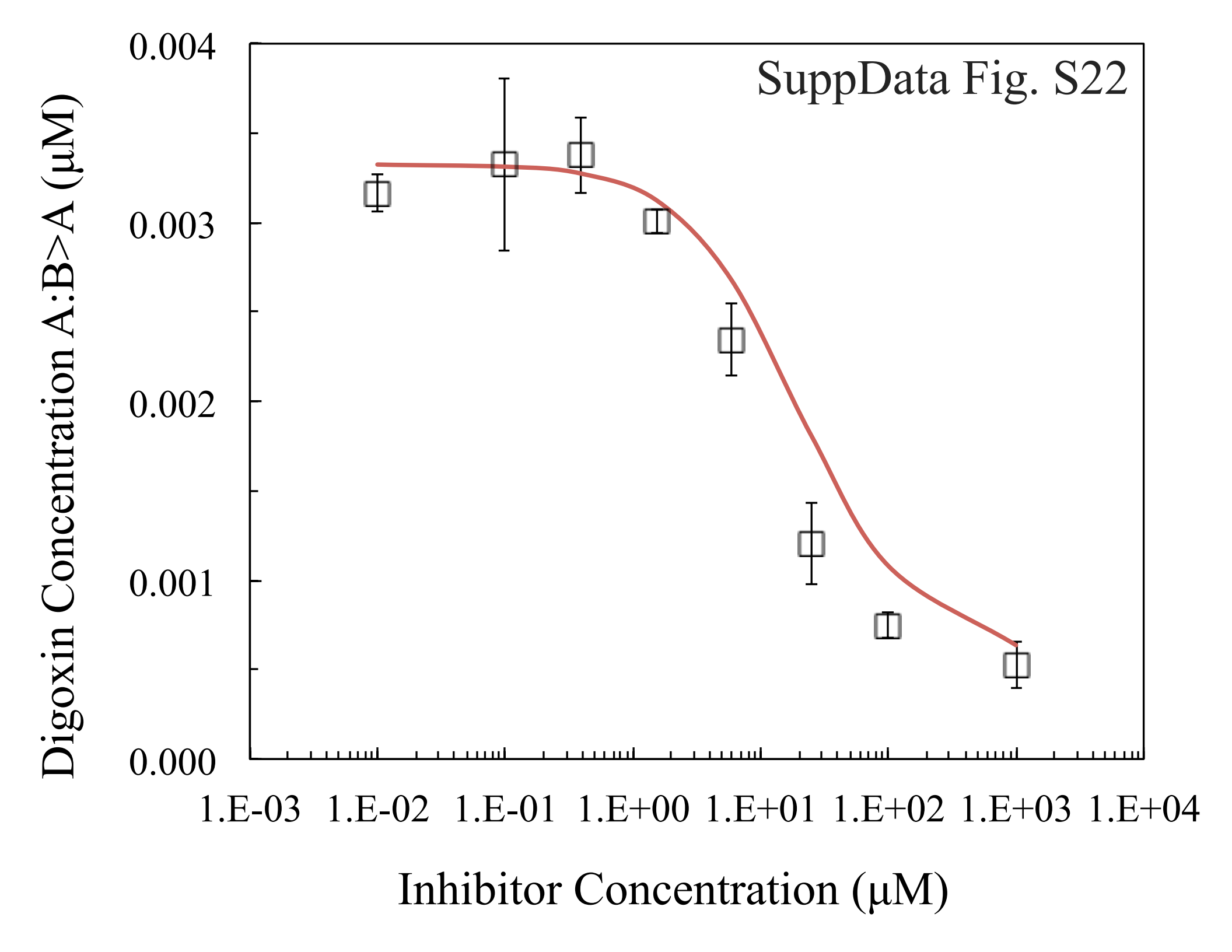
SuppData Fig. S22
Digoxin Concentration A:B>A (μM)
0.004
0.003
0.002
0.001
0.000
1.E-03
1.E-02
1.E-01
1.E+00
1.E+01
1.E+02
1.E+03
1.E+04
Inhibitor Concentration (μM)

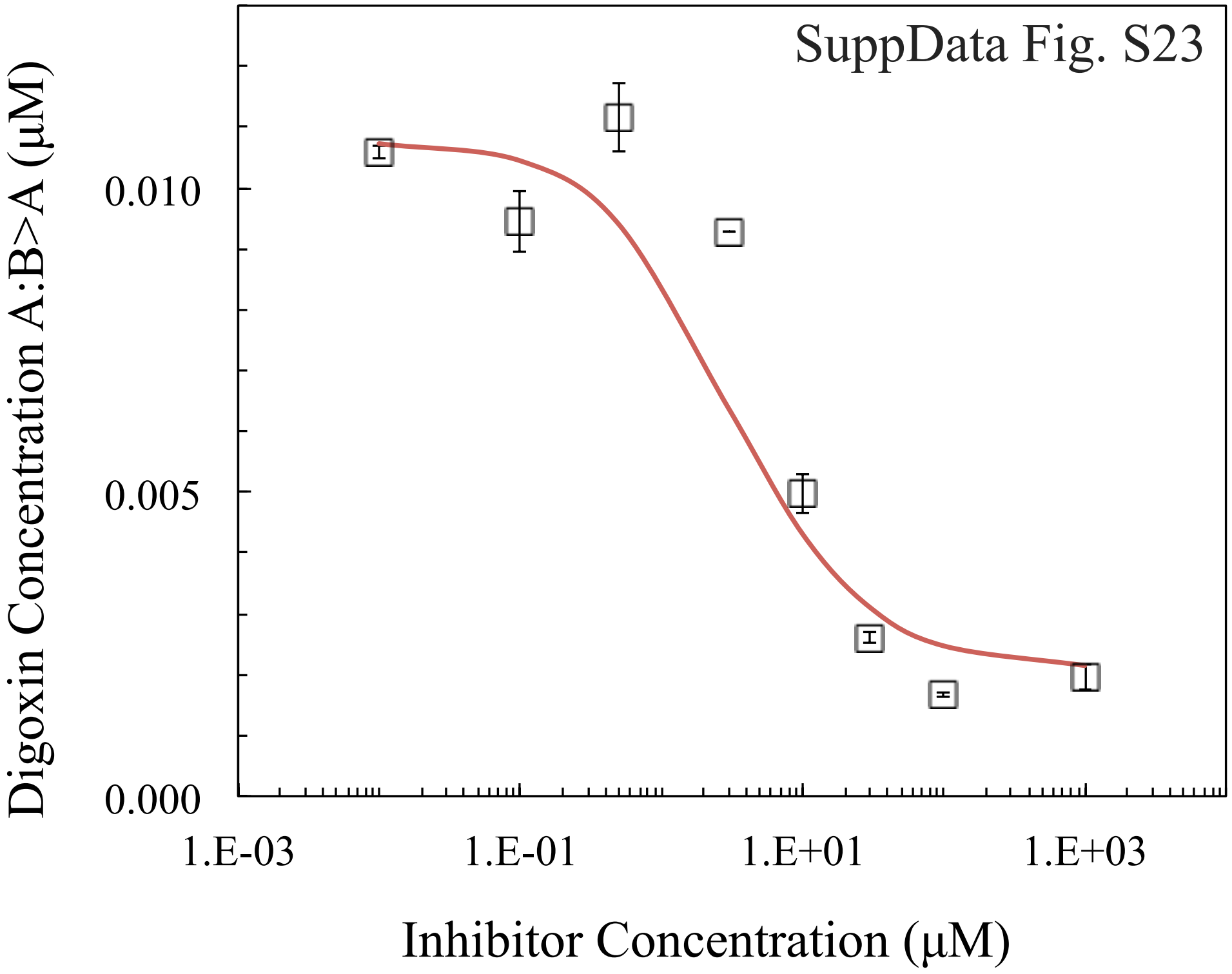
SuppData Fig. S23
Digoxin Concentration A:B>A (µM)
0.010
0.005
0.000
1.E-03
1.E-01
1.E+01
1.E+03
Inhibitor Concentration (µM)

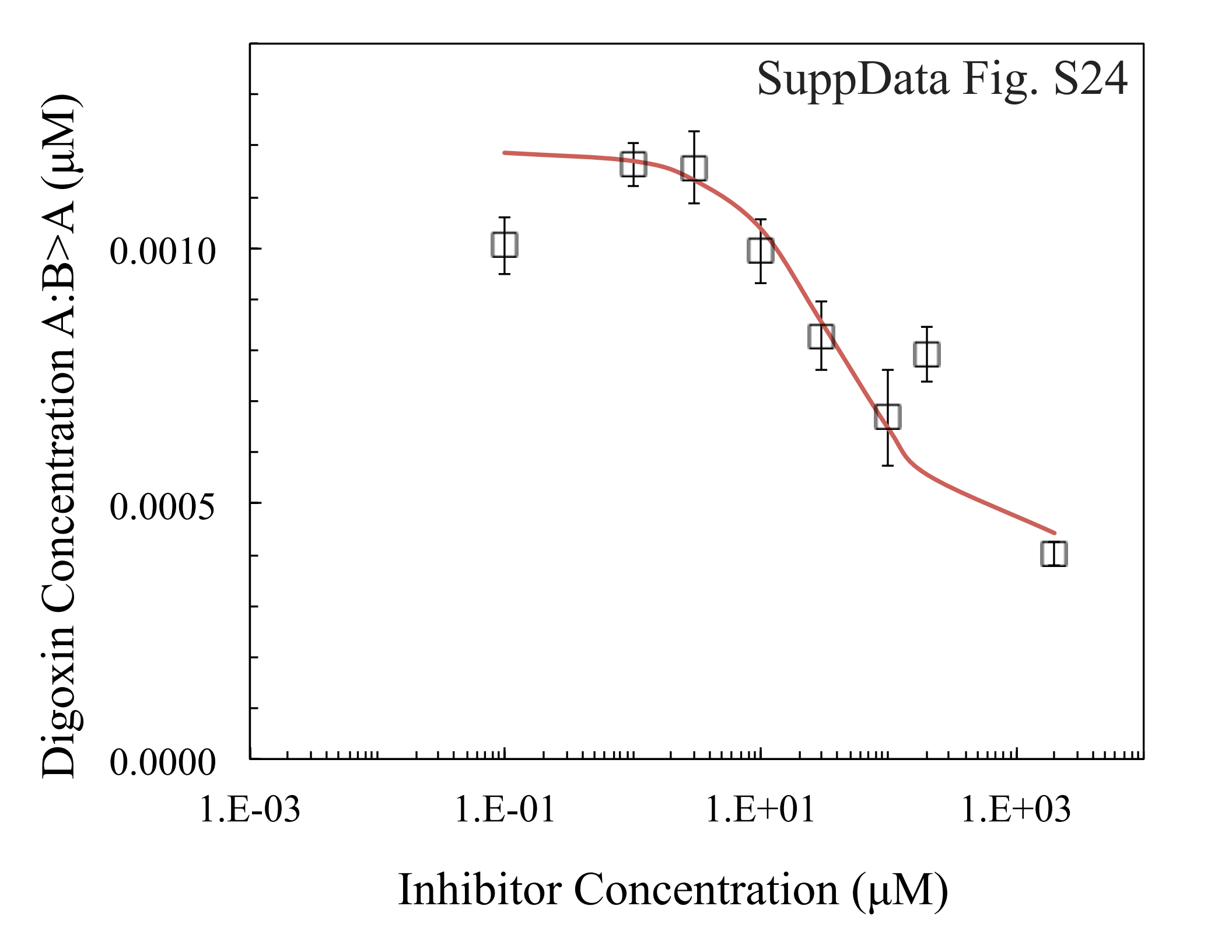
SuppData Fig. S24
Digoxin Concentration A:B>A (µM)
0.0010
0.0005
0.0000
1.E-03
1.E-01
1.E+01
1.E+03
Inhibitor Concentration (µM)

Supplemental Data Table S4. Figure Legends for Tables 2 and 4 in the main paper. For all figures, symbols show the B>A digoxin transport data, error bars show the data standard deviation and the line shows the fit to the data.

Fig. S25. Inhibition by carvedilol with MDCK-hMDR1-NKI cells from L02.
Fig. S26. Inhibition by diltiazem with MDCK-hMDR1-NKI cells from L02.
Fig. S27. Inhibition by isradipine with MDCK-hMDR1-NKI cells from L02.
Fig. S28. Inhibition by mibefradil with MDCK-hMDR1-NKI cells from L02.
Fig. S29. Inhibition by nicardipine with MDCK-hMDR1-NKI cells from L02.
Fig. S30. Inhibition by quinidine with MDCK-hMDR1-NKI cells from L02.
Fig. S31. Inhibition by ranolazine with MDCK-hMDR1-NKI cells from L02.
Fig. S32. Inhibition by verapamil with MDCK-hMDR1-NKI cells from L02.
Fig. S33. Inhibition by carvedilol with MDCK-hMDR1-NKI cells from L07.
Fig. S34. Inhibition by nicardipine with MDCK-hMDR1-NKI cells from L07.
Fig. S35. Inhibition by ranolazine with MDCK-hMDR1-NKI cells from L07.
Fig. S36. Inhibition by verapamil with MDCK-hMDR1-NKI cells from L07.
Fig. S37. Inhibition by carvedilol with Caco-2 cells from L06.
Fig. S38. Inhibition by diltiazem with Caco-2 cells from L06.
Fig. S39. Inhibition by isradipine with Caco-2 cells from L06.
Fig. S40. Inhibition by nicardipine with Caco-2 cells from L06.
Fig. S41. Inhibition by quinidine with Caco-2 cells from L06.
Fig. S42. Inhibition by ranolazine with Caco-2 cells from L06.
Fig. S43. Inhibition by verapamil with Caco-2 cells from L06.
Fig. S44. Inhibition by carvedilol with Caco-2 cells from L11.
Fig. S45. Inhibition by diltiazem with Caco-2 cells from L11.
Fig. S46. Inhibition by isradipine with Caco-2 cells from L11.
Fig. S47. Inhibition by nicardipine with Caco-2 cells from L11.
Fig. S48. Inhibition by quinidine with Caco-2 cells from L11.
Fig. S49. Inhibition by ranolazine with Caco-2 cells from L11.
Fig. S50. Inhibition by mibefradil with LLC-PK1-hMDR1-NKI cells from L02.
Fig. S51. Inhibition by quinidine with LLC-PK1-hMDR1-NKI cells from L02.

Fig. S52. Inhibition by ranolazine with LLC-PK1-hMDR1-NKI cells from L02.
Fig. S53. Inhibition by verapamil with LLC-PK1-hMDR1-NKI cells from L02.

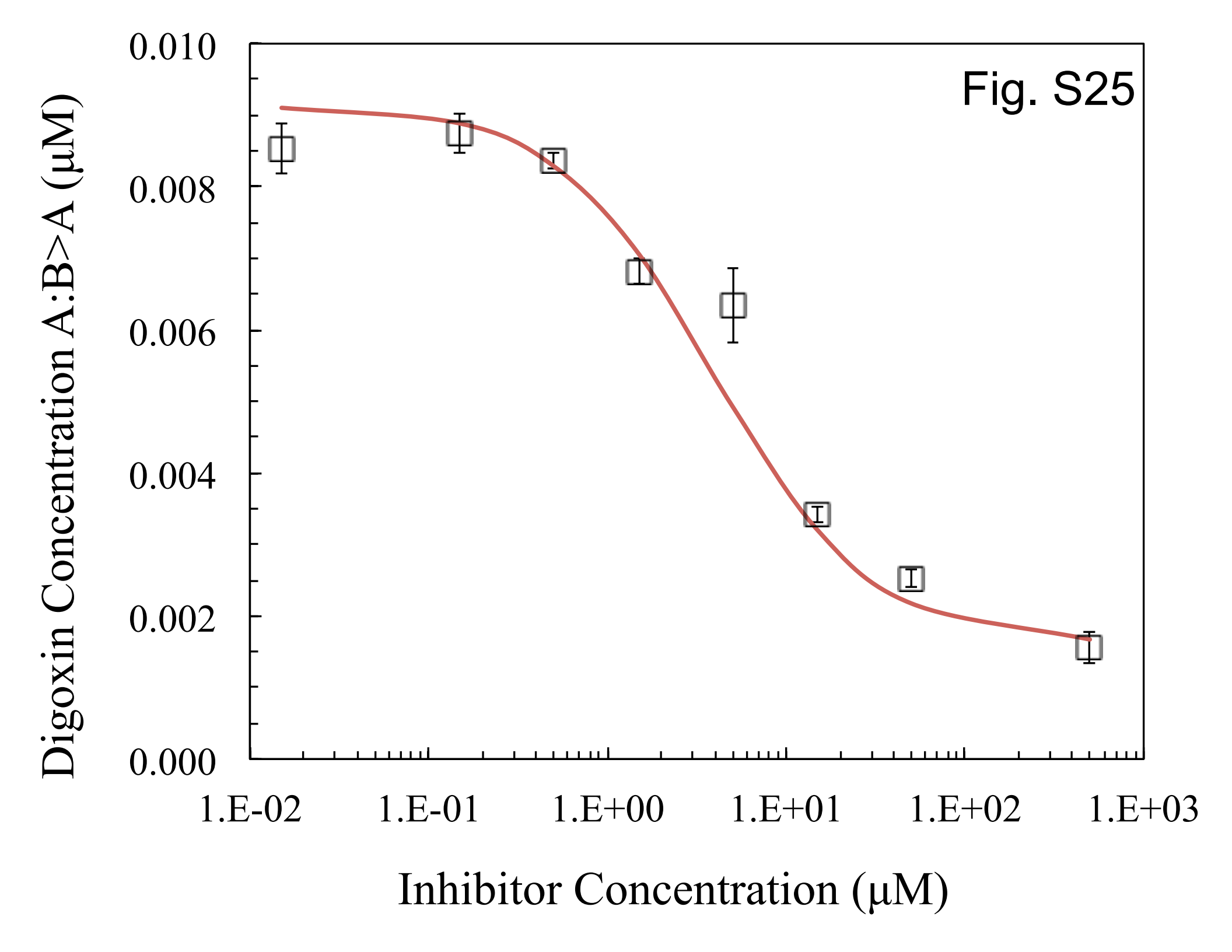
Fig. S25
Digoxin Concentration A:B>A (μM)
0.010
0.008
0.006
0.004
0.002
0.000
1.E-02
1.E-01
1.E+00
1.E+01
1.E+02
1.E+03
Inhibitor Concentration (μM)

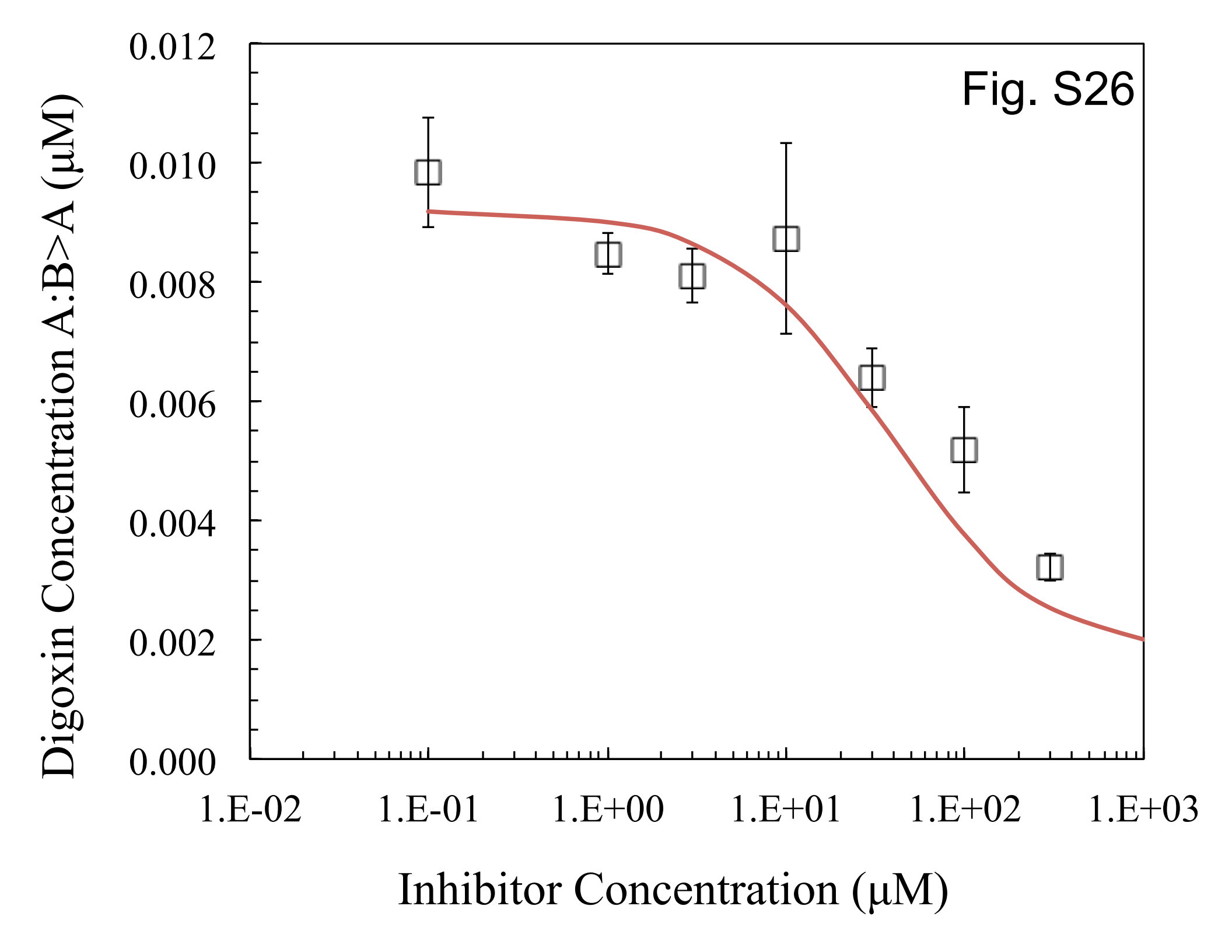
Fig. S26
Digoxin Concentration A:B>A (μM)
0.012
0.010
0.008
0.006
0.004
0.002
0.000
1.E-02
1.E-01
1.E+00
1.E+01
1.E+02
1.E+03
Inhibitor Concentration (μM)

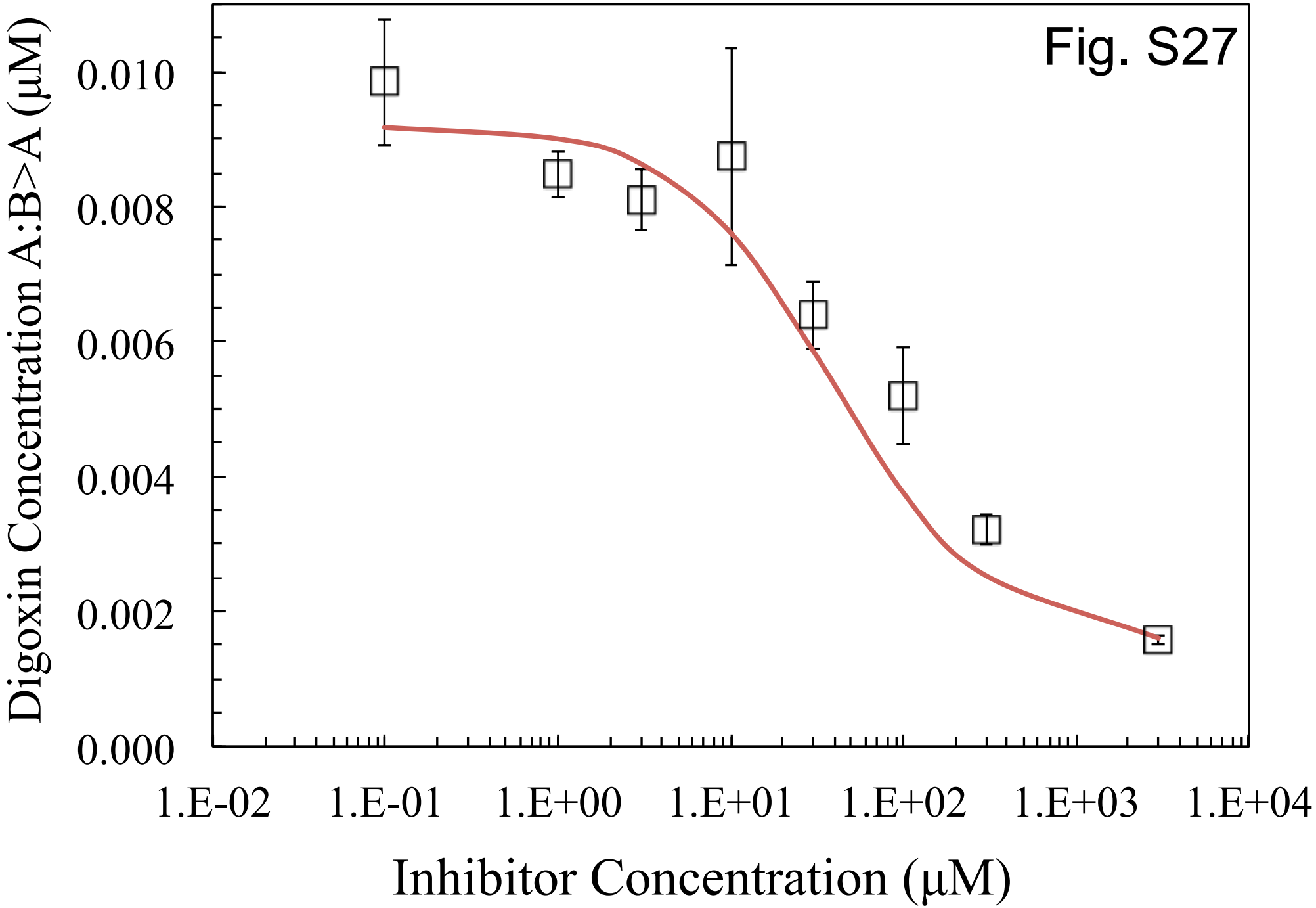
Fig. S27
Digoxin Concentration A:B>A (μM)
0.010
0.008
0.006
0.004
0.002
0.000
1.E-02
1.E-01
1.E+00
1.E+01
1.E+02
1.E+03
1.E+04
Inhibitor Concentration (μM)

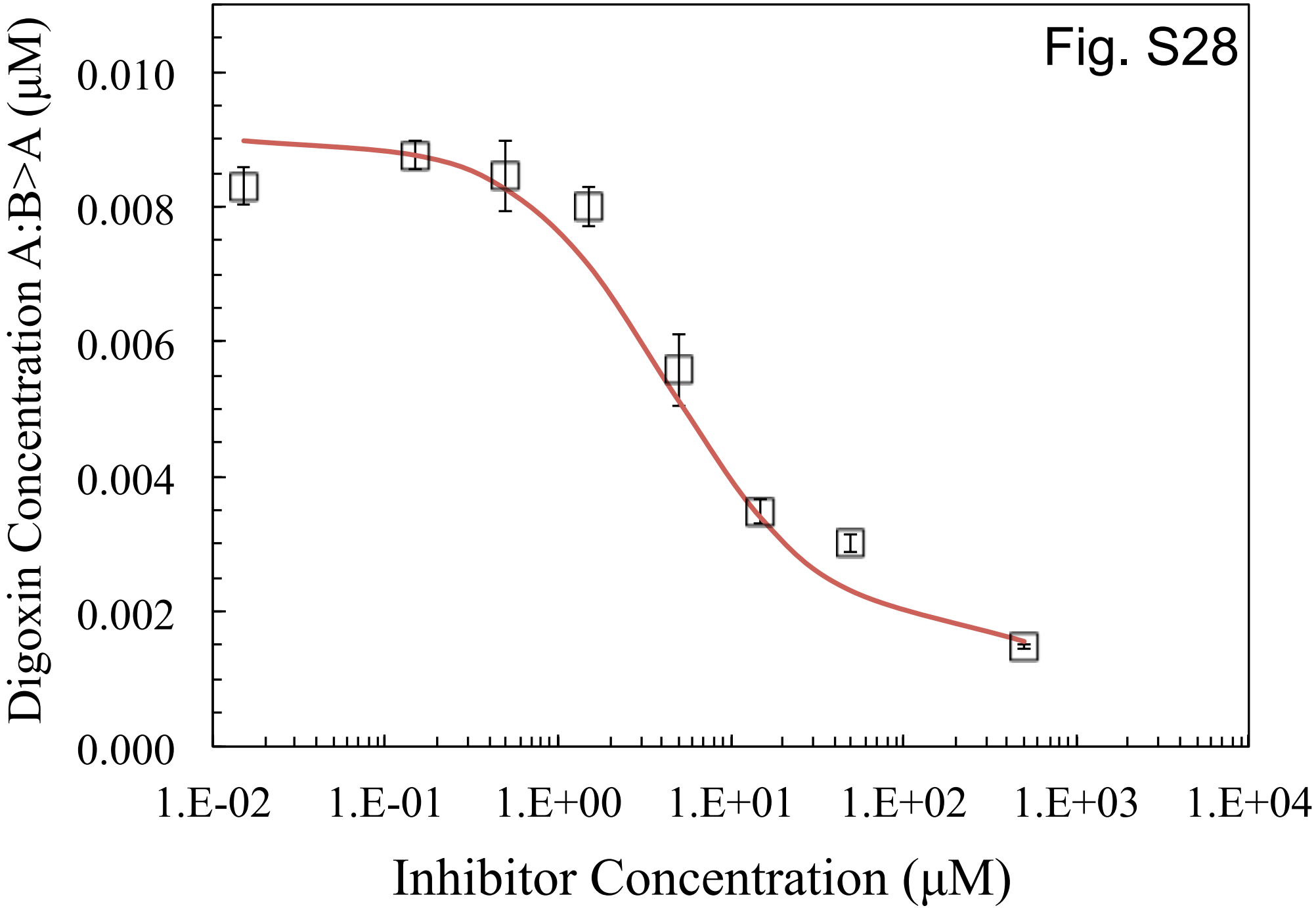
Fig. S28
Digoxin Concentration A:B>A (μM)
0.010
0.008
0.006
0.004
0.002
0.000
1.E-02
1.E-01
1.E+00
1.E+01
1.E+02
1.E+03
1.E+04
Inhibitor Concentration (μM)

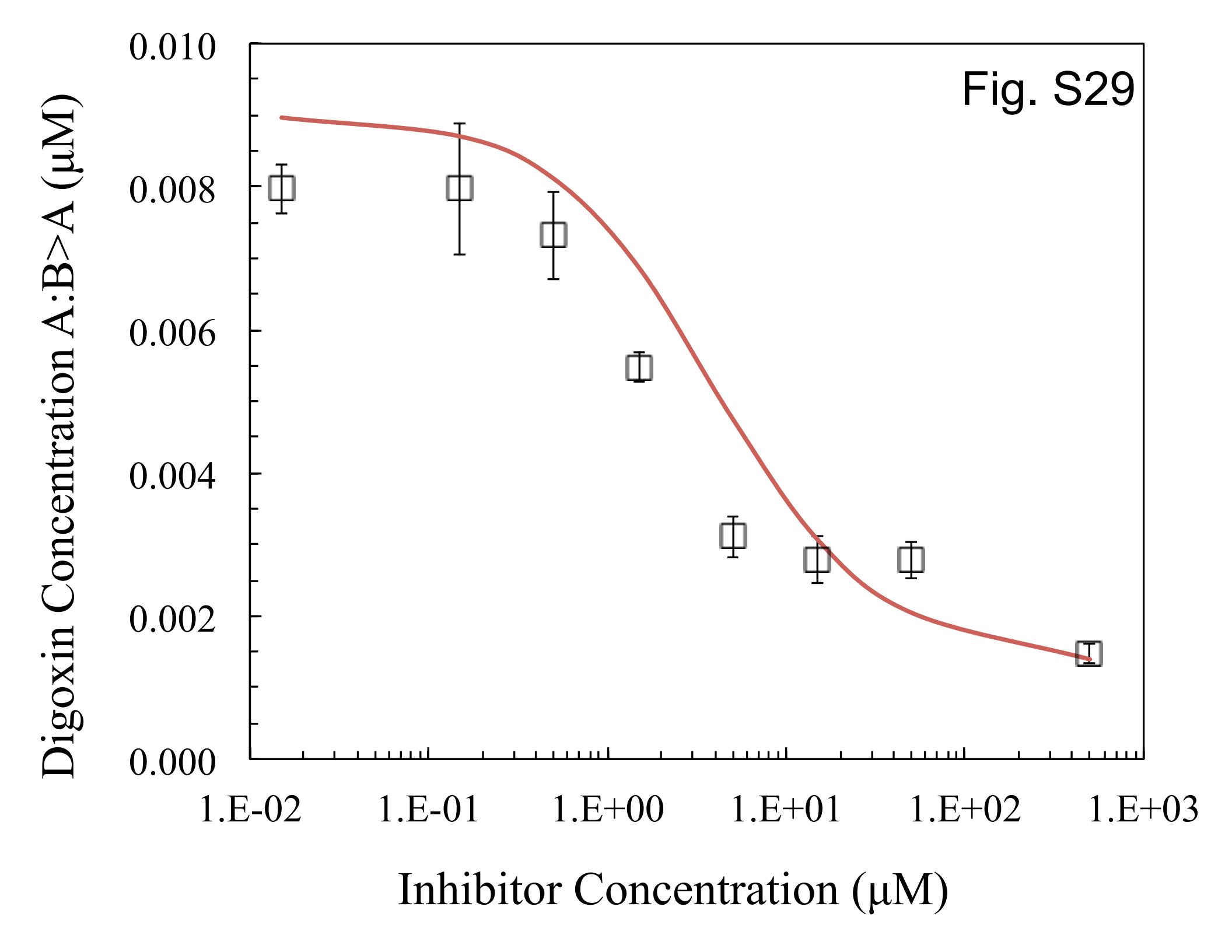
Fig. S29
Digoxin Concentration A:B>A (μM)
0.010
0.008
0.006
0.004
0.002
0.000
1.E-02
1.E-01
1.E+00
1.E+01
1.E+02
1.E+03
Inhibitor Concentration (μM)

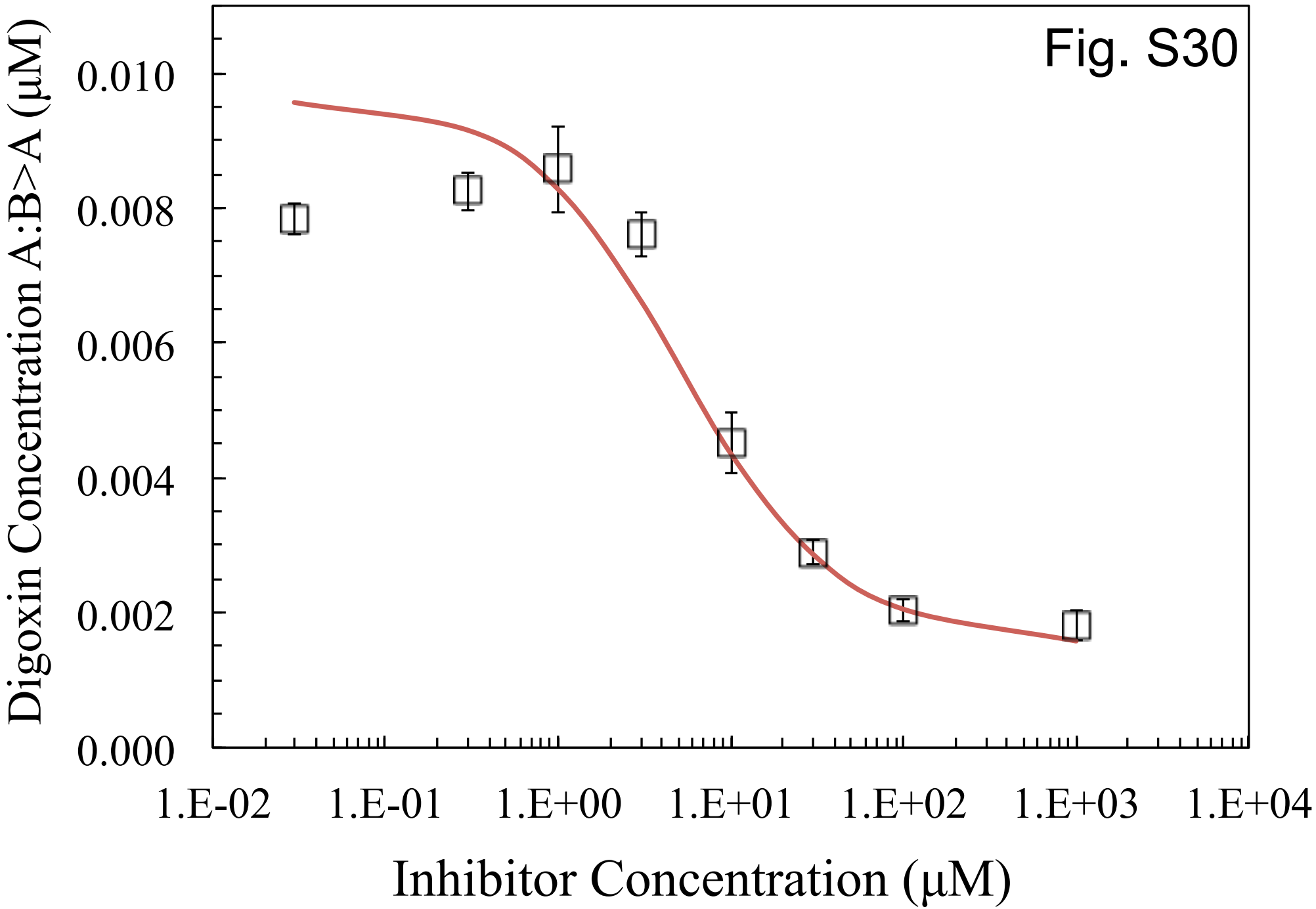
Fig. S30
Digoxin Concentration A:B>A (μM)
0.010
0.008
0.006
0.004
0.002
0.000
1.E-02
1.E-01
1.E+00
1.E+01
1.E+02
1.E+03
1.E+04
Inhibitor Concentration (μM)

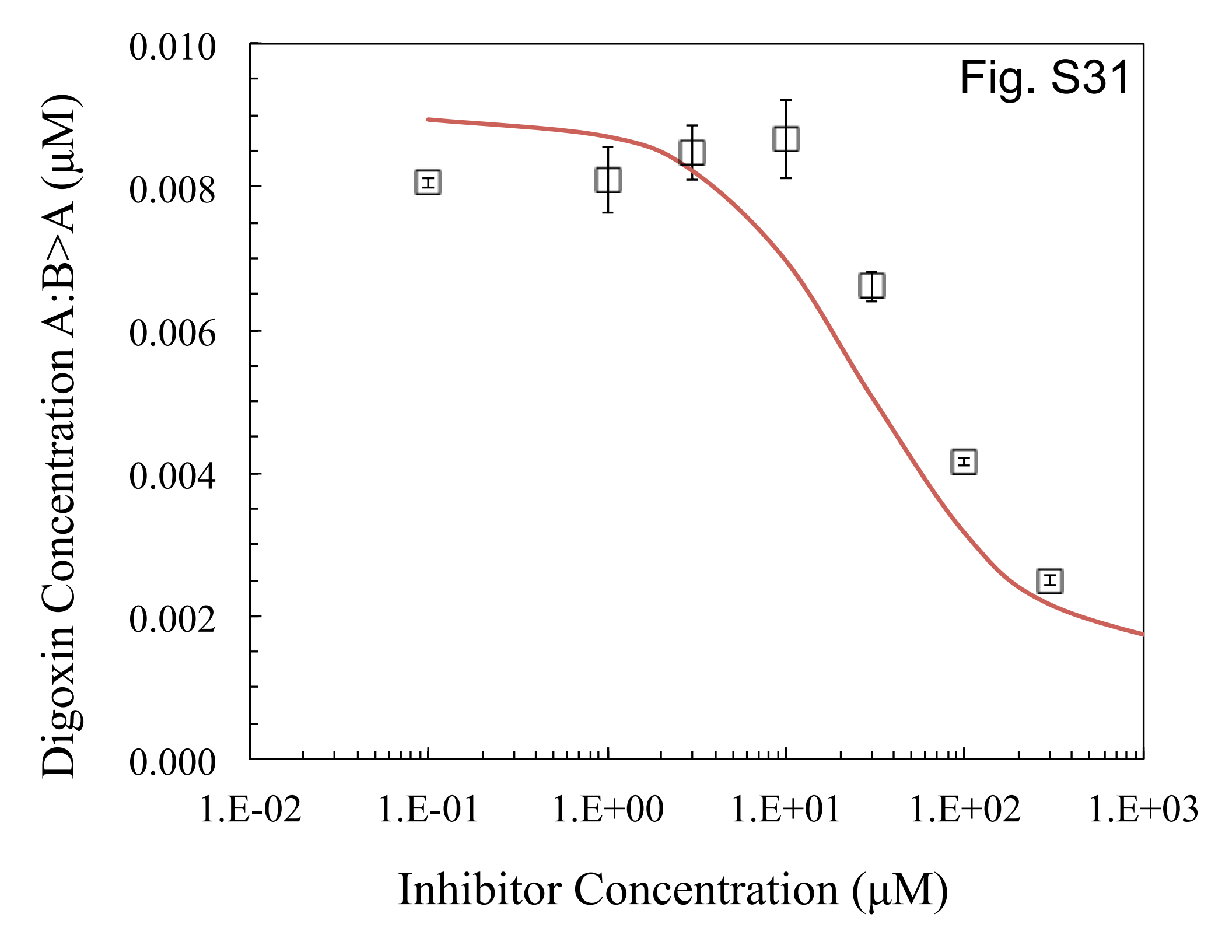
Fig. S31
Digoxin Concentration A:B>A (μM)
0.010
0.008
0.006
0.004
0.002
0.000
1.E-02
1.E-01
1.E+00
1.E+01
1.E+02
1.E+03
Inhibitor Concentration (μM)

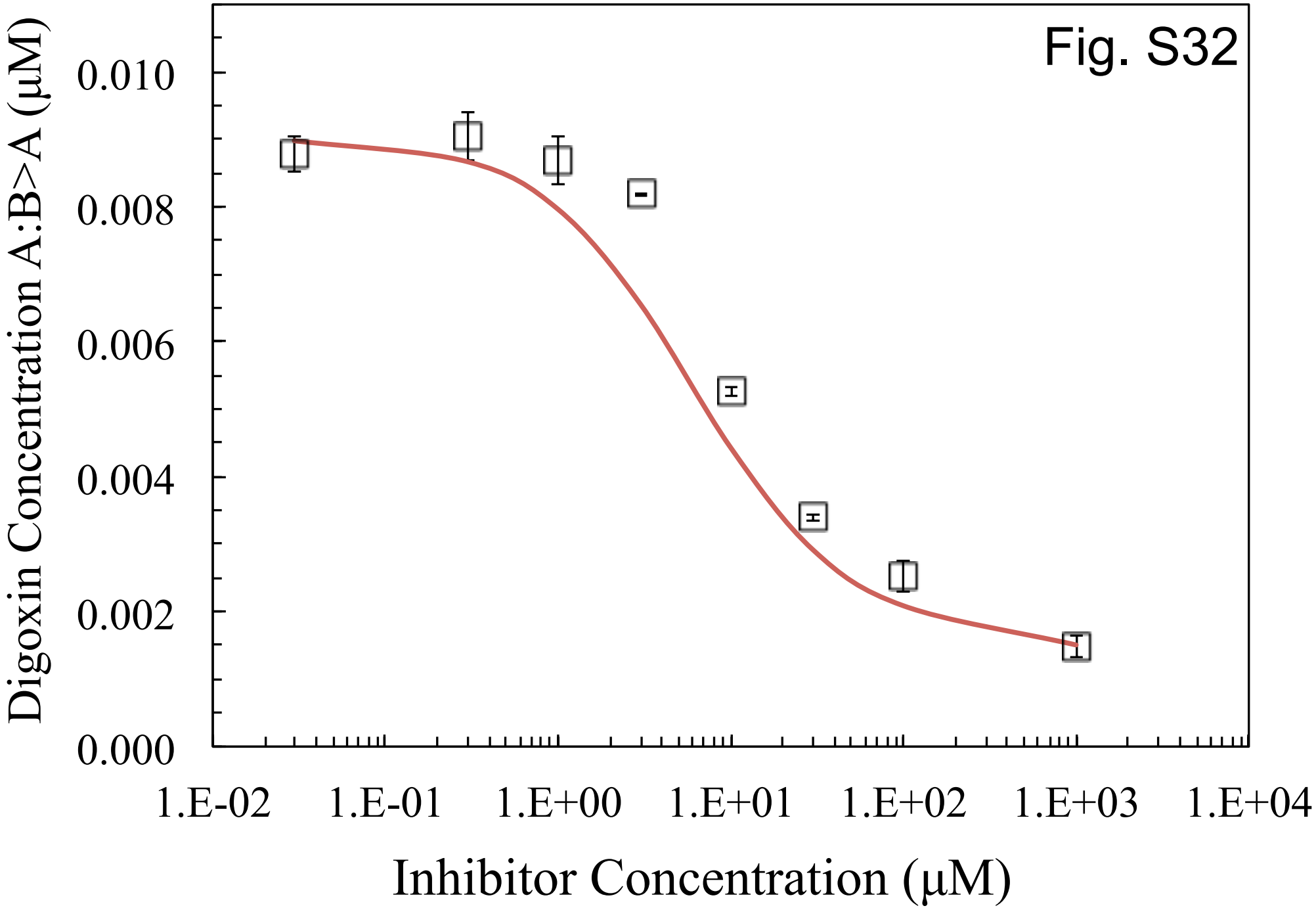
Fig. S32
Digoxin Concentration A:B>A (μM)
0.010
0.008
0.006
0.004
0.002
0.000
1.E-02
1.E-01
1.E+00
1.E+01
1.E+02
1.E+03
1.E+04
Inhibitor Concentration (μM)

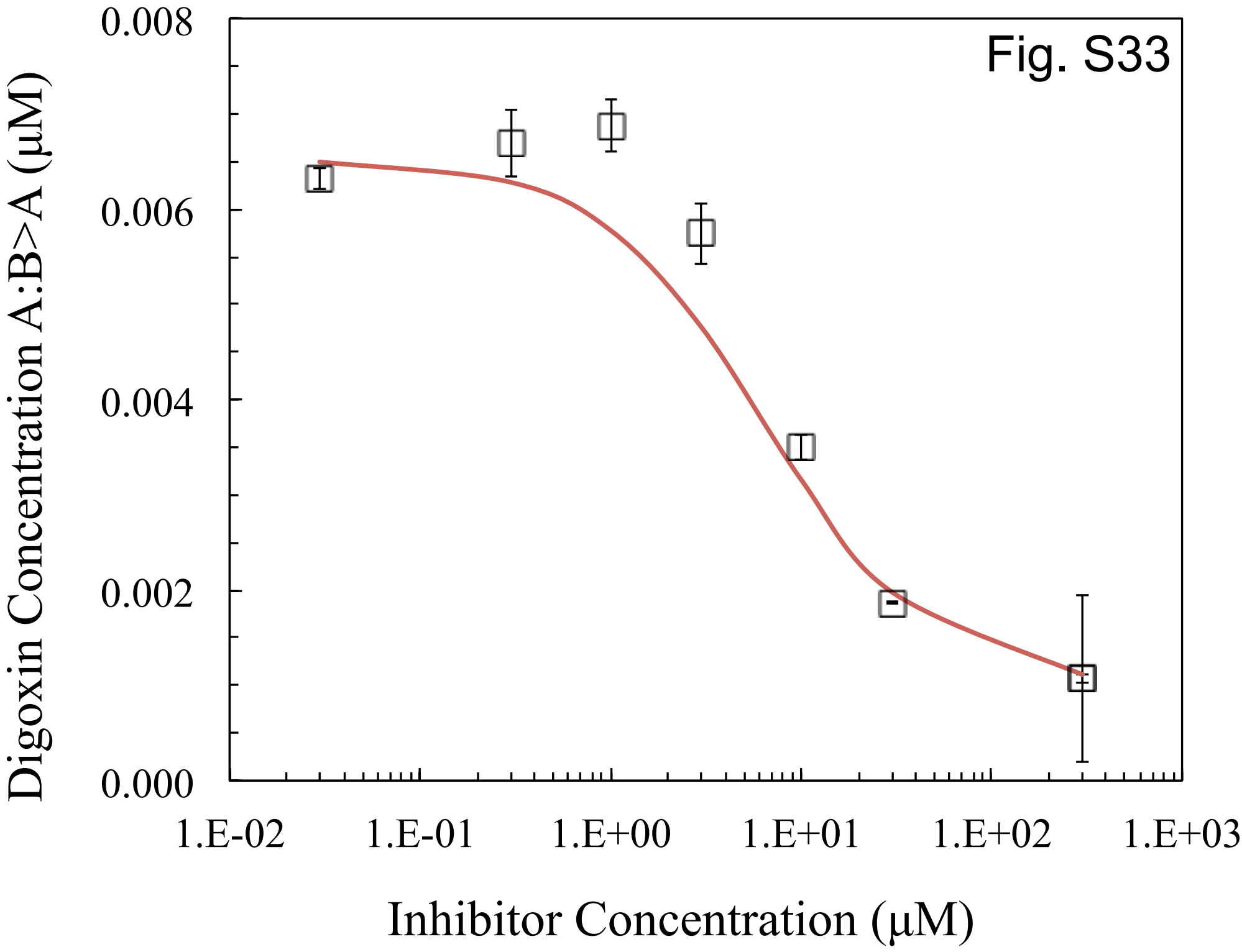
Fig. S33
Digoxin Concentration A:B>A (μM)
0.008
0.006
0.004
0.002
0.000
1.E-02
1.E-01
1.E+00
1.E+01
1.E+02
1.E+03
Inhibitor Concentration (μM)

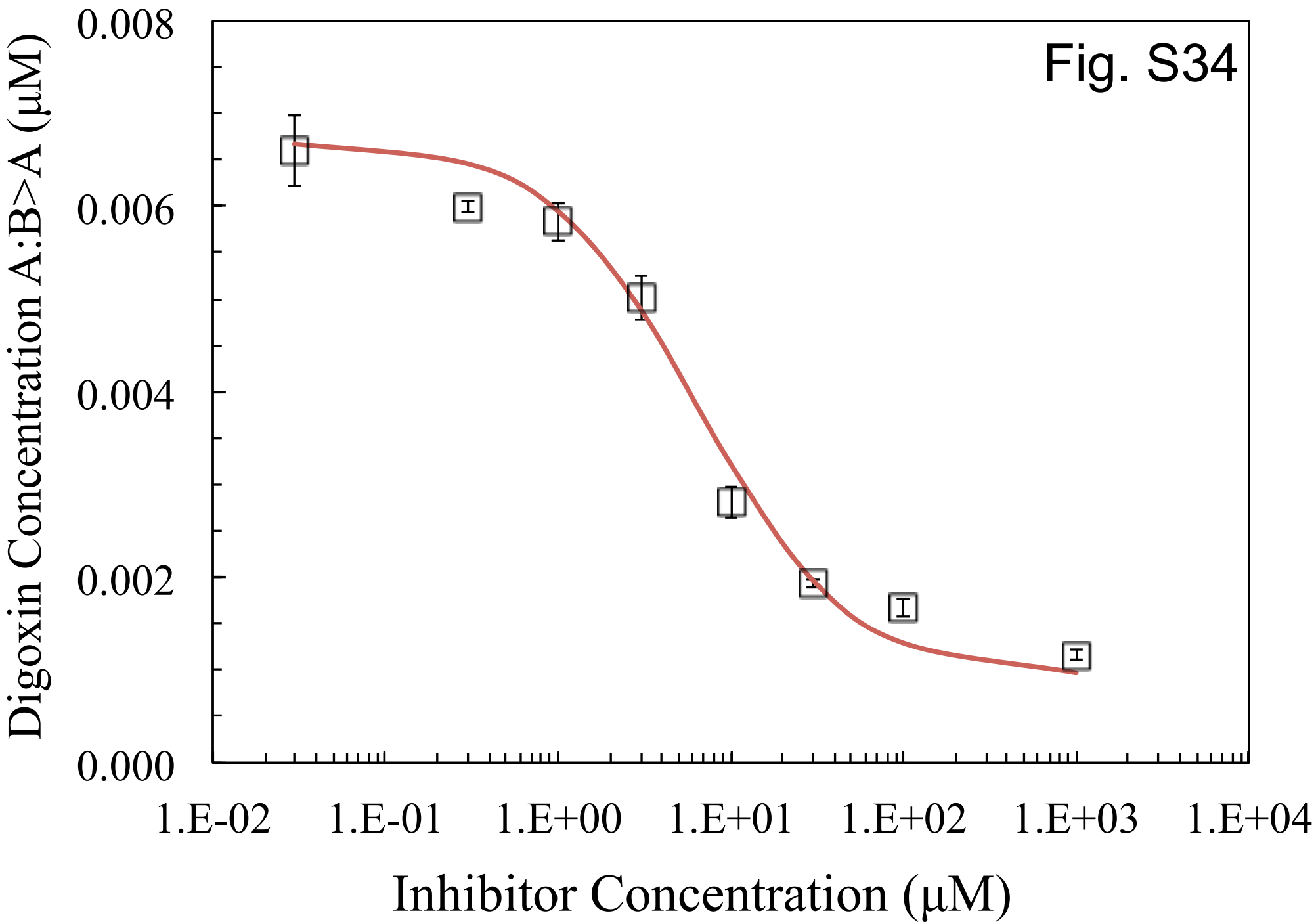
Fig. S34
Digoxin Concentration A:B>A (μM)
0.008
0.006
0.004
0.002
0.000
1.E-02
1.E-01
1.E+00
1.E+01
1.E+02
1.E+03
1.E+04
Inhibitor Concentration (μM)

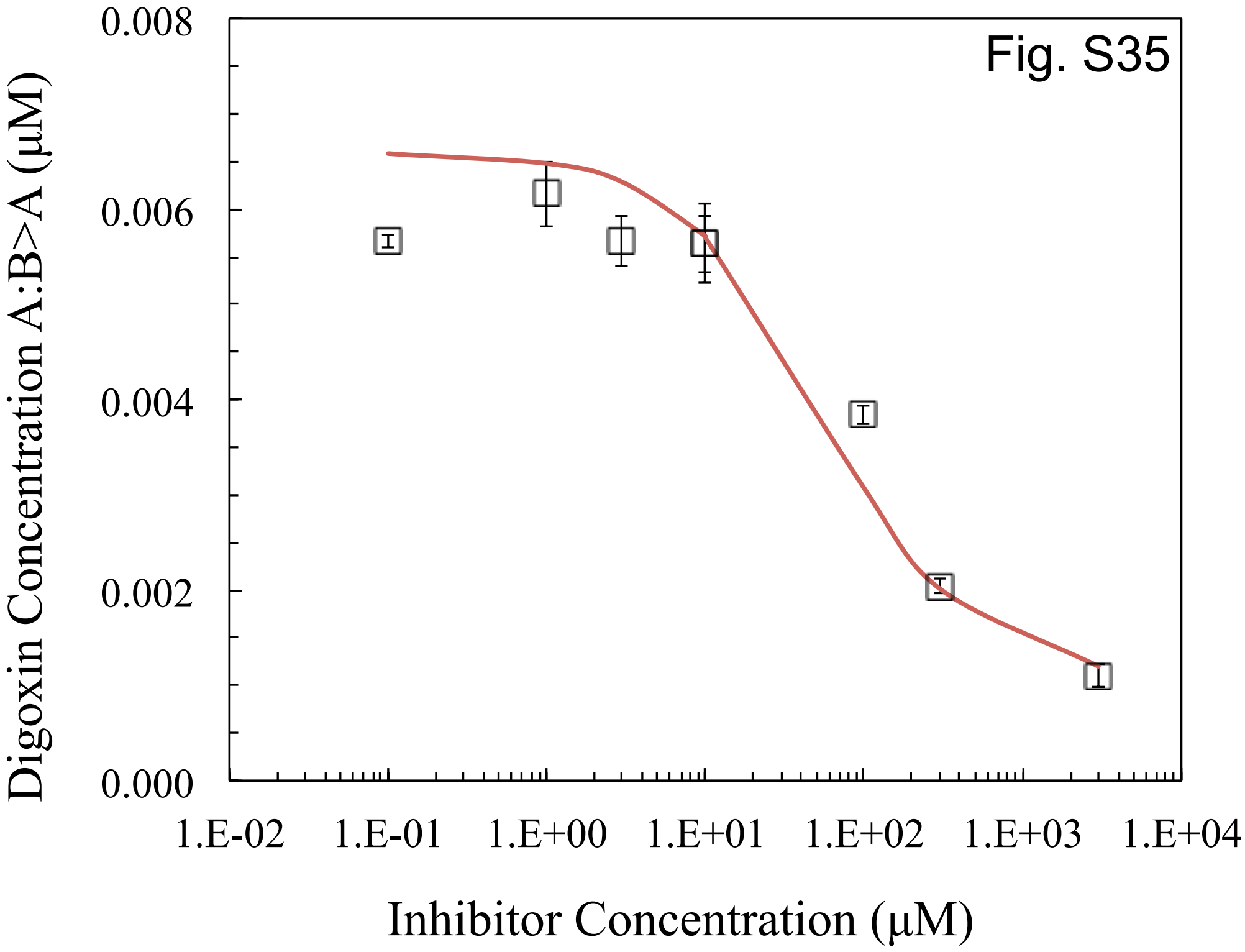
Fig. S35
Digoxin Concentration A:B>A (μM)
0.008
0.006
0.004
0.002
0.000
1.E-02
1.E-01
1.E+00
1.E+01
1.E+02
1.E+03
1.E+04
Inhibitor Concentration (μM)

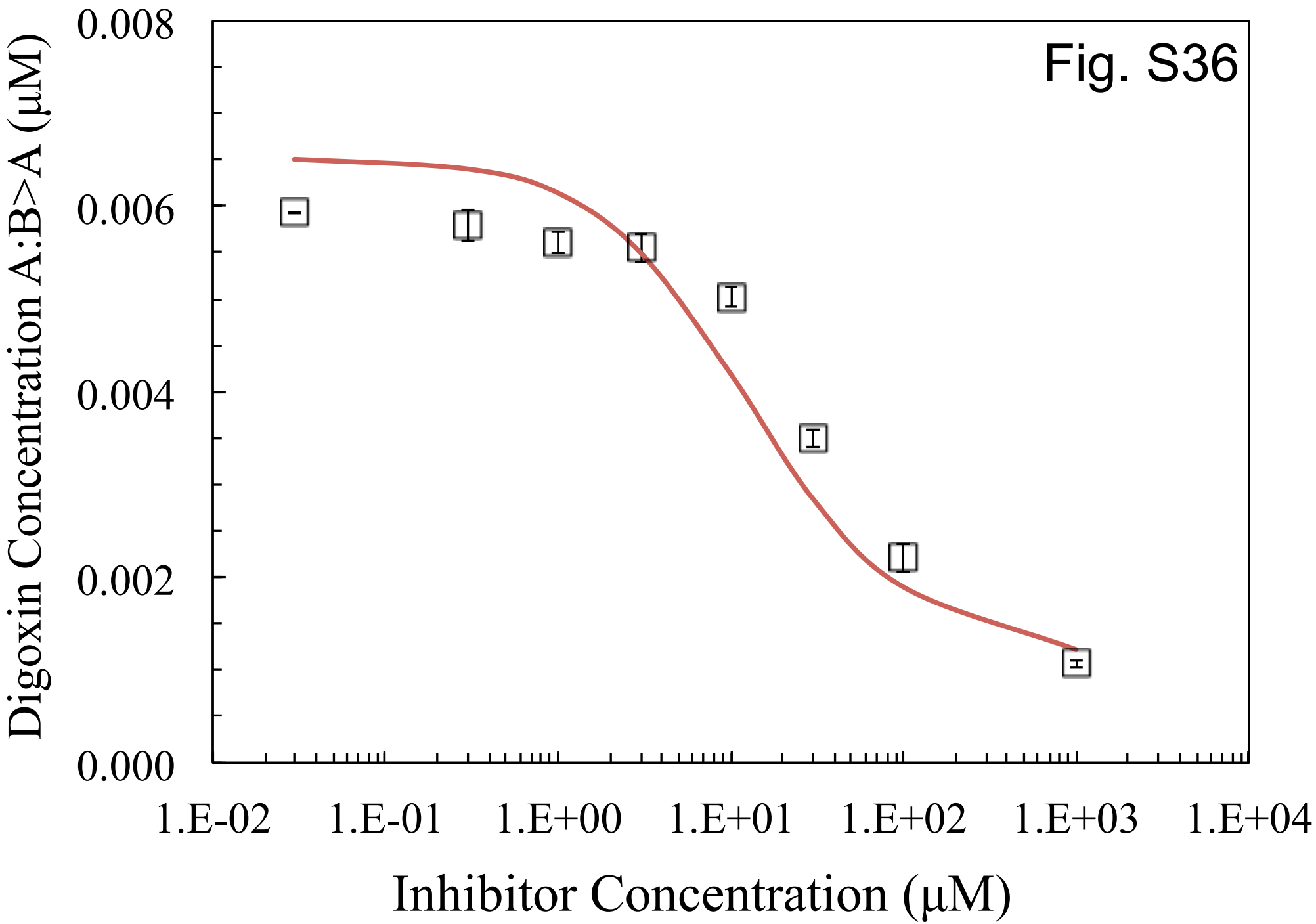
Fig. S36
Digoxin Concentration A:B>A (μM)
0.008
0.006
0.004
0.002
0.000
1.E-02
1.E-01
1.E+00
1.E+01
1.E+02
1.E+03
1.E+04
Inhibitor Concentration (μM)

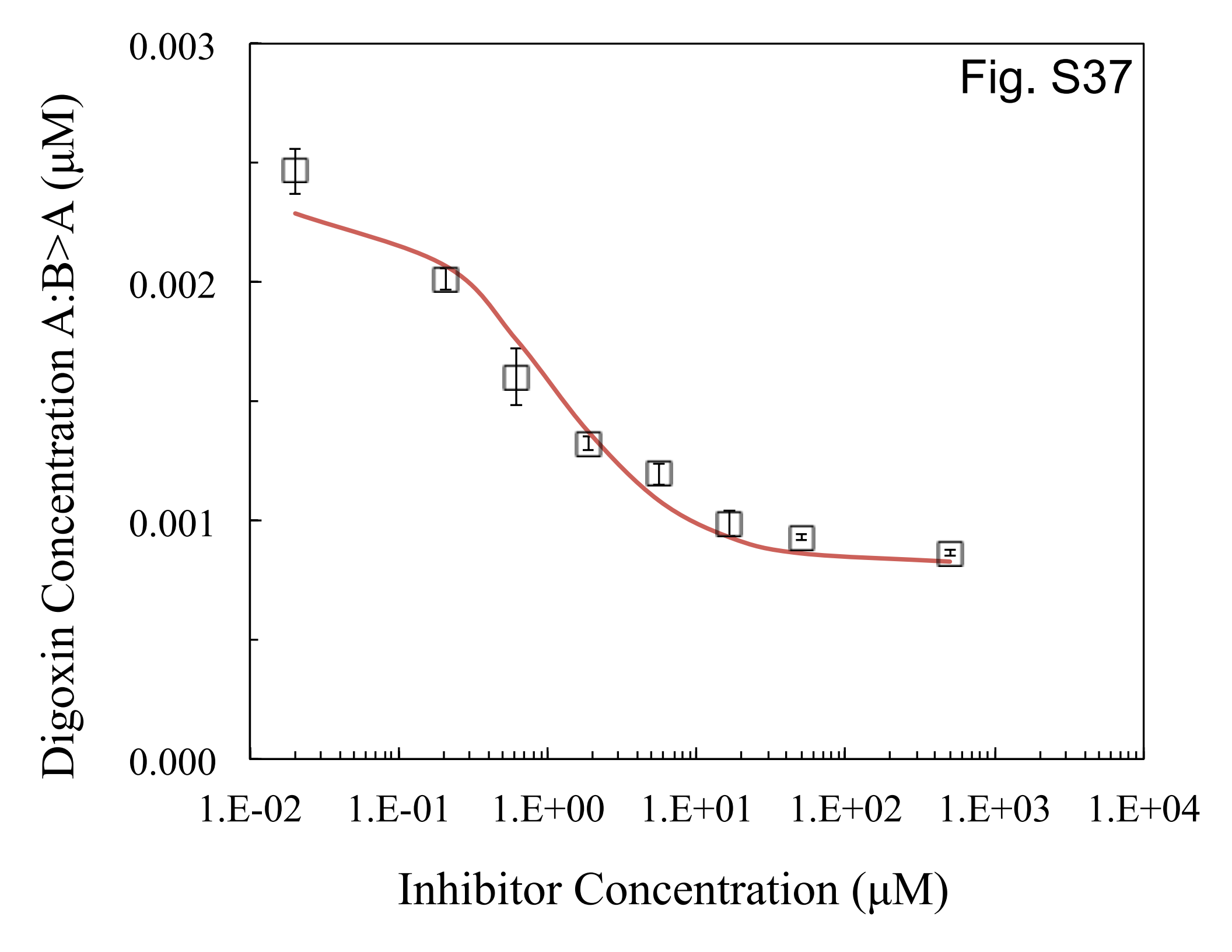
Fig. S37
0.003
0.002
0.001
0.000
Digoxin Concentration A:B>A (μM)
1.E-02
1.E-01
1.E+00
1.E+01
1.E+02
1.E+03
1.E+04
Inhibitor Concentration (μM)

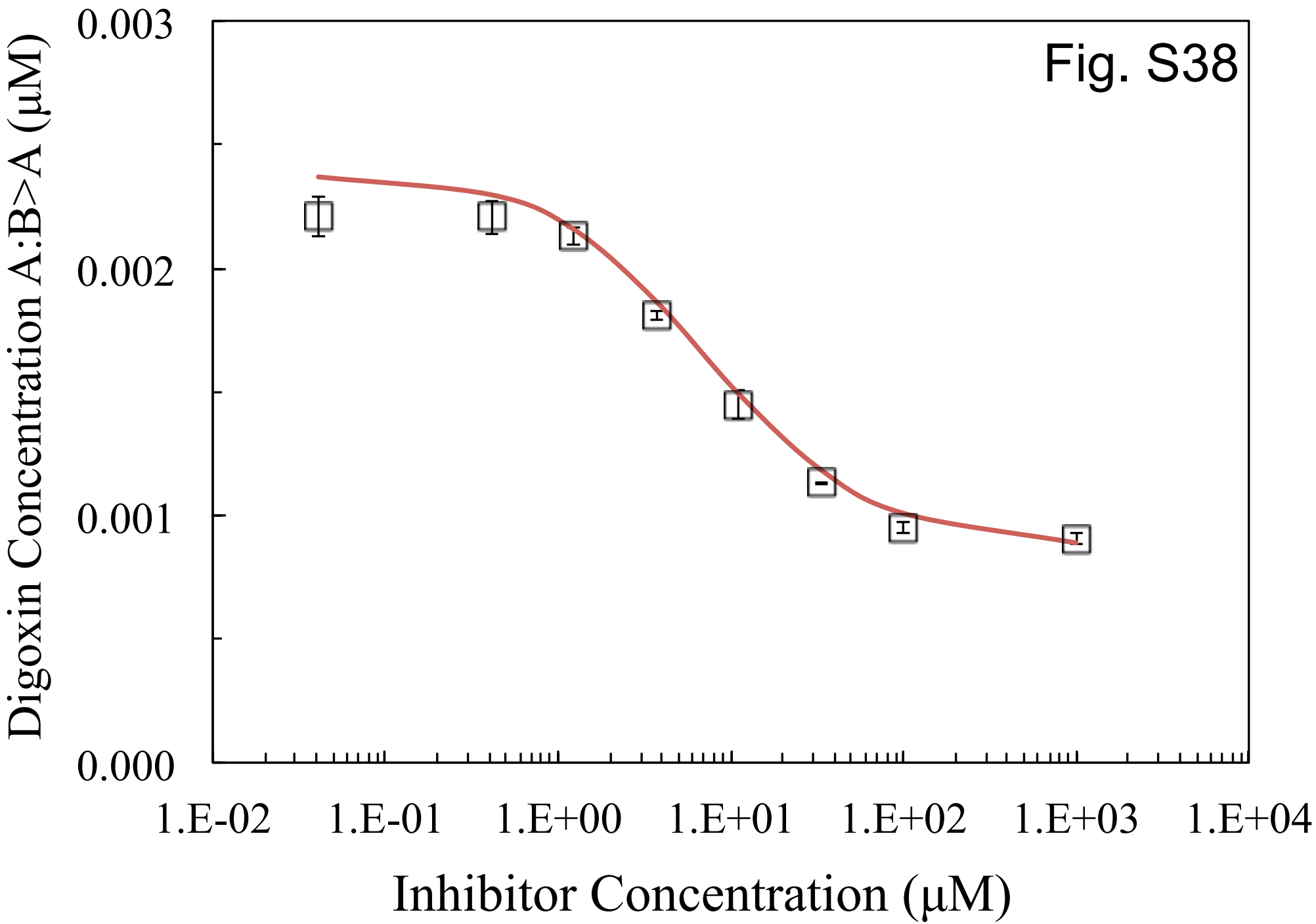
Fig. S38
Digoxin Concentration A:B>A (μM)
0.003
0.002
0.001
0.000
1.E-02
1.E-01
1.E+00
1.E+01
1.E+02
1.E+03
1.E+04
Inhibitor Concentration (μM)

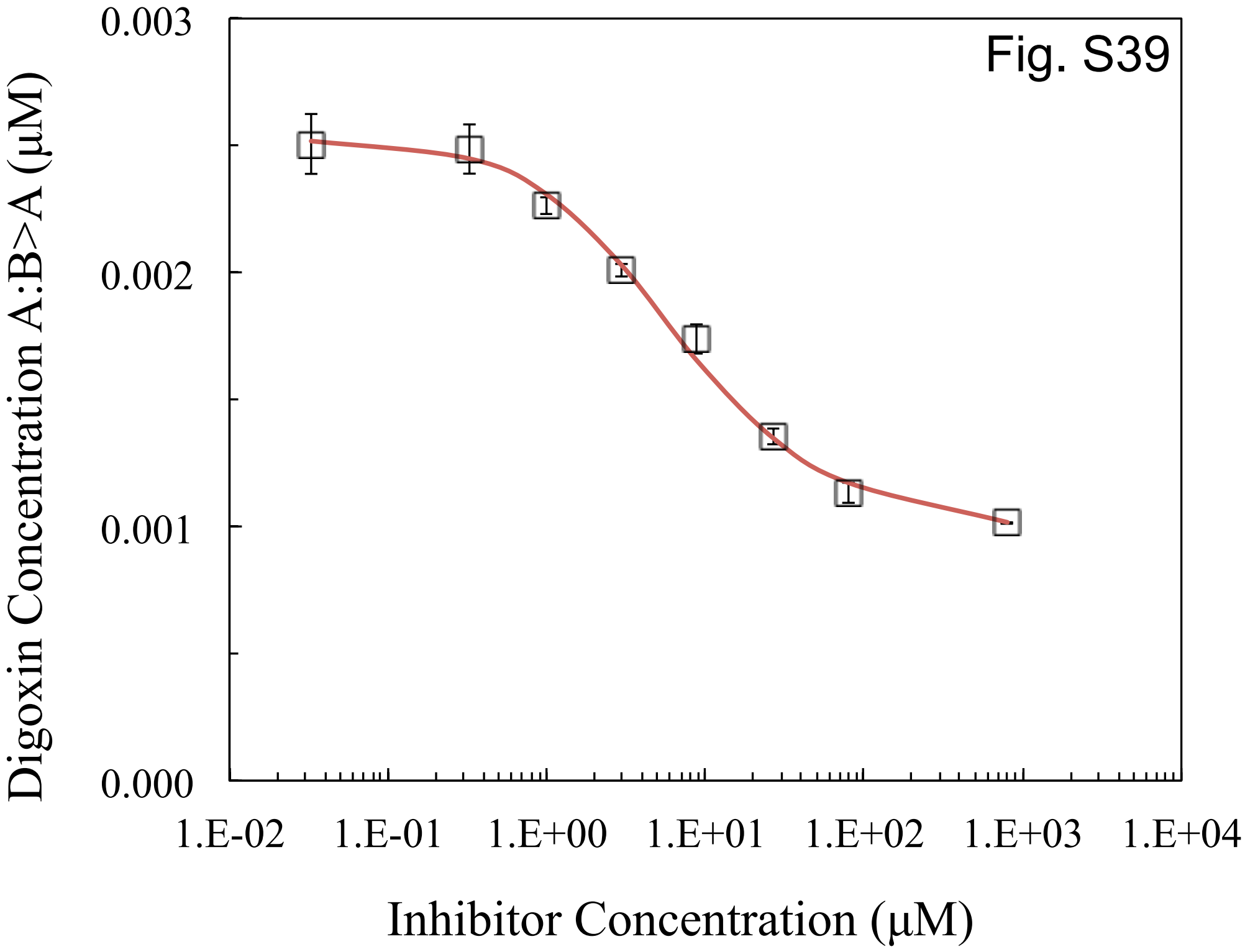
Fig. S39
0.003
0.002
0.001
0.000
Digoxin Concentration A:B>A (μM)
1.E-02
1.E-01
1.E+00
1.E+01
1.E+02
1.E+03
1.E+04
Inhibitor Concentration (μM)

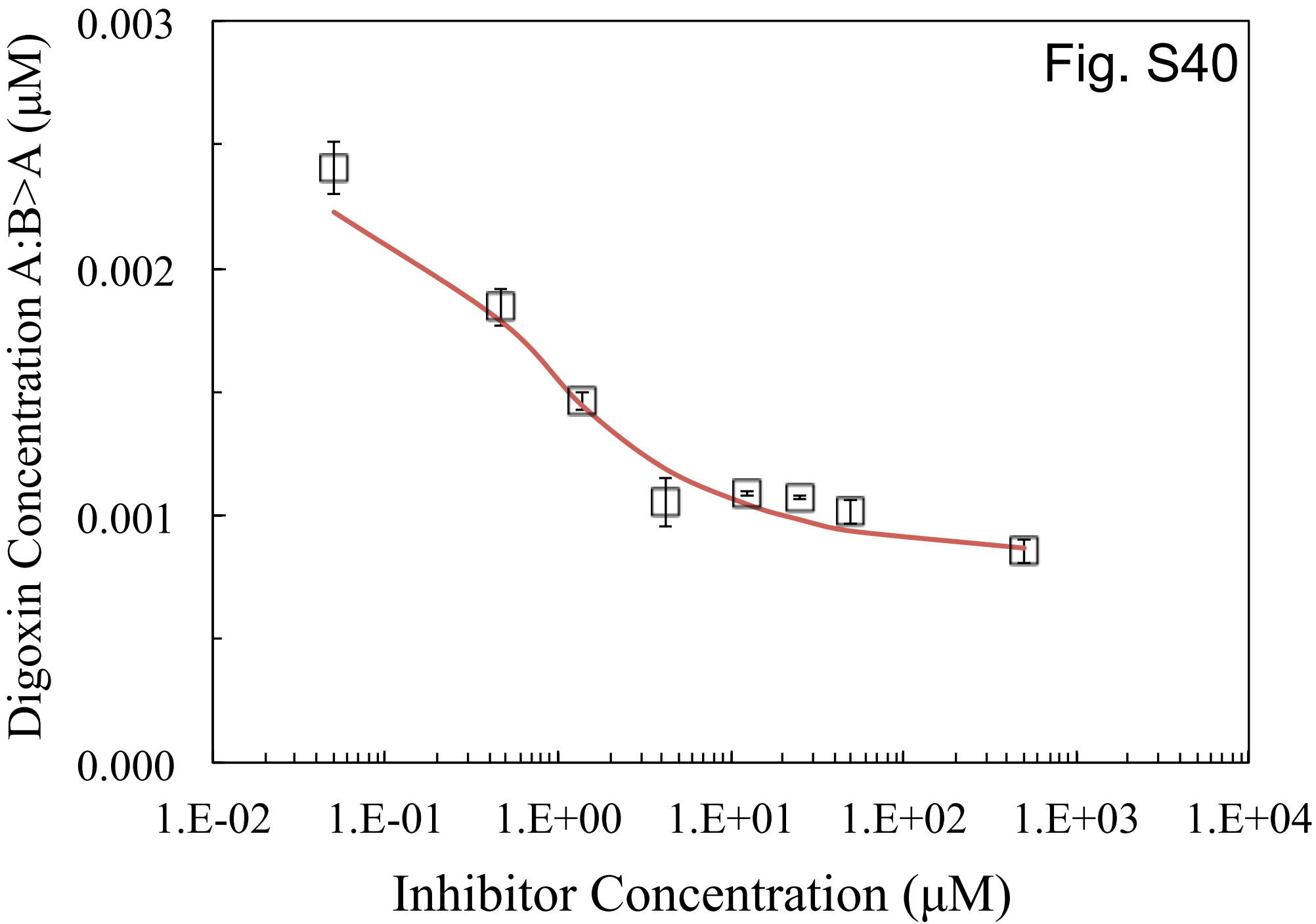
Fig. S40
Digoxin Concentration A:B>A (μM)
0.003
0.002
0.001
0.000
1.E-02
1.E-01
1.E+00
1.E+01
1.E+02
1.E+03
1.E+04
Inhibitor Concentration (μM)

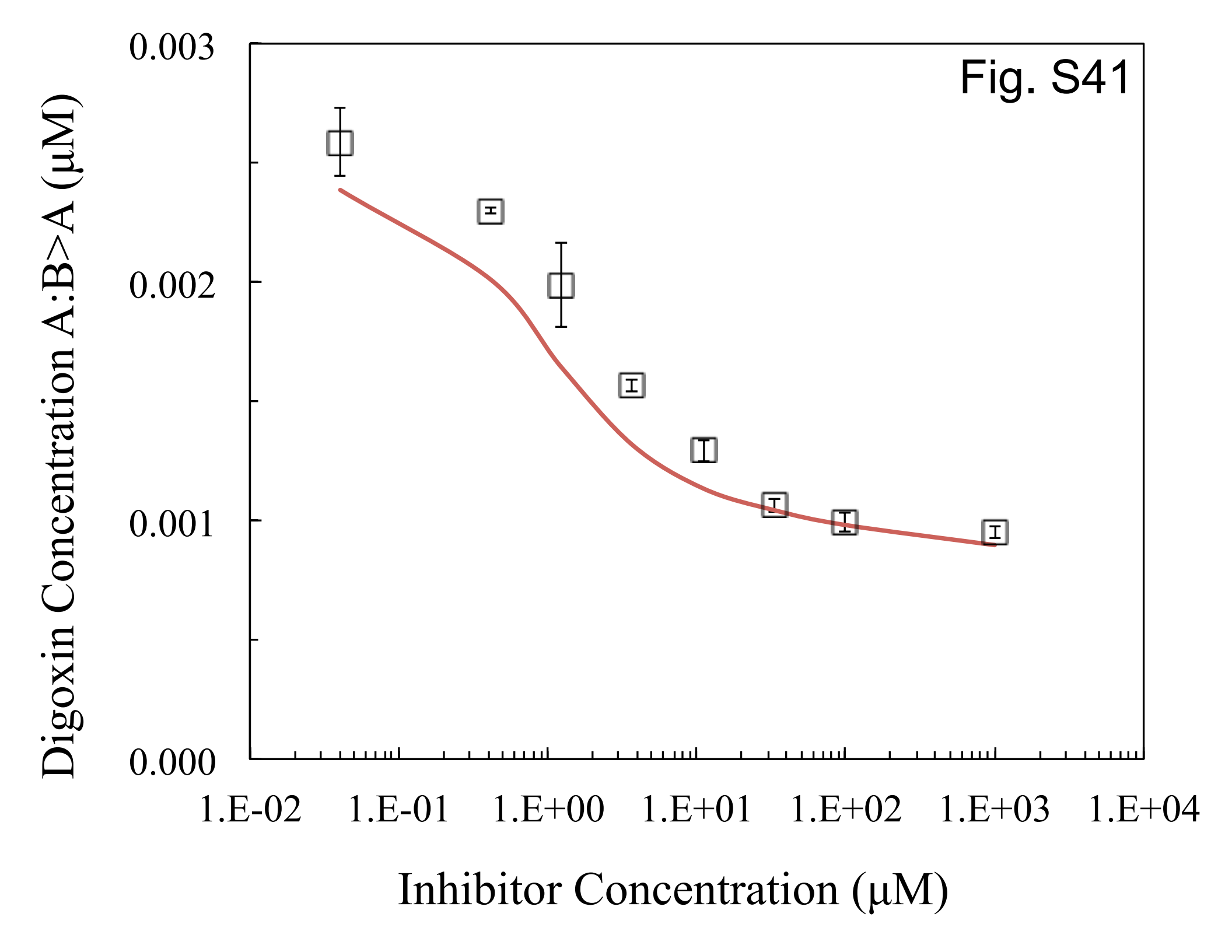
Fig. S41
0.003
0.002
0.001
0.000
Digoxin Concentration A:B>A (μM)
1.E-02
1.E-01
1.E+00
1.E+01
1.E+02
1.E+03
1.E+04
Inhibitor Concentration (μM)

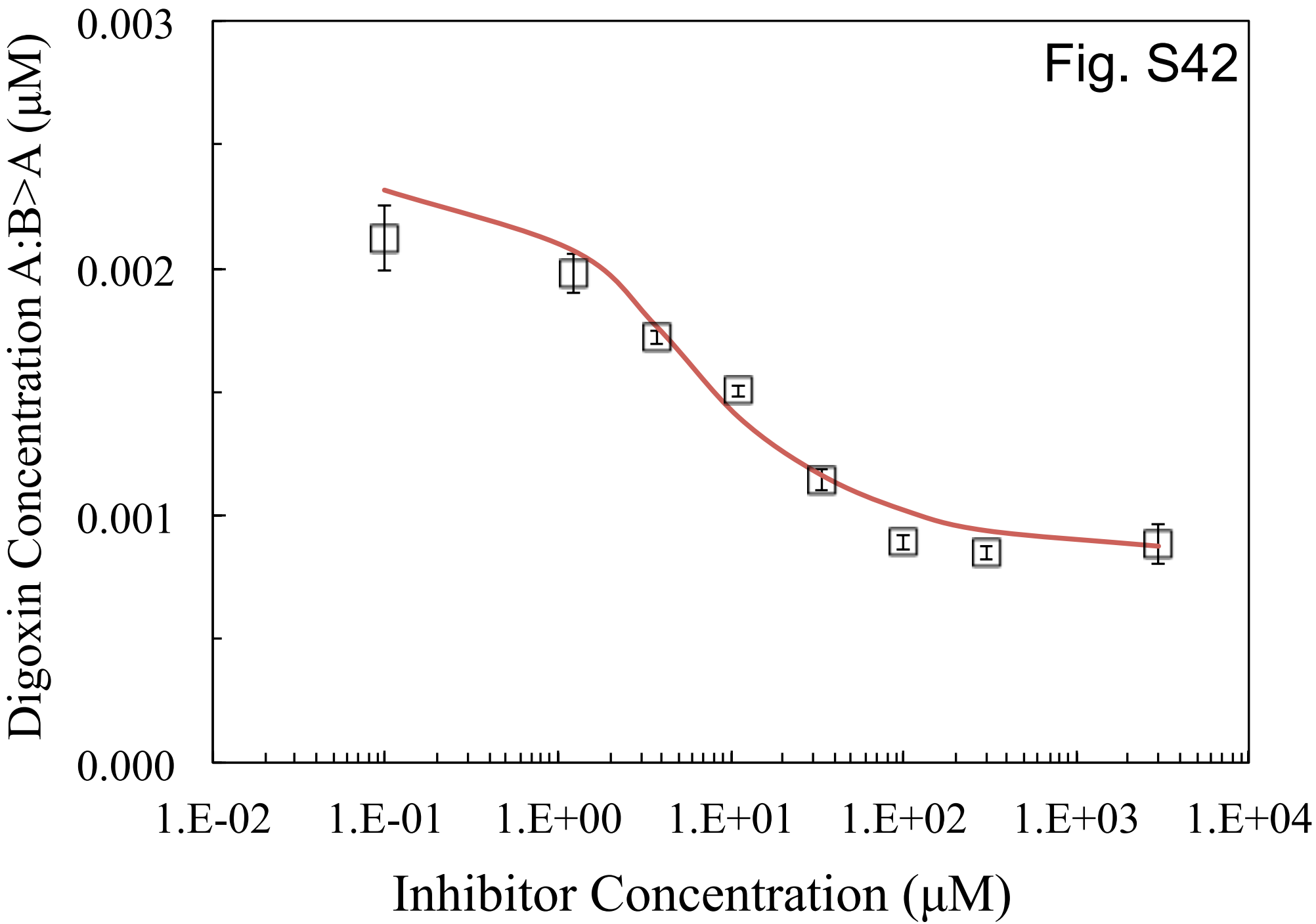
Fig. S42
Digoxin Concentration A:B>A (μM)
0.003
0.002
0.001
0.000
1.E-02
1.E-01
1.E+00
1.E+01
1.E+02
1.E+03
1.E+04
Inhibitor Concentration (μM)

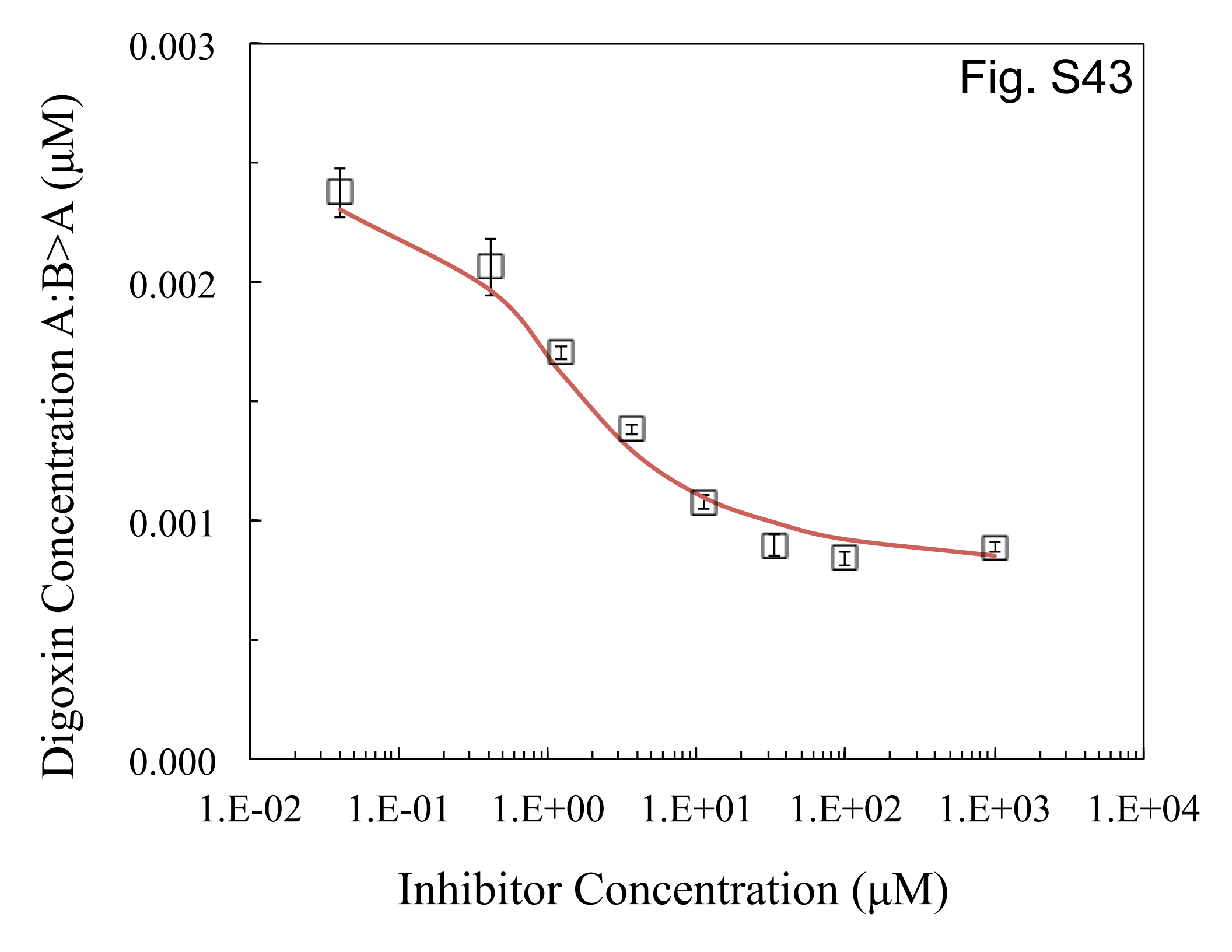
Fig. S43
Digoxin Concentration A:B>A (μM)
0.003
0.002
0.001
0.000
1.E-02
1.E-01
1.E+00
1.E+01
1.E+02
1.E+03
1.E+04
Inhibitor Concentration (μM)

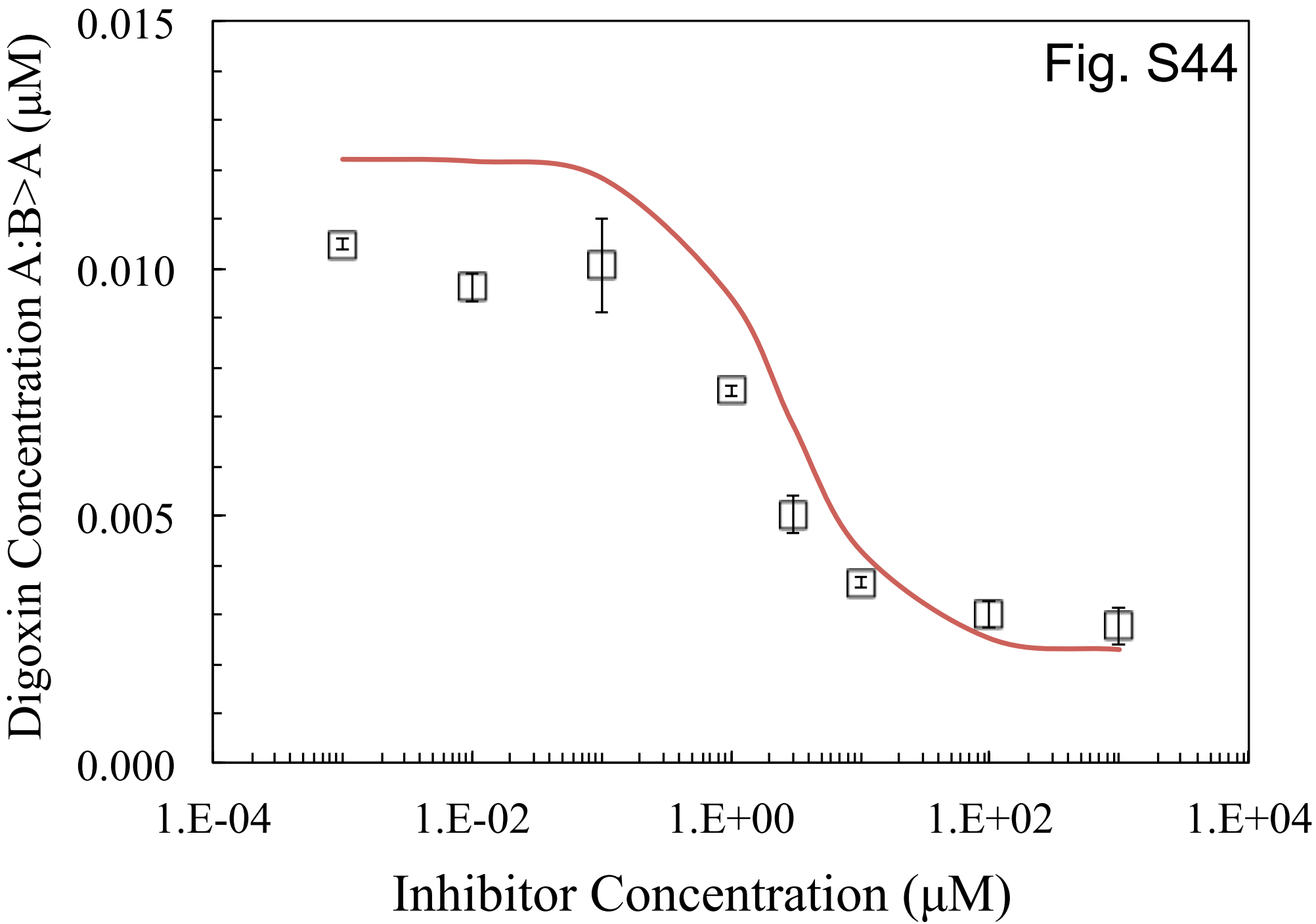
Fig. S44
Digoxin Concentration A:B>A (μM)
0.015
0.010
0.005
0.000
1.E-04
1.E-02
1.E+00
1.E+02
1.E+04
Inhibitor Concentration (μM)

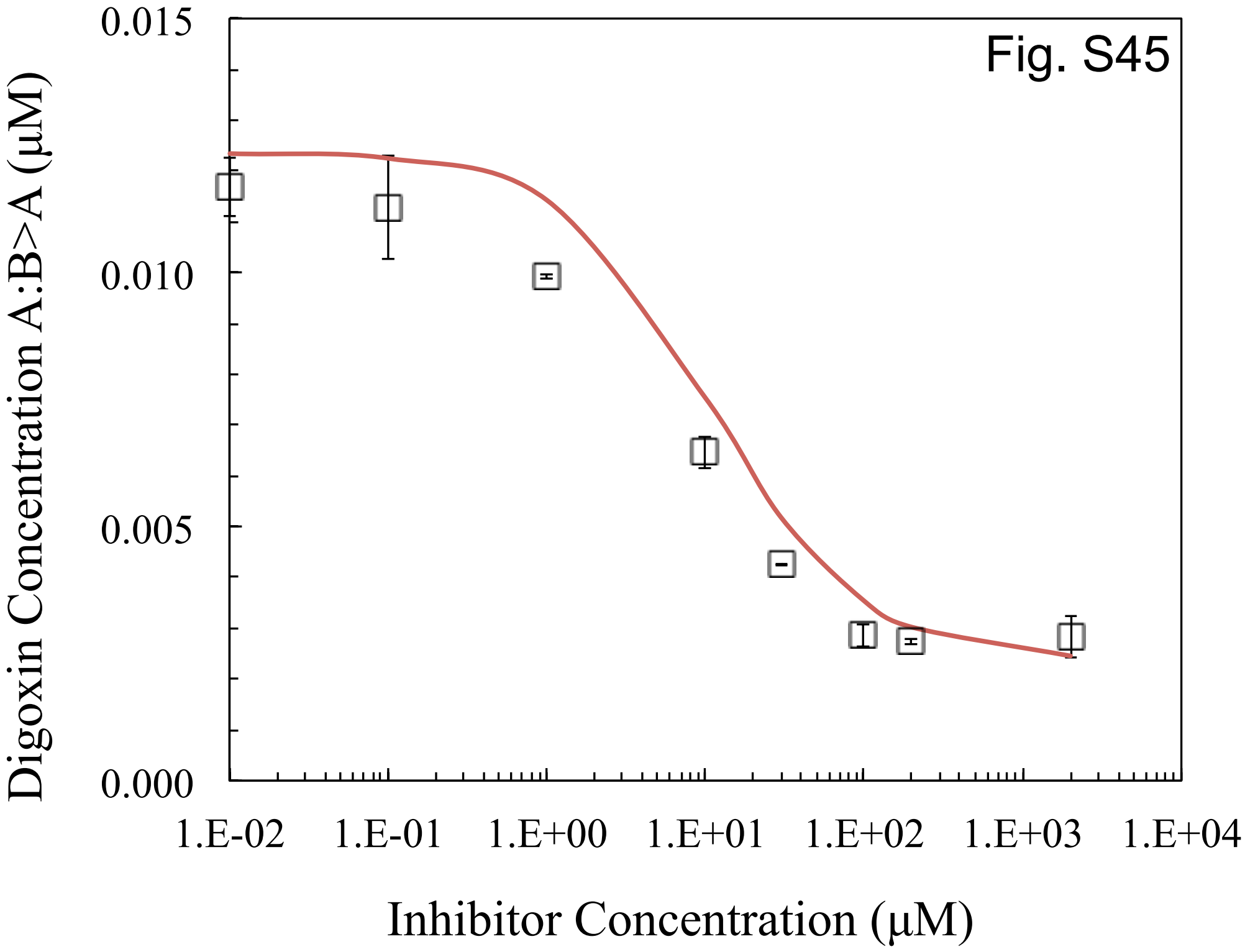
Fig. S45
0.015
0.010
0.005
0.000
Digoxin Concentration A:B>A (μM)
1.E-02
1.E-01
1.E+00
1.E+01
1.E+02
1.E+03
1.E+04
Inhibitor Concentration (μM)

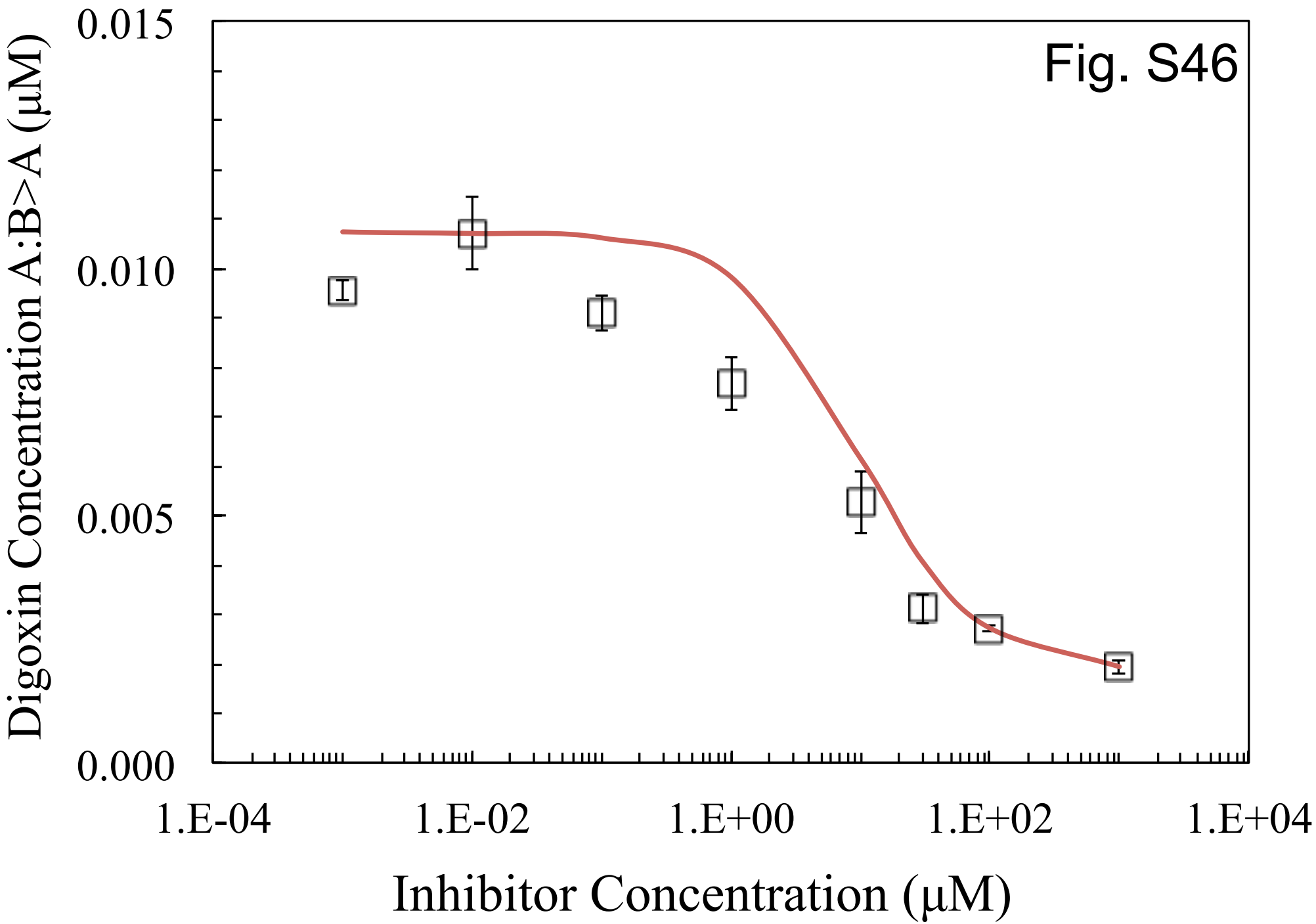
Fig. S46
Digoxin Concentration A:B>A (μM)
0.015
0.010
0.005
0.000
1.E-04
1.E-02
1.E+00
1.E+02
1.E+04
Inhibitor Concentration (μM)

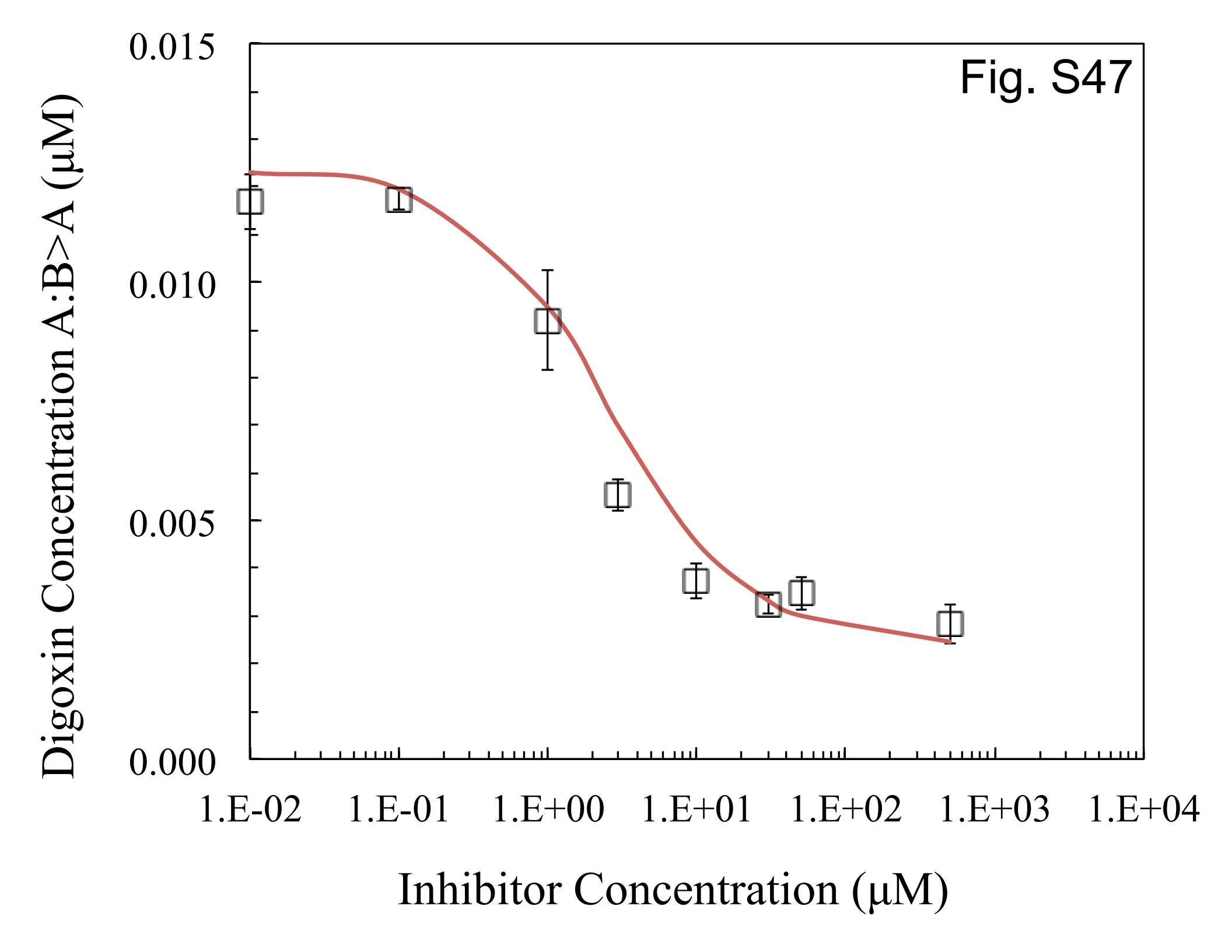
Fig. S47
0.015
0.010
0.005
0.000
Digoxin Concentration A:B>A (μM)
1.E-02
1.E-01
1.E+00
1.E+01
1.E+02
1.E+03
1.E+04
Inhibitor Concentration (μM)

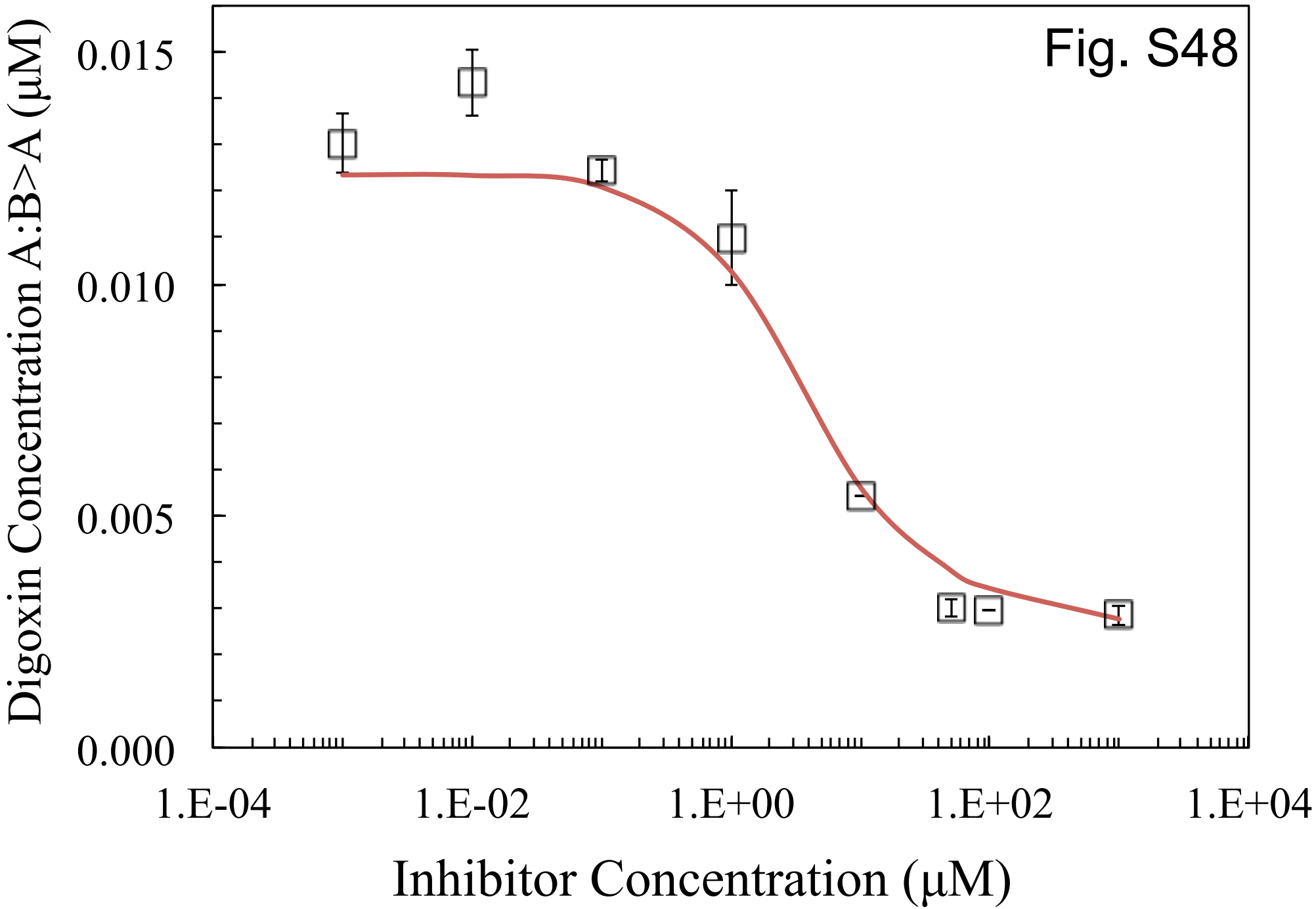
Fig. S48
Digoxin Concentration A:B>A (μM)
0.015
0.010
0.005
0.000
1.E-04
1.E-02
1.E+00
1.E+02
1.E+04
Inhibitor Concentration (μM)

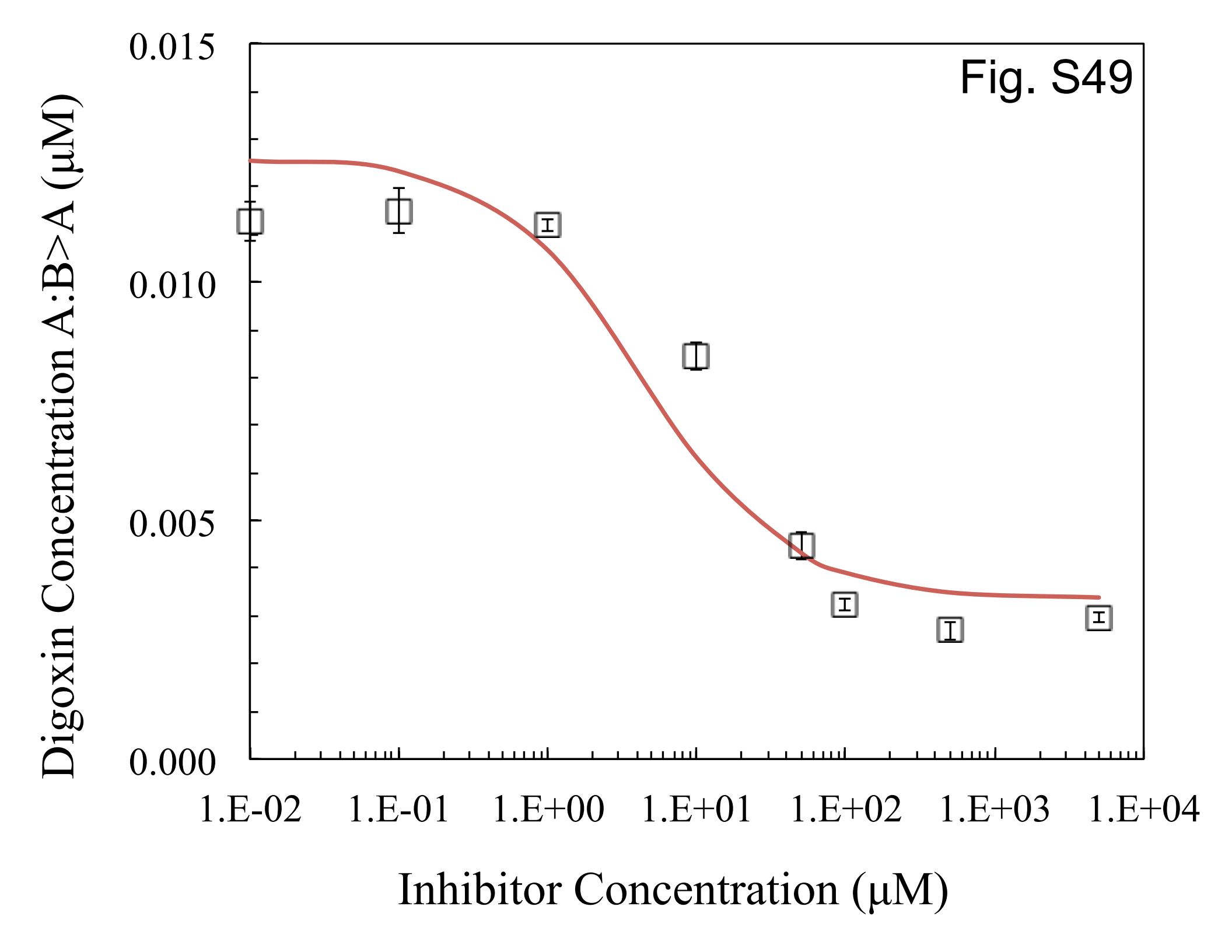
Fig. S49
0.015
0.010
0.005
0.000
Digoxin Concentration A:B>A (μM)
1.E-02
1.E-01
1.E+00
1.E+01
1.E+02
1.E+03
1.E+04
Inhibitor Concentration (μM)

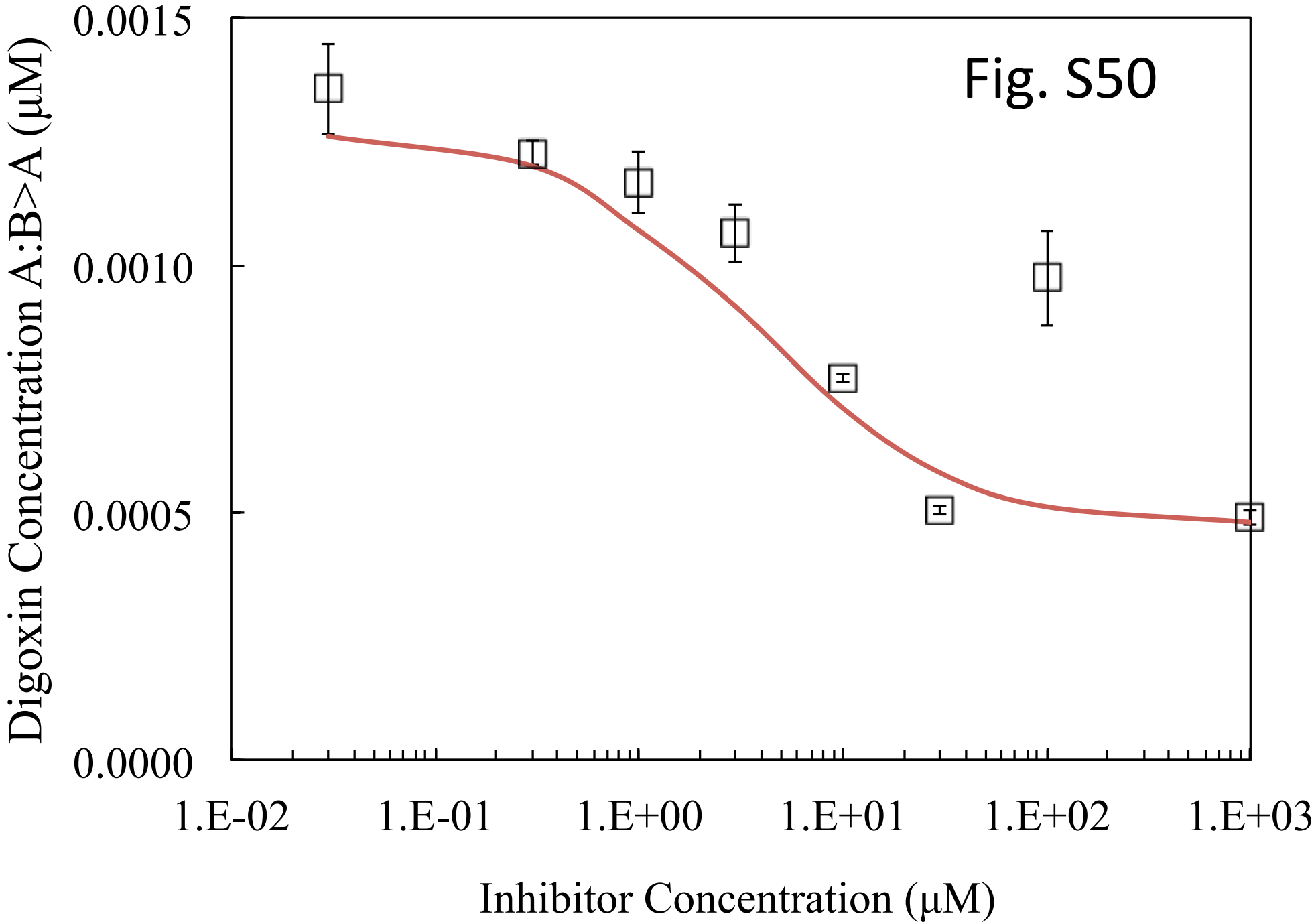
Fig. S50
0.0015
0.0010
0.0005
0.0000
Digoxin Concentration A:B>A (μM)
1.E-02
1.E-01
1.E+00
1.E+01
1.E+02
1.E+03
Inhibitor Concentration (μM)

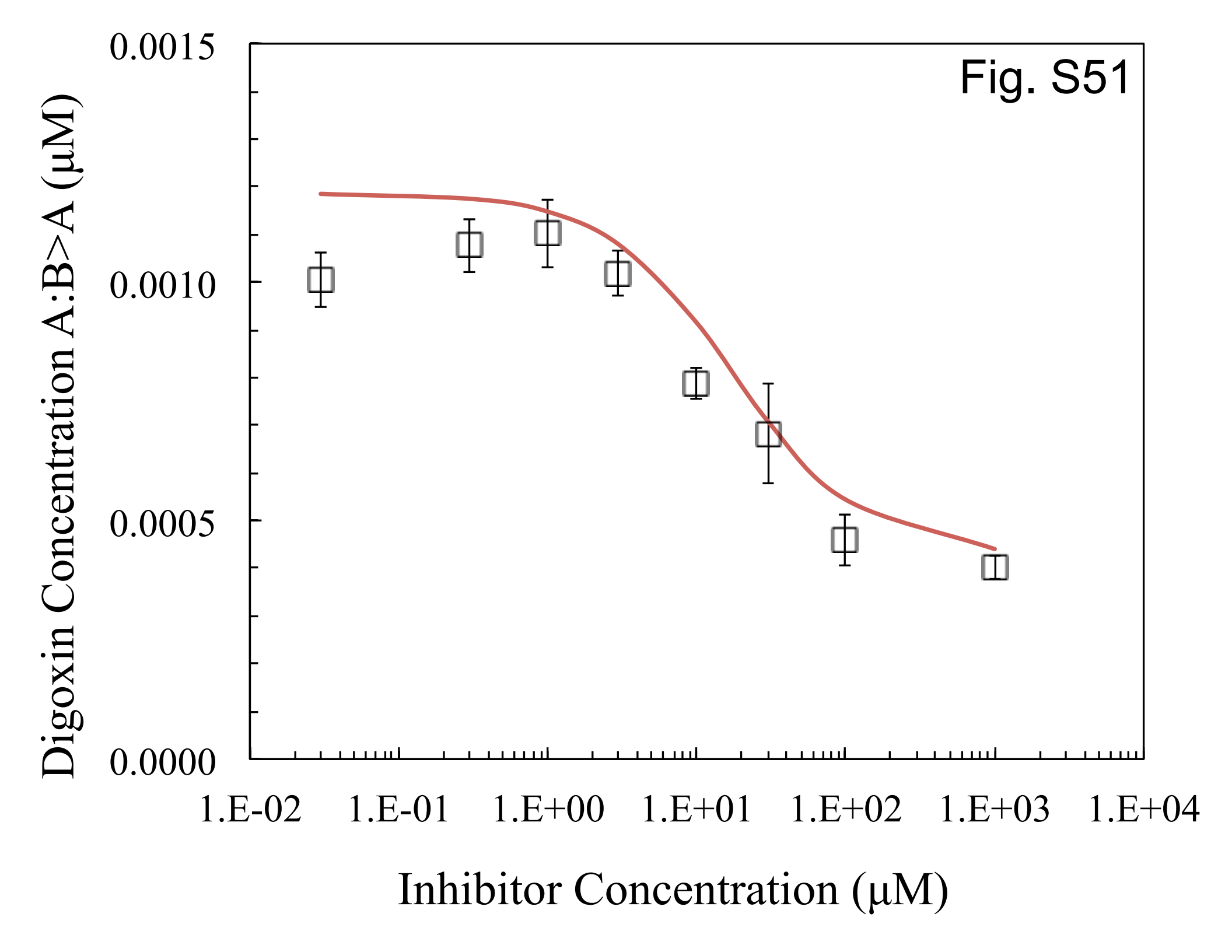
Fig. S51
0.0015
0.0010
0.0005
0.0000
Digoxin Concentration A:B>A (μM)
1.E-02
1.E-01
1.E+00
1.E+01
1.E+02
1.E+03
1.E+04
Inhibitor Concentration (μM)

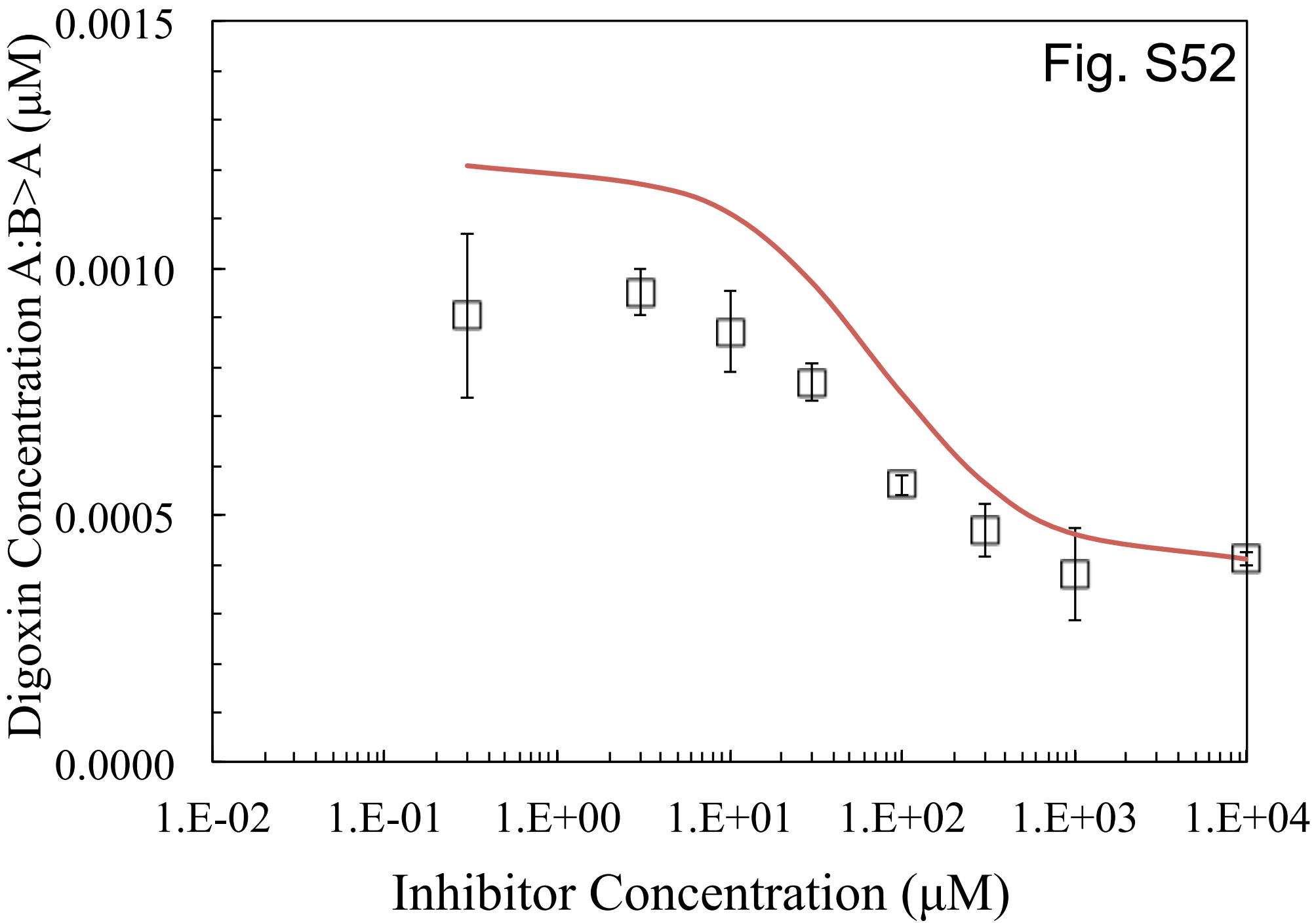
Fig. S52
Digoxin Concentration A:B>A (μM)
0.0015
0.0010
0.0005
0.0000
1.E-02
1.E-01
1.E+00
1.E+01
1.E+02
1.E+03
1.E+04
Inhibitor Concentration (μM)

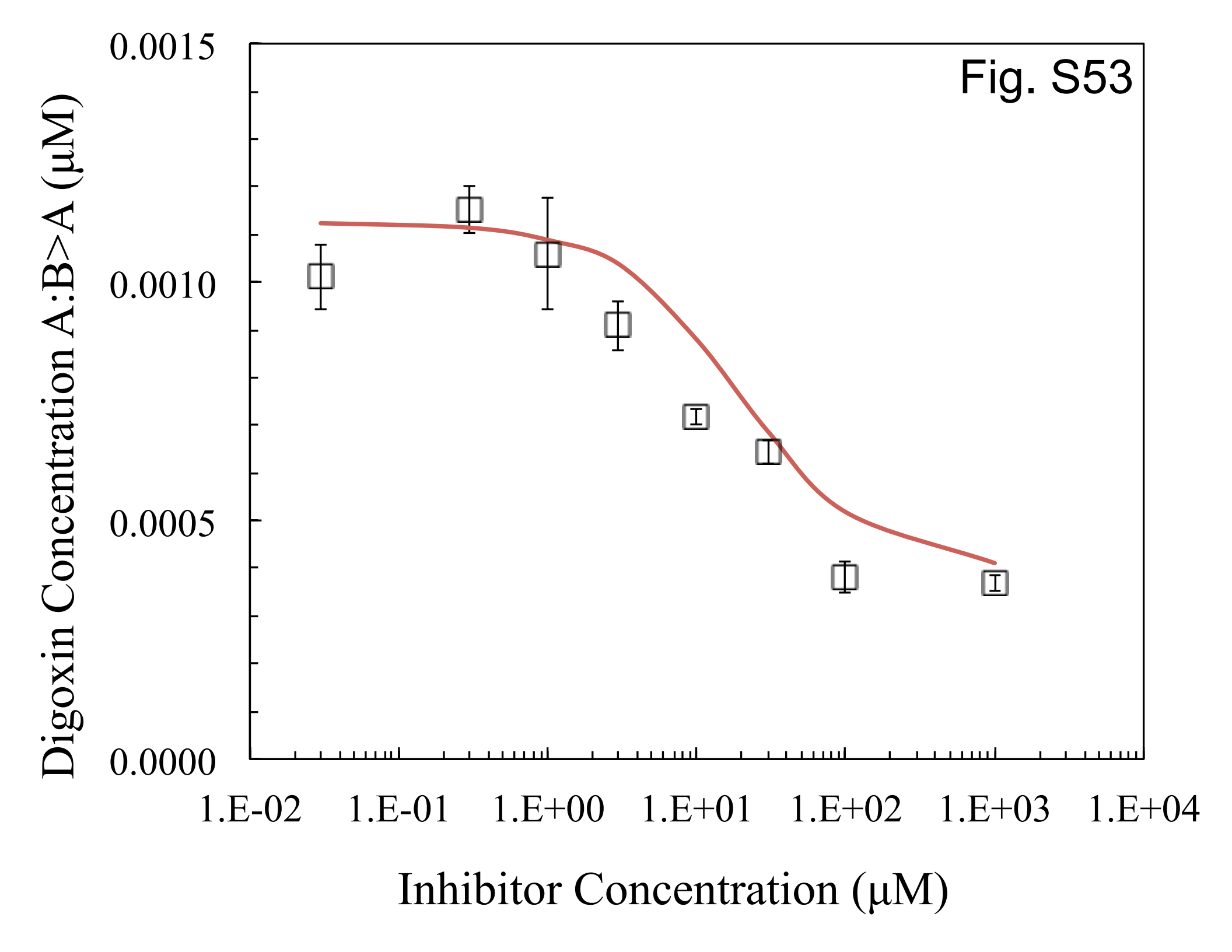
Fig. S53
0.0015
0.0010
0.0005
0.0000
Digoxin Concentration A:B>A (μM)
1.E-02
1.E-01
1.E+00
1.E+01
1.E+02
1.E+03
1.E+04
Inhibitor Concentration (μM)

Supplemental Data Table S5. Figure Legends for Tables 5A and 5B in the main paper. For all figures, symbols show the B>A digoxin transport data, error bars show the data standard deviation and the line shows the fit to the data.

Fig. S54. Inhibition by carvedilol with HPTC cells from K06.
Fig. S55. Inhibition by carvedilol with HPTC cells from K10.
Fig. S56. Inhibition by diltiazem with HPTC cells from K13.
Fig. S57. Inhibition by isradipine with HPTC cells from K08.
Fig. S58. Inhibition by ketoconazole with HPTC cells from K02.
Fig. S59. Inhibition by ketoconazole with HPTC cells from K11.
Fig. S60. Inhibition by mibefradil with HPTC cells from K07.
Fig. S61. Inhibition by nicardipine with HPTC cells from K04.
Fig. S62. Inhibition by nicardipine with HPTC cells from K13.
Fig. S63. Inhibition by quinidine with HPTC cells from K01.
Fig. S64. Inhibition by quinidine with HPTC cells from K02.
Fig. S65. Inhibition by ranolazine with HPTC cells from K12.
Fig. S66. Inhibition by verapamil with HPTC cells from K01.
Fig. S67. Inhibition by verapamil with HPTC cells from K10.

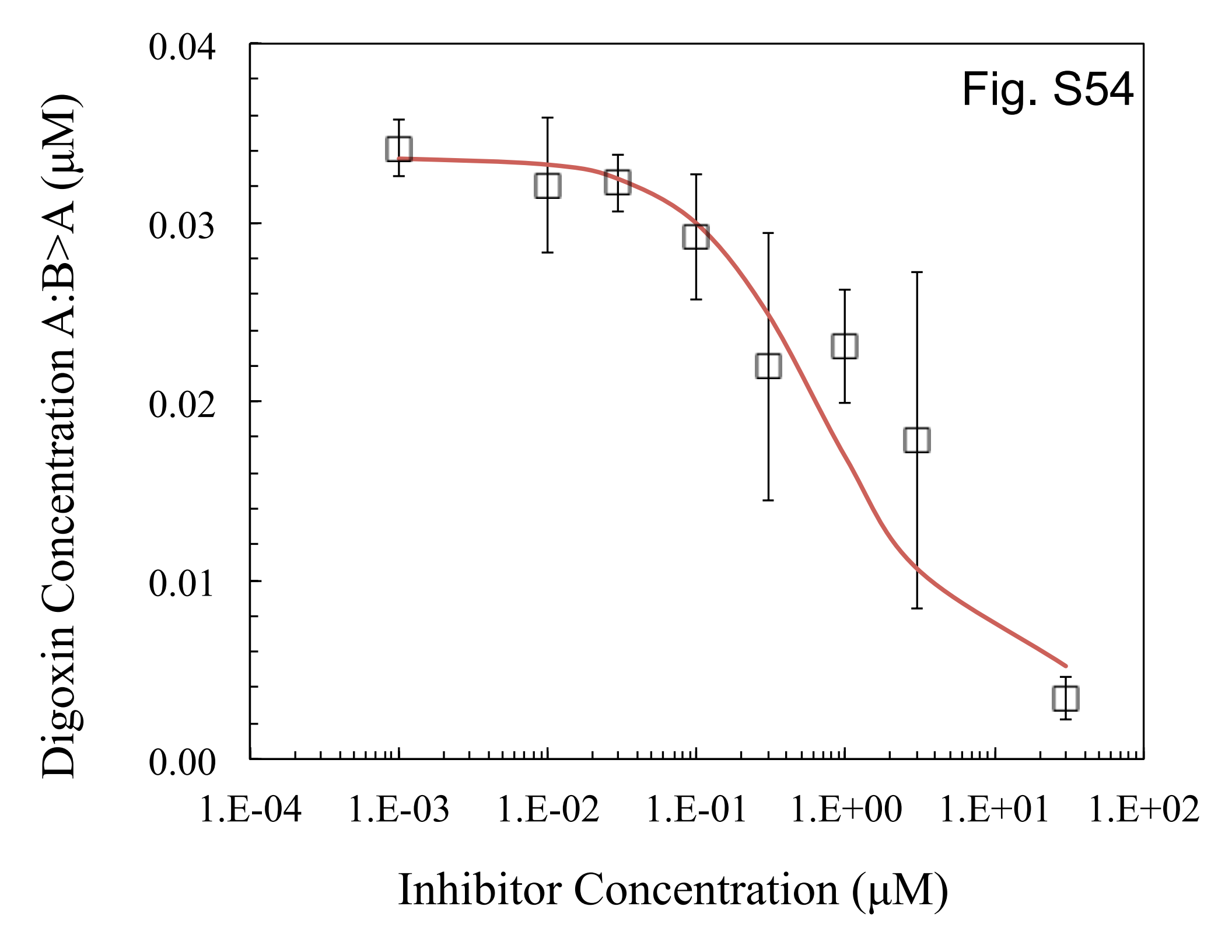
Fig. S54
Digoxin Concentration A:B>A (μM)
0.04
0.03
0.02
0.01
0.00
1.E-04
1.E-03
1.E-02
1.E-01
1.E+00
1.E+01
1.E+02
Inhibitor Concentration (μM)

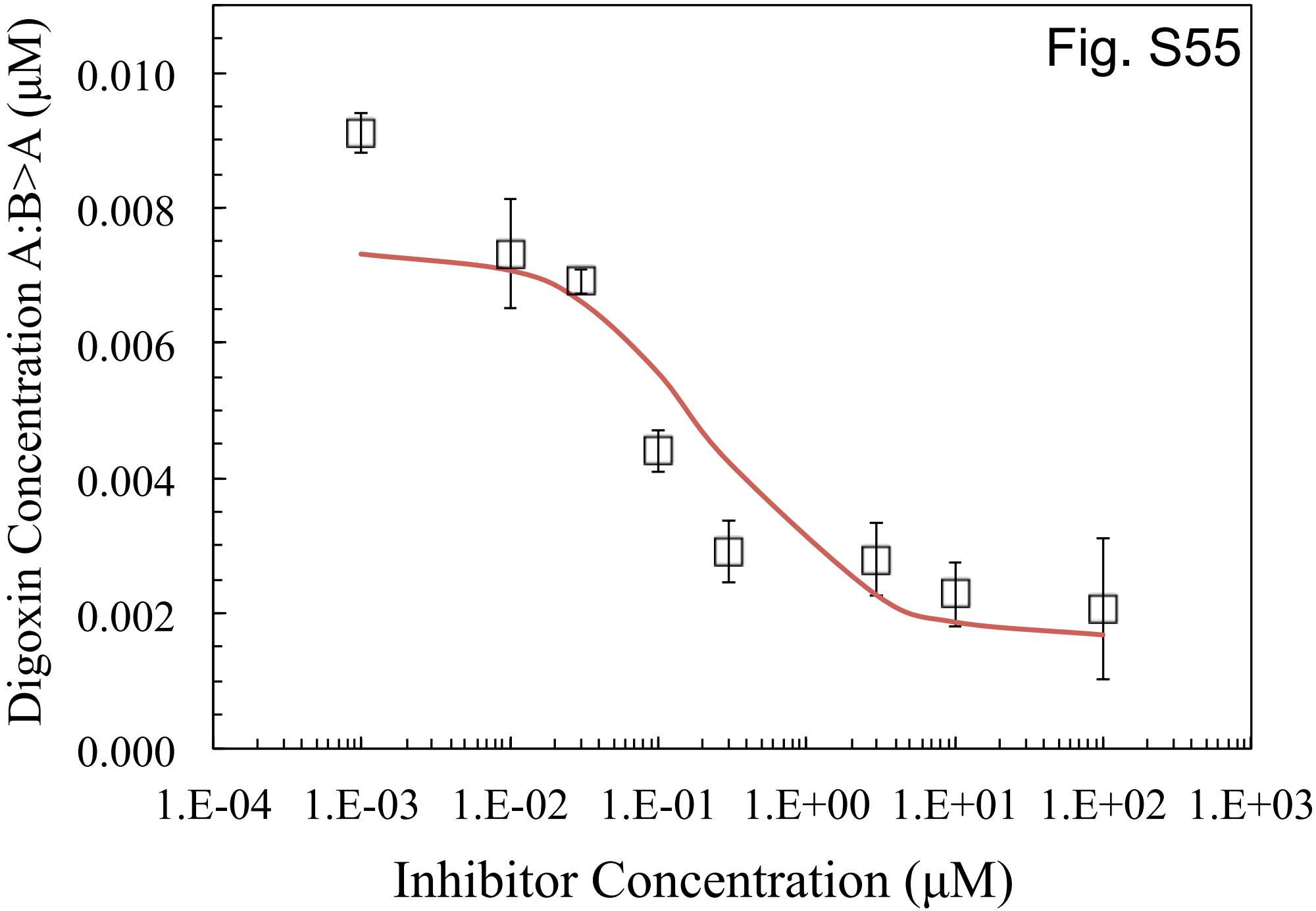
Fig. S55
Digoxin Concentration A:B>A (μM)
0.010
0.008
0.006
0.004
0.002
0.000
1.E-04
1.E-03
1.E-02
1.E-01
1.E+00
1.E+01
1.E+02
1.E+03
Inhibitor Concentration (μM)

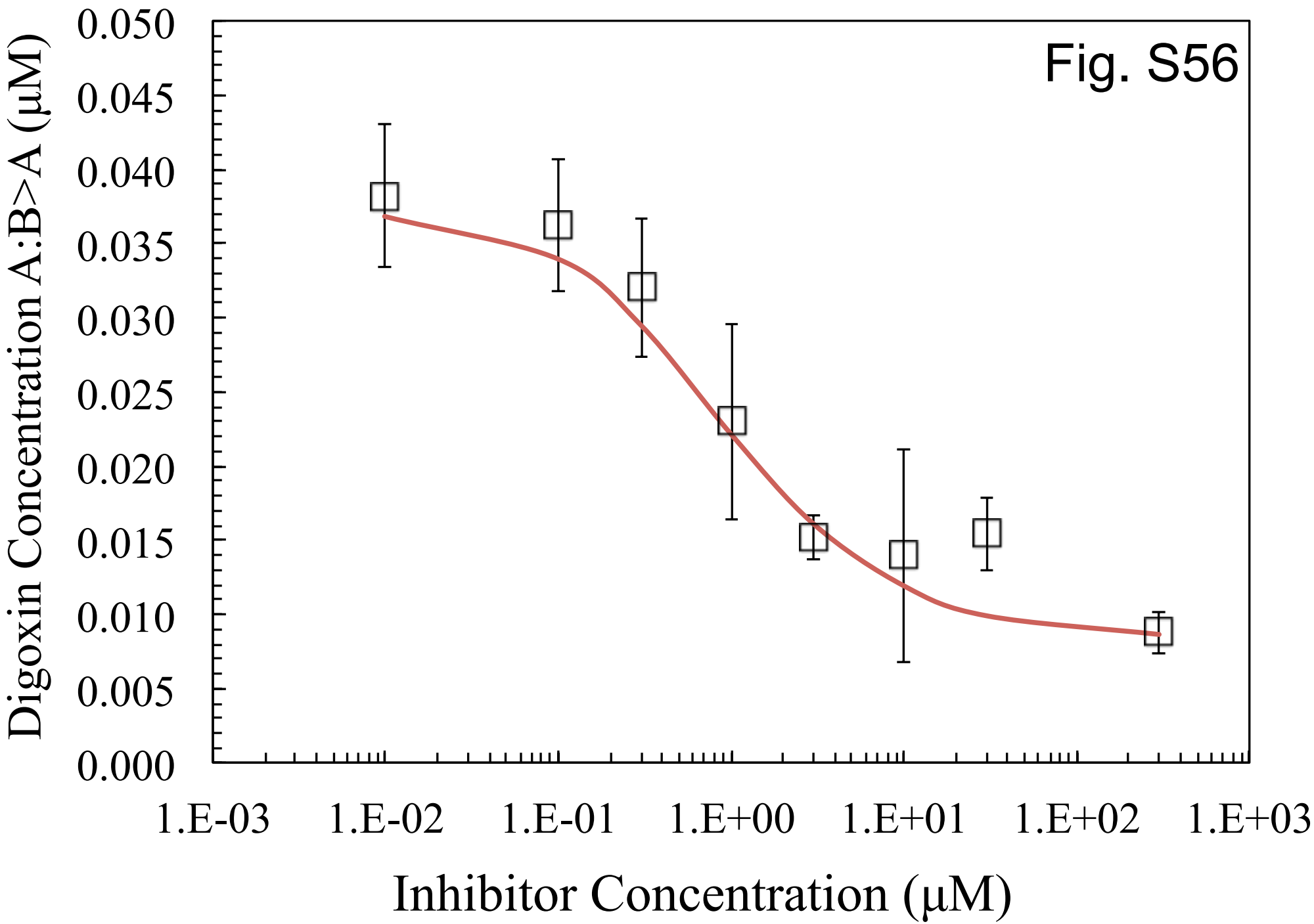
Fig. S56
Digoxin Concentration A:B>A (μM)
0.050
0.045
0.040
0.035
0.030
0.025
0.020
0.015
0.010
0.005
0.000
1.E-03
1.E-02
1.E-01
1.E+00
1.E+01
1.E+02
1.E+03
Inhibitor Concentration (μM)

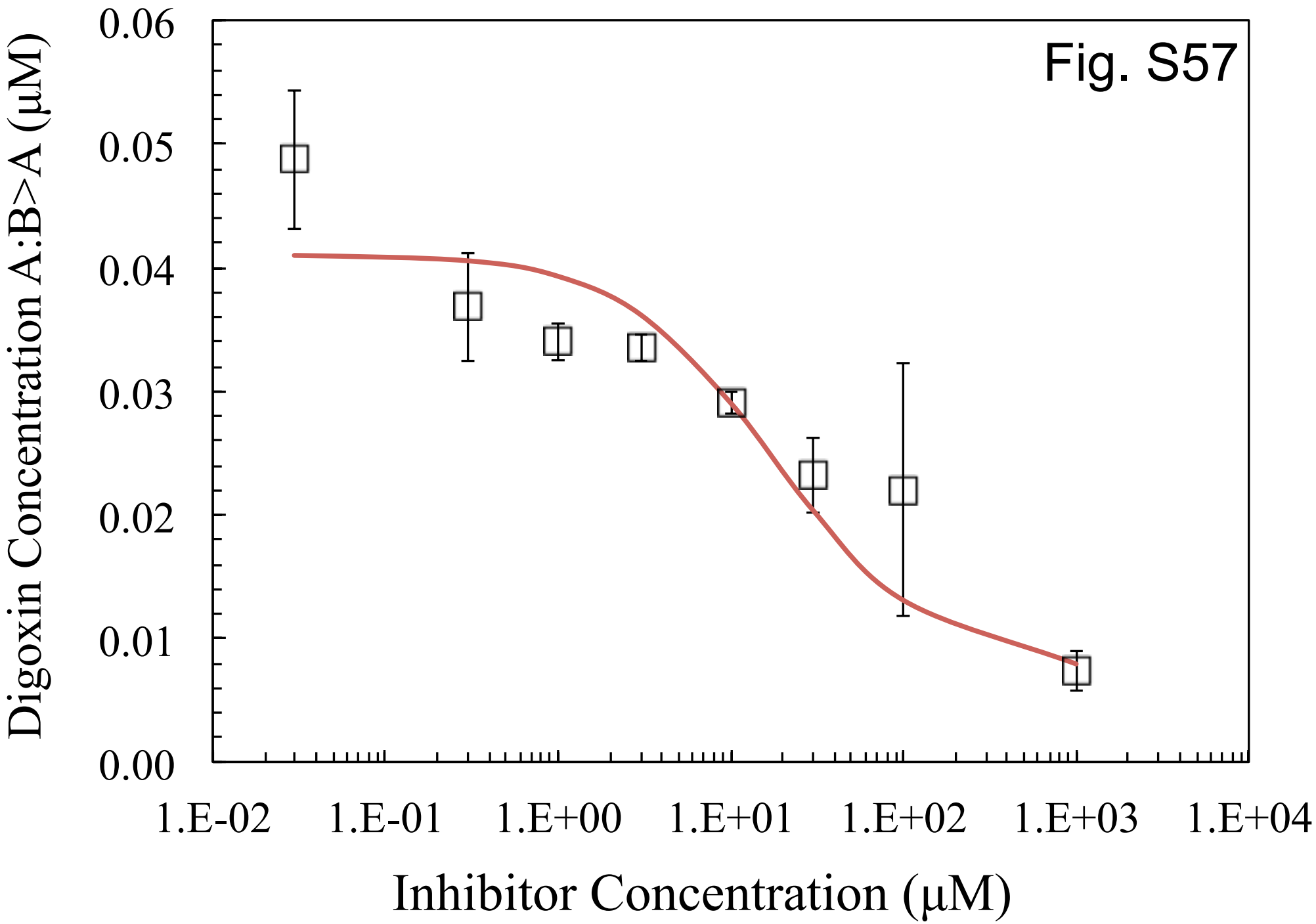
Fig. S57
Digoxin Concentration A:B>A (μM)
0.06
0.05
0.04
0.03
0.02
0.01
0.00
1.E-02
1.E-01
1.E+00
1.E+01
1.E+02
1.E+03
1.E+04
Inhibitor Concentration (μM)

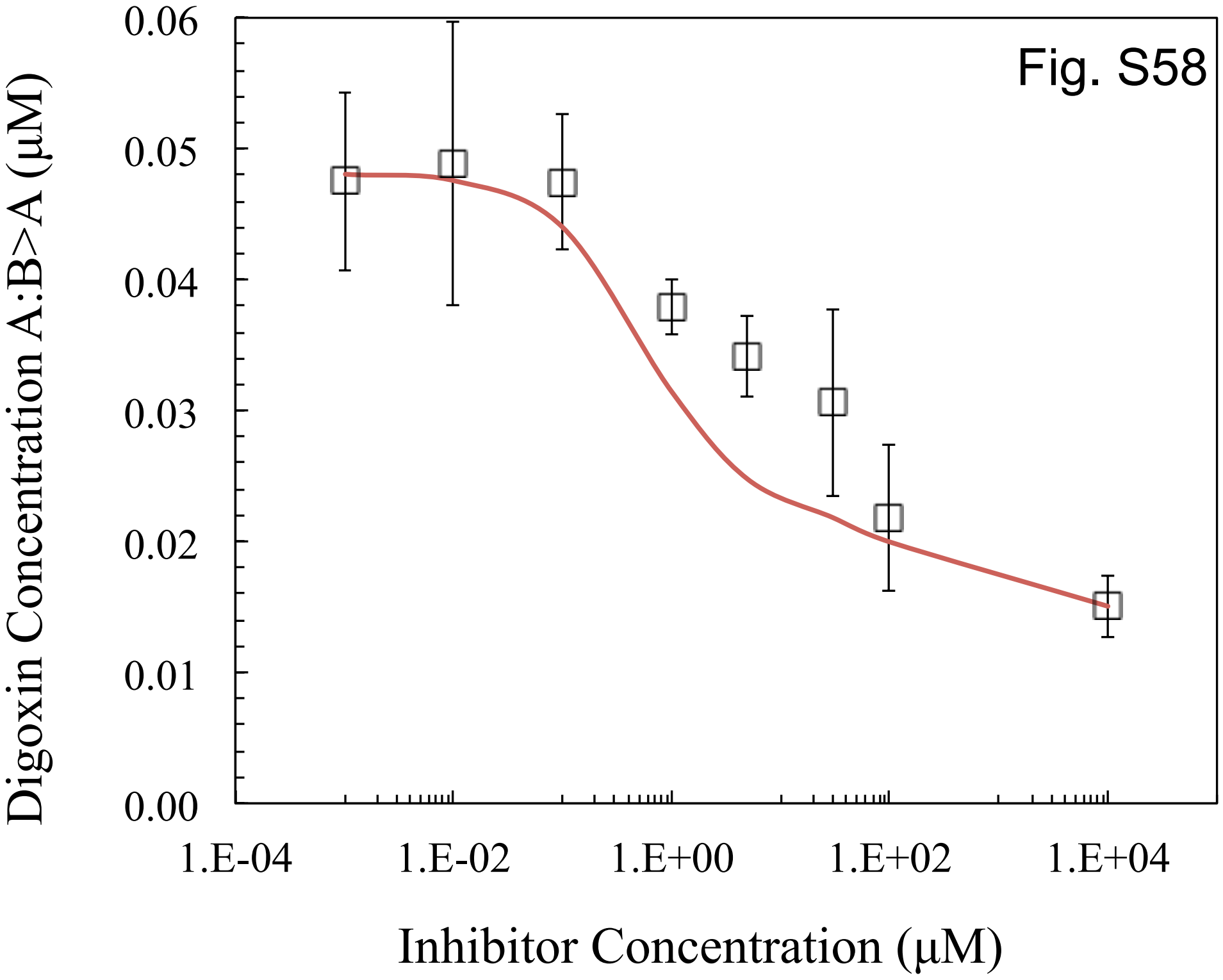
Fig. S58
Digoxin Concentration A:B>A (μM)
0.06
0.05
0.04
0.03
0.02
0.01
0.00
1.E-04
1.E-02
1.E+00
1.E+02
1.E+04
Inhibitor Concentration (μM)

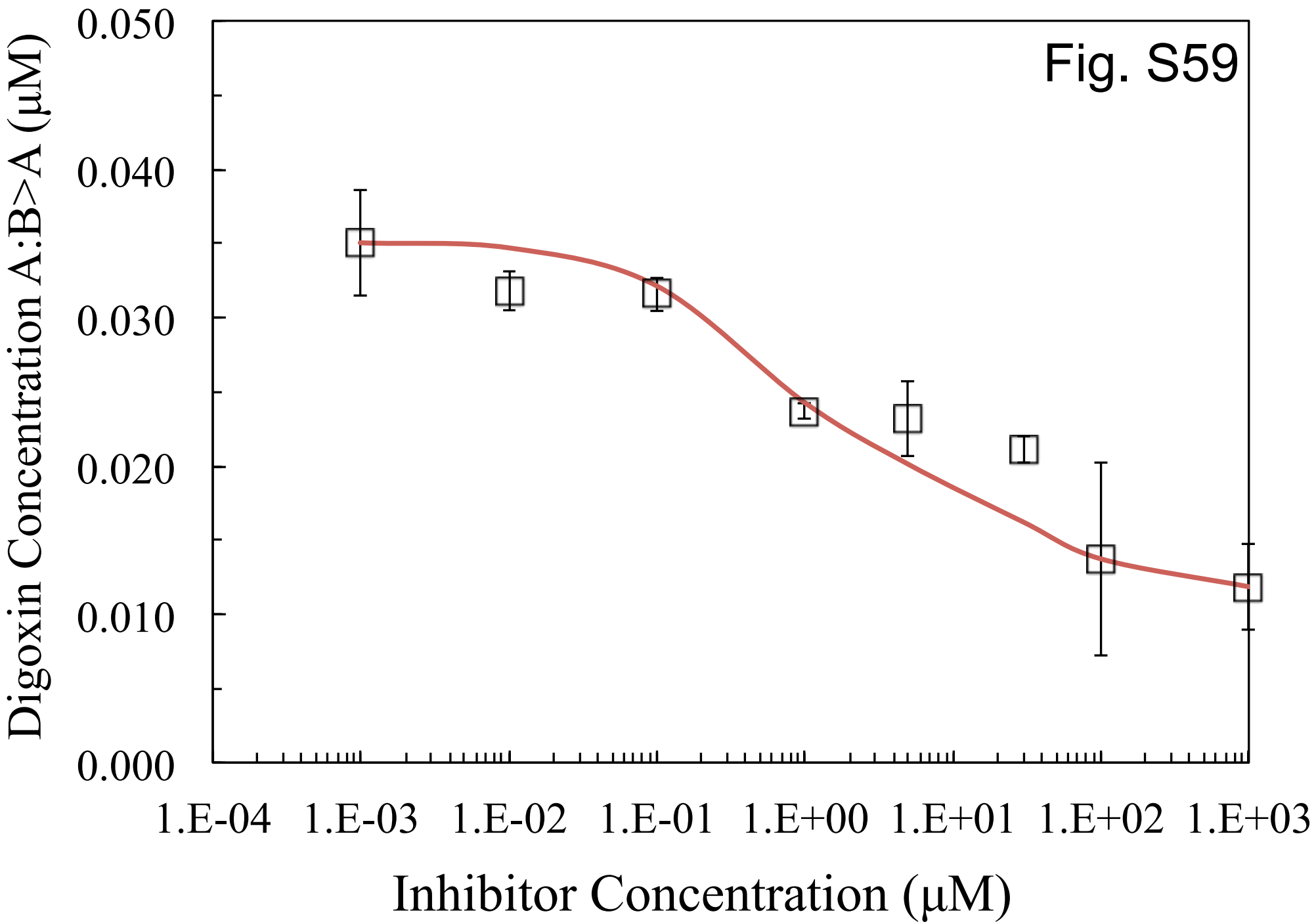
Fig. S59
Digoxin Concentration A:B>A (μM)
0.050
0.040
0.030
0.020
0.010
0.000
1.E-04
1.E-03
1.E-02
1.E-01
1.E+00
1.E+01
1.E+02
1.E+03
Inhibitor Concentration (μM)

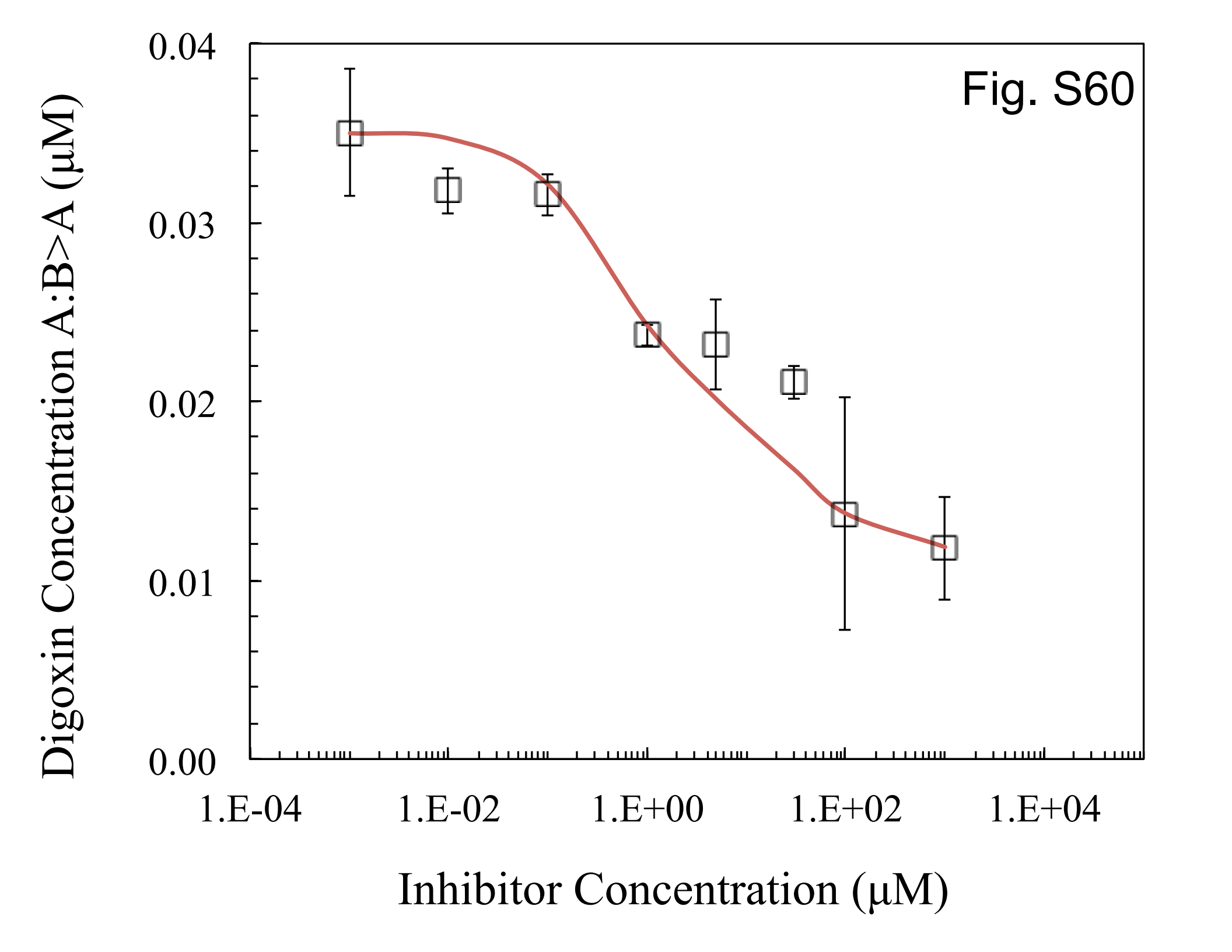
Fig. S60
Digoxin Concentration A:B>A (μM)
0.04
0.03
0.02
0.01
0.00
1.E-04
1.E-02
1.E+00
1.E+02
1.E+04
Inhibitor Concentration (μM)

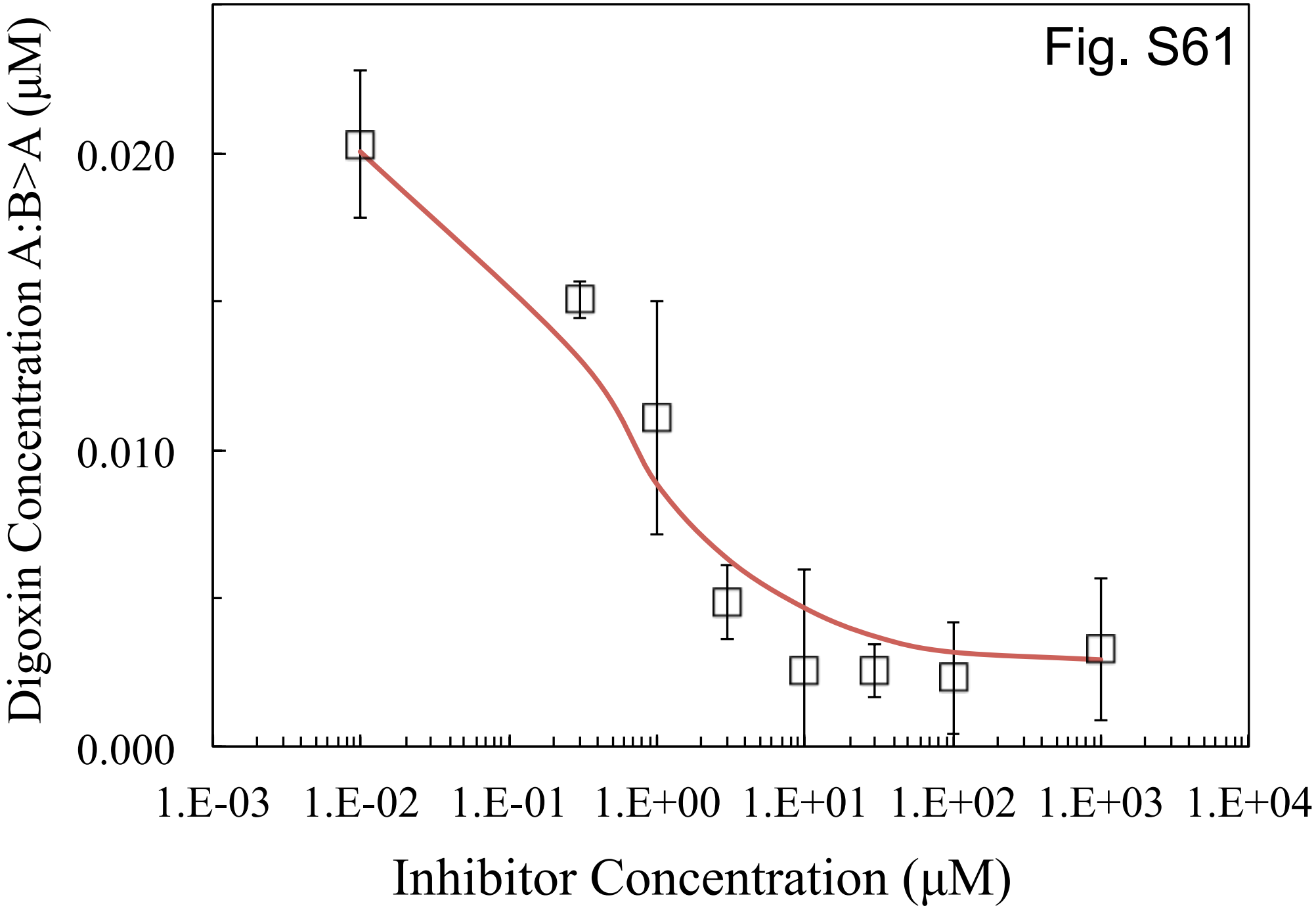
Fig. S61
Digoxin Concentration A:B>A (μM)
0.020
0.010
0.000
1.E-03
1.E-02
1.E-01
1.E+00
1.E+01
1.E+02
1.E+03
1.E+04
Inhibitor Concentration (μM)

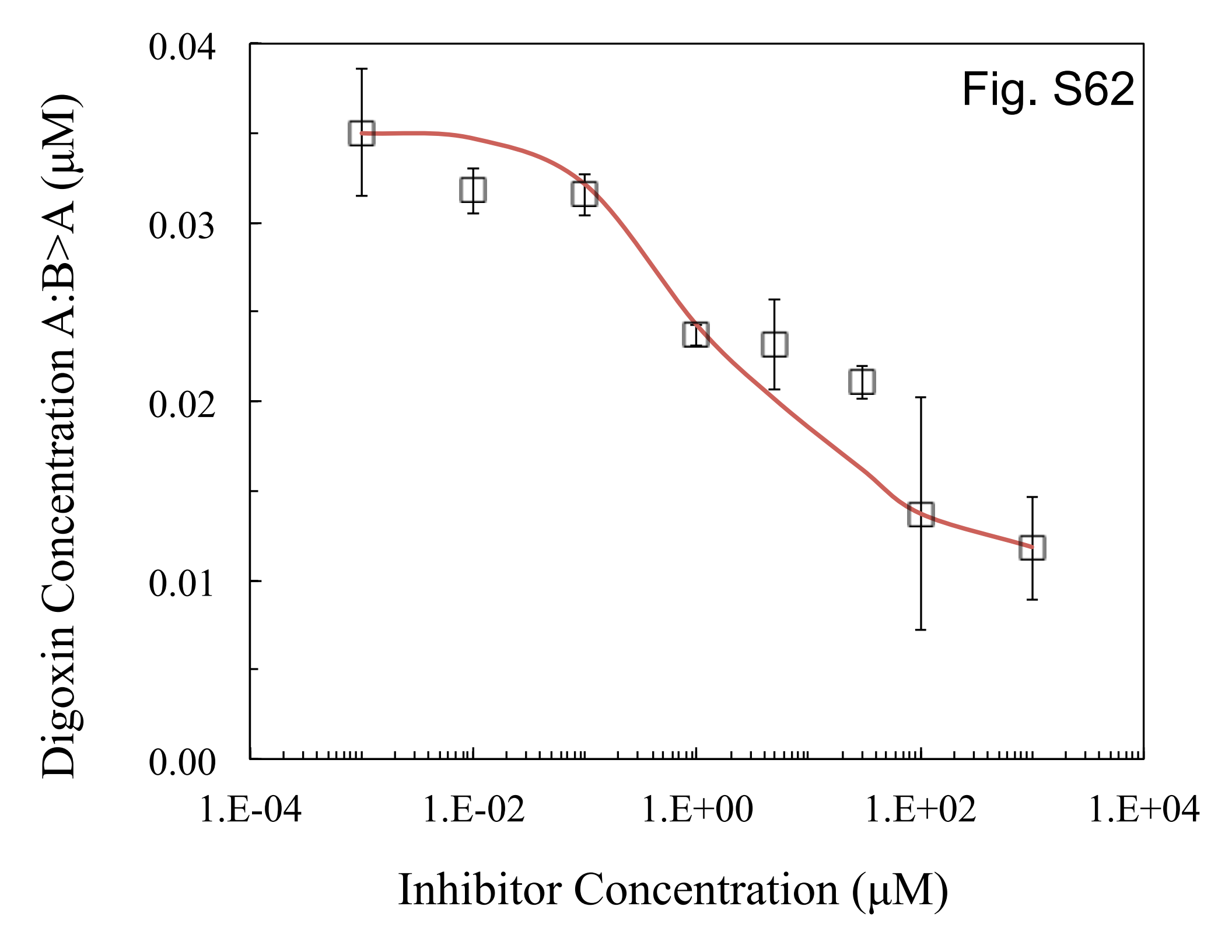
Fig. S62
Digoxin Concentration A:B>A (μM)
0.04
0.03
0.02
0.01
0.00
1.E-04
1.E-02
1.E+00
1.E+02
1.E+04
Inhibitor Concentration (μM)

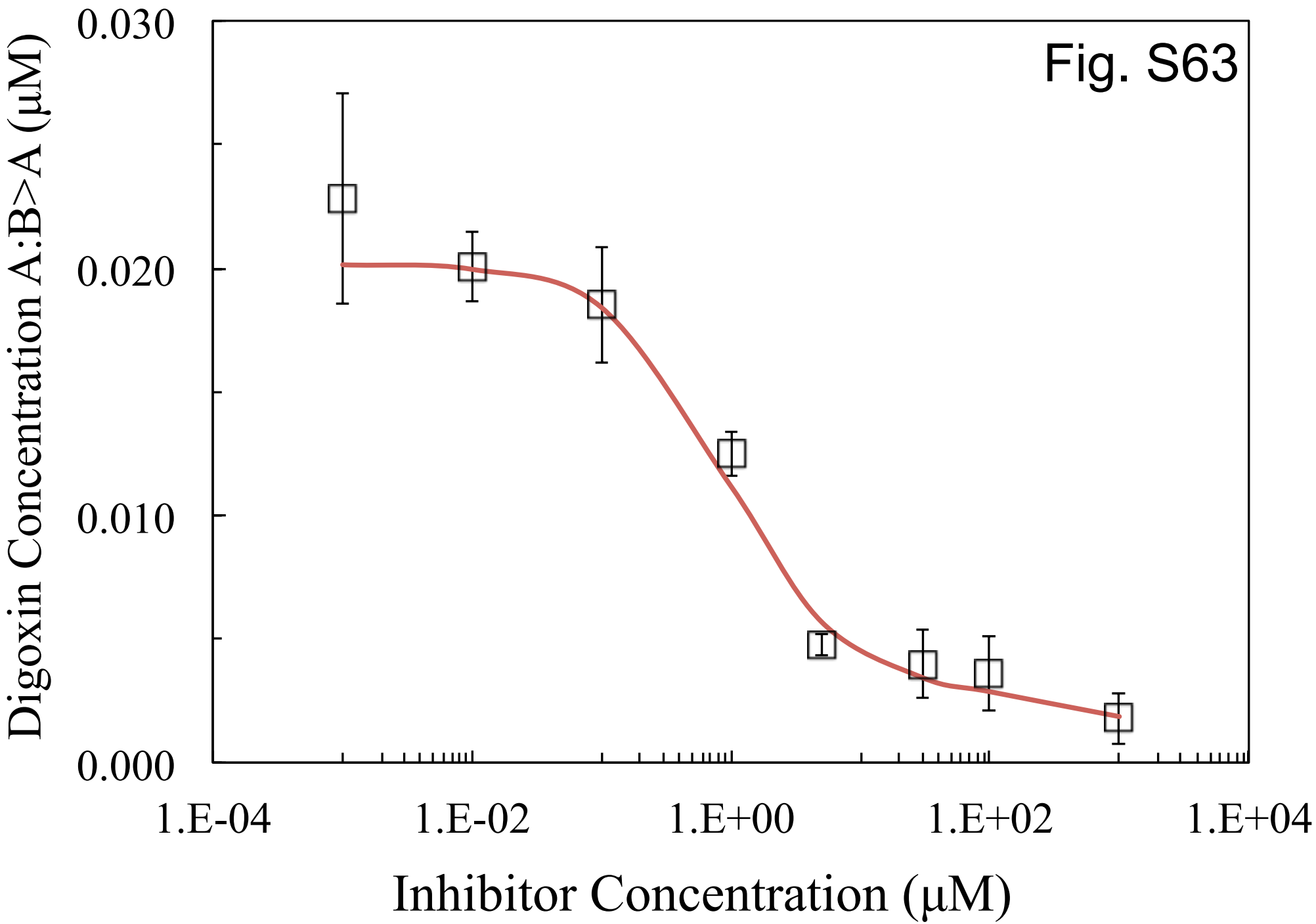
Fig. S63
Digoxin Concentration A:B>A (μM)
0.030
0.020
0.010
0.000
1.E-04
1.E-02
1.E+00
1.E+02
1.E+04
Inhibitor Concentration (μM)

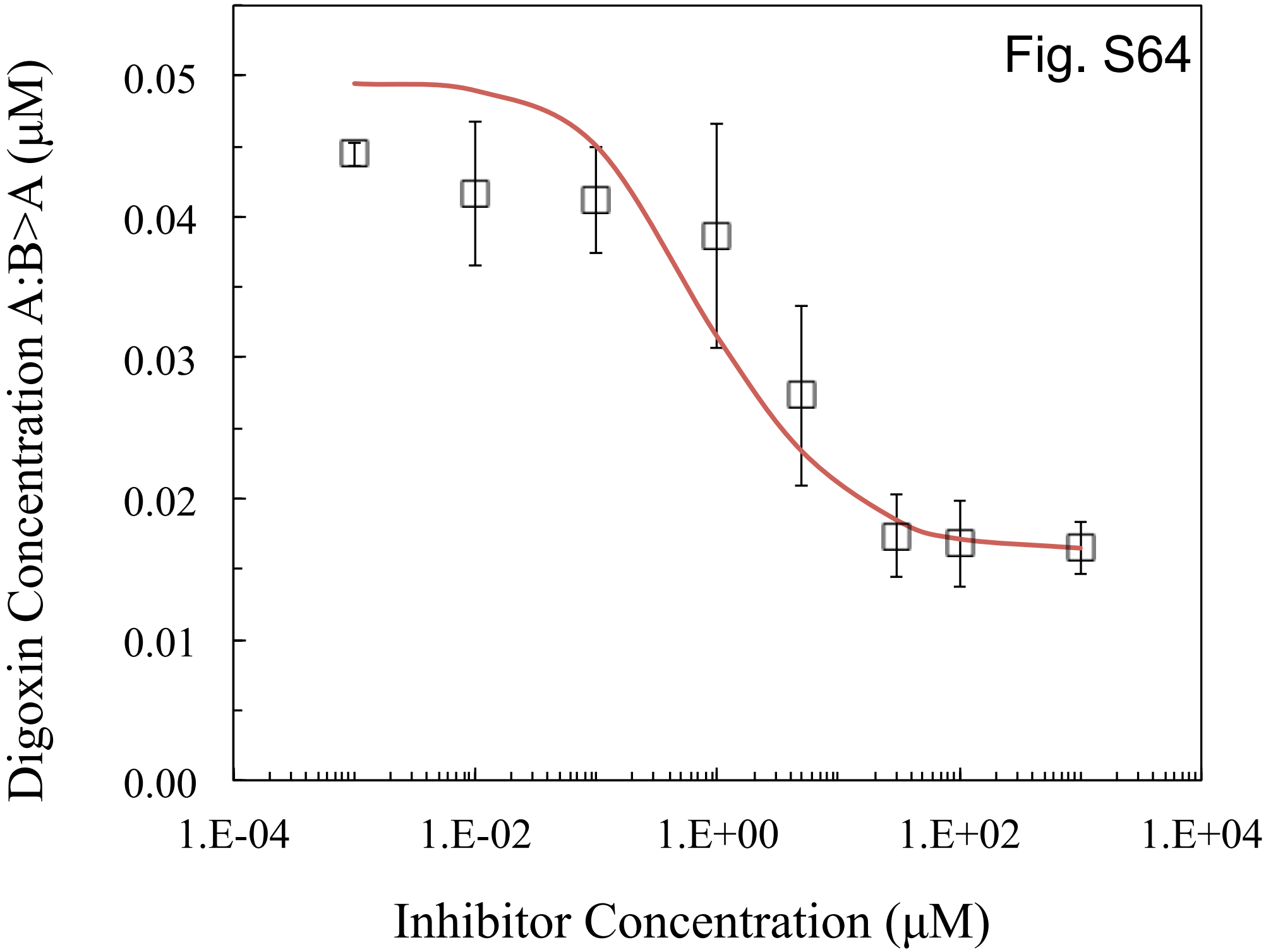
Fig. S64
Digoxin Concentration A:B>A (μM)
0.05
0.04
0.03
0.02
0.01
0.00
1.E-04
1.E-02
1.E+00
1.E+02
1.E+04
Inhibitor Concentration (μM)

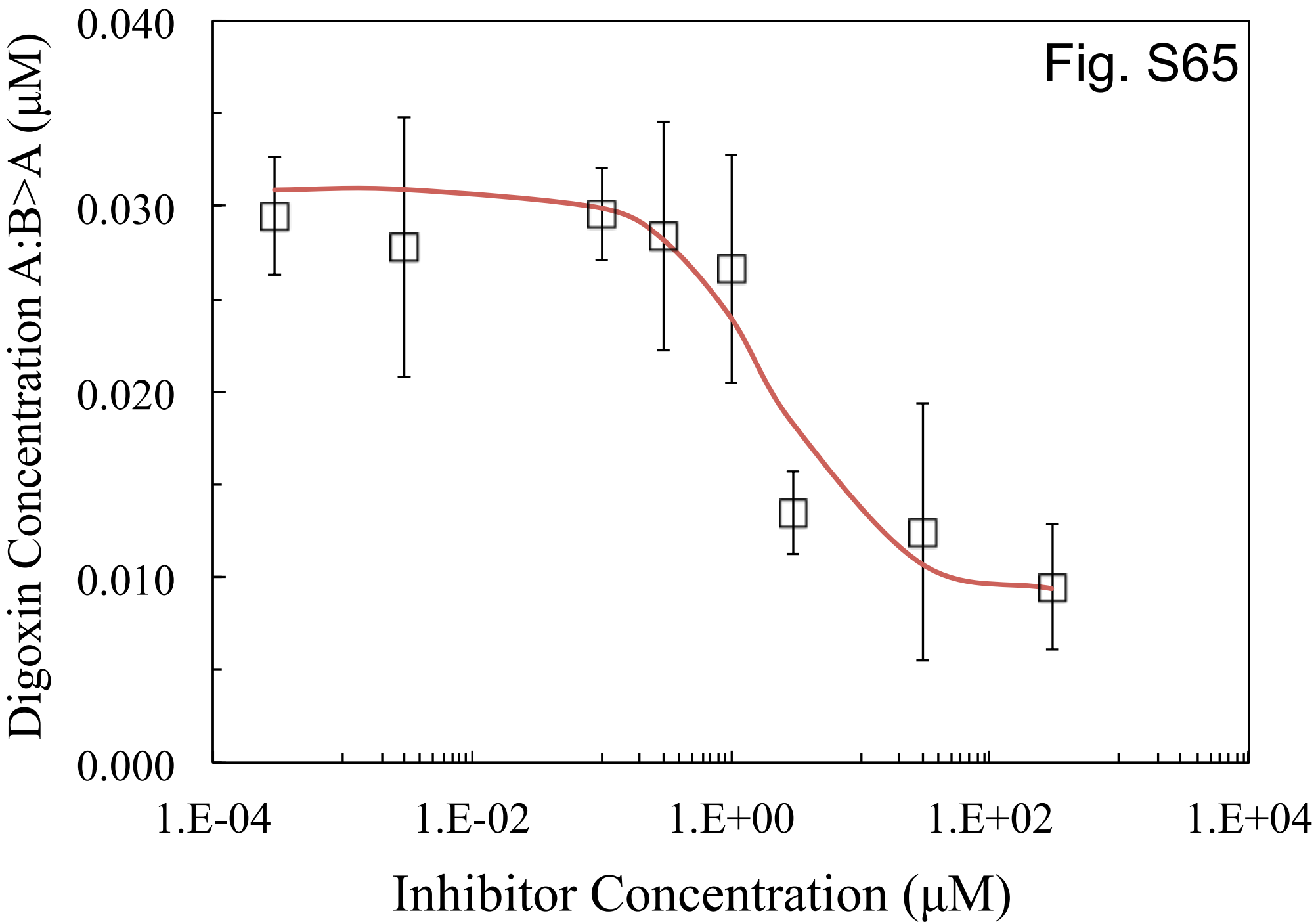
Fig. S65
Digoxin Concentration A:B>A (μM)
0.040
0.030
0.020
0.010
0.000
1.E-04
1.E-02
1.E+00
1.E+02
1.E+04
Inhibitor Concentration (μM)

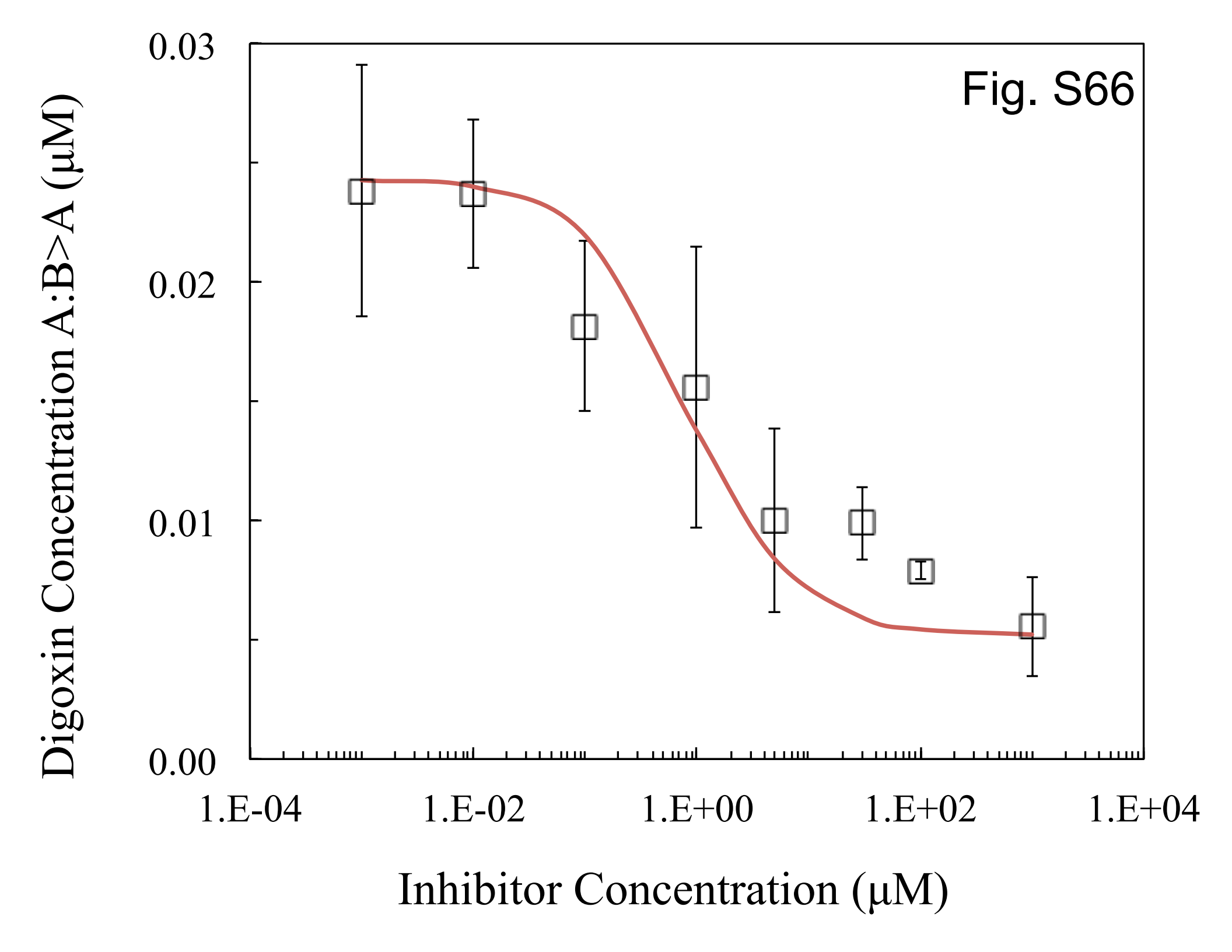
Fig. S66
Digoxin Concentration A:B>A (μM)
0.03
0.02
0.01
0.00
1.E-04
1.E-02
1.E+00
1.E+02
1.E+04
Inhibitor Concentration (μM)

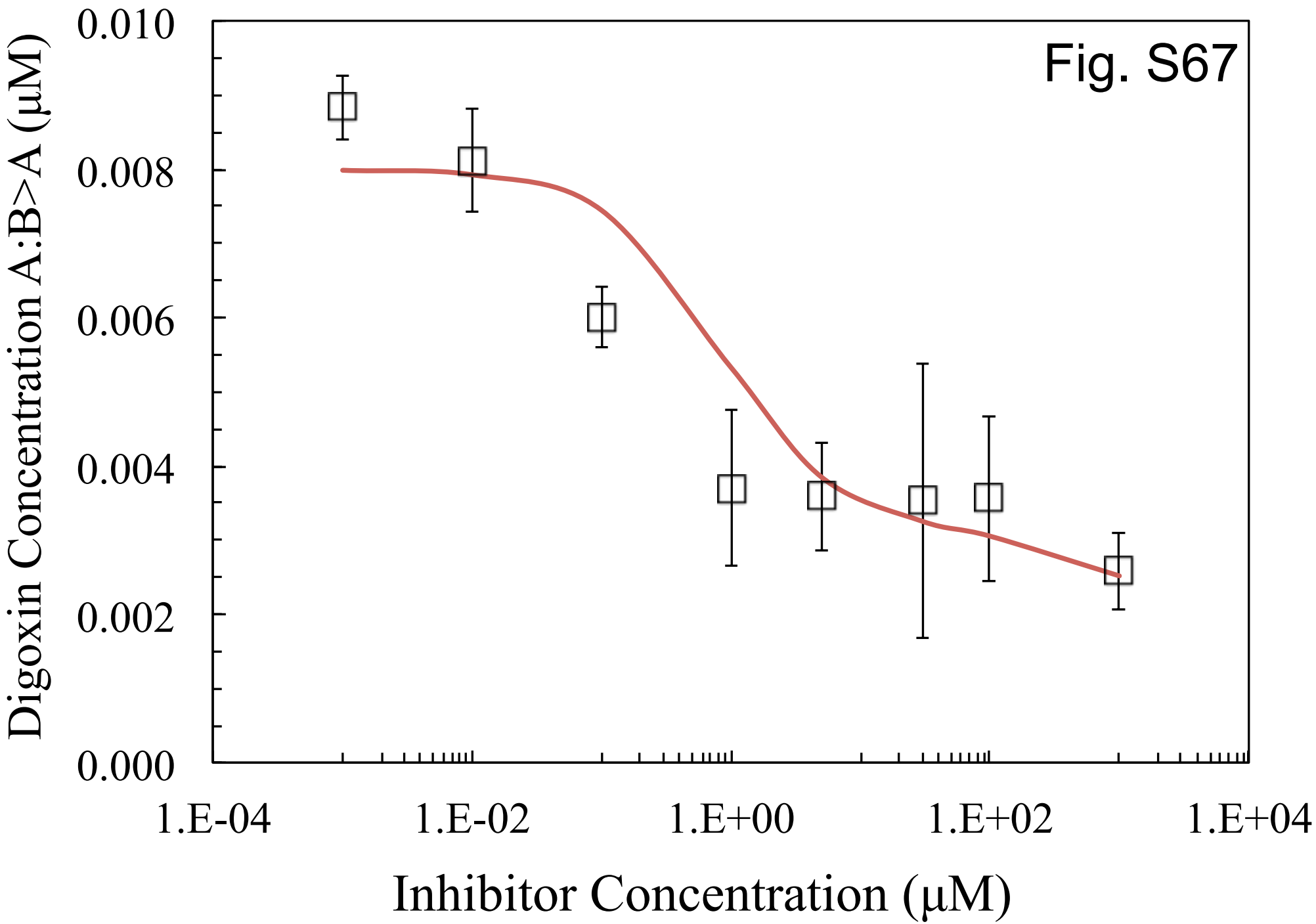
Fig. S67
Digoxin Concentration A:B>A (μM)
0.010
0.008
0.006
0.004
0.002
0.000
1.E-04
1.E-02
1.E+00
1.E+02
1.E+04
Inhibitor Concentration (μM)

Supplemental Data Table S6. Figure Legends for HPTC digoxin in the main paper. For all figures, S54-S67, symbols show the B>A digoxin transport data, error bars show the data standard deviation and the line shows the fit to the data.

Fig. S68. Inhibition by T3 of digoxin uptake into HPTC cells.
Fig. S69. Inhibition by T3 of digoxin transport, $J_{B>A}$, through HPTC cells.

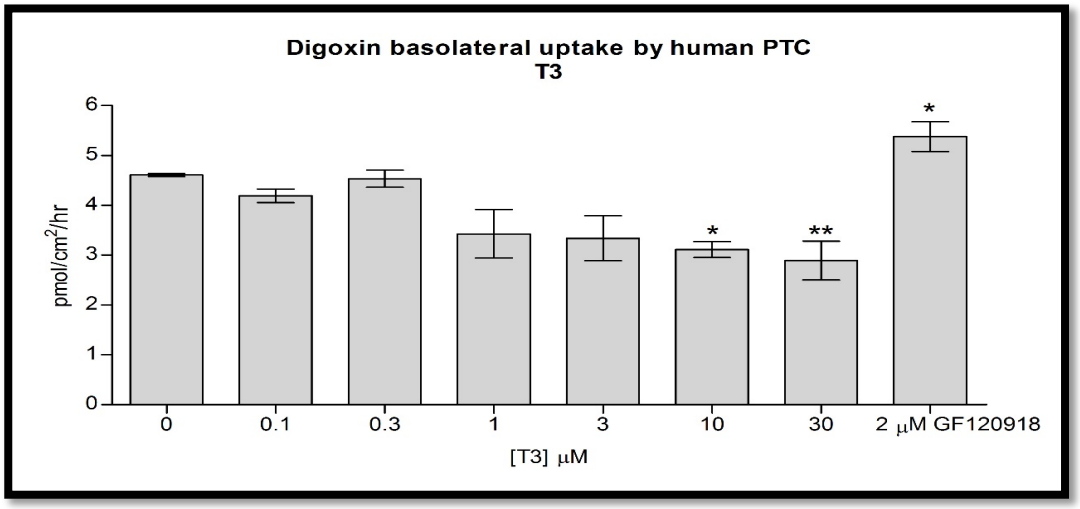

S68

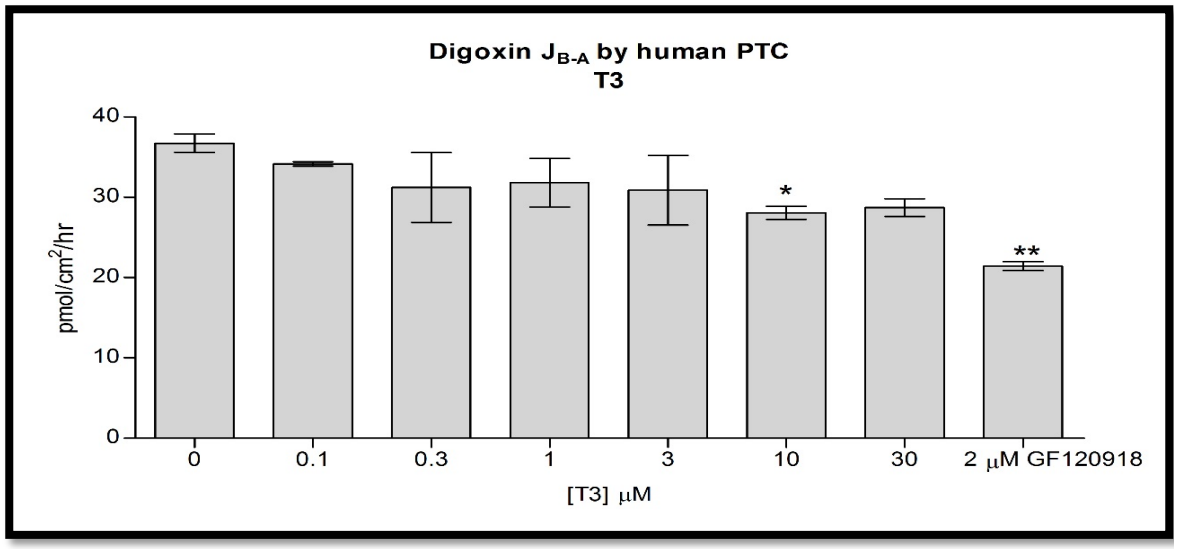
Digoxin J_{B-A} by human PTC
T3
pmol/cm^2/hr
40
30
20
10
0
*
**
0
0.1
0.3
1
3
10
30
2 μM GF120918
[T3] μM

Supplemental Data Table S7. Individual Lab fits for $\log_{10}\{k_{rQ}\}$ for Main Table 3

Cell [a]	lab	Inhb [b]	$\log_{10}\{k_{rQ}\}$ [c]	k_{rQ} [c]	$\langle\log_{10}\{k_{rQ}\}\rangle$ [d]	$\langle k_{rQ}\rangle$ [d]
1	2	CRV	3.80	6.28E+03		
1	7	CRV	3.91	8.10E+03		
2	6	CRV	4.49	3.12E+04		
2	11	CRV	3.72	5.30E+03	3.98	9.6E+03
1	2	DLT	5.00	1.01E+05		
2	6	DLT	5.23	1.69E+05		
2	11	DLT	4.22	1.64E+04	4.82	6.5E+04
1	2	IZR	4.58	3.80E+04		
2	6	IZR	5.02	1.06E+05		
2	11	IZR	4.70	5.02E+04	4.77	5.9E+04
1	2	MBF	3.90	7.90E+03		
3	2	MBF	3.93	8.52E+03	3.91	8.2E+03
1	2	NCD	3.59	3.90E+03		
1	7	NCD	3.71	5.10E+03		
2	6	NCD	4.52	3.31E+04		
2	11	NCD	3.48	3.03E+03	3.82	6.7E+03
1	2	QND	3.79	6.20E+03		
2	6	QND	4.46	2.91E+04		

2	11	QND	4.17	1.48E+04		
3	2	QND	4.08	1.20E+04	4.13	1.3E+04
1	2	RNO	4.76	5.80E+04		
1	7	RNO	4.99	9.70E+04		
2	6	RNO	4.94	8.71E+04		
2	11	RNO	4.32	2.07E+04		
3	2	RNO	4.53	3.41E+04	4.71	5.1E+04
1	2	VRP	4.08	1.20E+04		
1	7	VRP	4.52	3.30E+04		
2	6	VRP	4.30	2.00E+04		
3	2	VRP	4.51	3.22E+04	4.35	2.2E+04

Footnotes for Supplemental Data Table S7:

[a] Cells 1, 2 and 3 are MDCKII-hMDR1-NKI, Caco-2 and LLC-PK1-hMDR1-NKI, respectively.

[b] Inhibitors: CRV (carvedilol); DLT (Diltiazem); IZR (Isradipine); MBF (Mibefradil); NCD (Nicardipine); QND (Quinidine); RNO (Ranolazine); VRP (Verapamil).

[c] $\log_{10}\{k_{rQ}\}$ is the fitted value.

[d] $< \log_{10}\{k_{rQ}\} >$ is the inhibitor average over the fitted labs. <krQ>=10^< $\log_{10}\{k_{rQ}\}$ >.